UNIVERSITY OF CALGARY

SPEED GENERATION IN THE GOLF SWING: AN ANALYSIS OF ANGULAR KINEMATICS, KINETIC ENERGY AND ANGULAR MOMENTUM IN PLAYER BODY SEGMENTS

by

Brady C. Anderson

A THESIS SUBMITTED TO THE FACULTY OF GRADUATE
STUDIES IN PARTIAL FULFILMENT OF THE REQUIREMENTS
FOR THE CROSS-DISCIPLINARY DEGREE OF MASTER OF SCIENCE

FACULTY OF KINESIOLOGY
and
DEPARTMENT OF MECHANICAL ENGINEERING

CALGARY, ALBERTA

MAY 2007

UNIVERSITY OF CALGARY

FACULTY OF GRADUATE STUDIES

The undersigned certify that they have read, and recommend to the Faculty of Graduate Studies for acceptance, a thesis entitled "Speed Generation in the Golf Swing: An Analysis of Angular Kinematics, Kinetic Energy and Angular Momentum in Player Body Segments" submitted by Brady C. Anderson in partial fulfilment of the requirements of the degree of Co-disciplinary Master of Science.

_____

Supervisor, Dr. Darren Stefanyshyn
Faculty of Kinesiology, Engineering

_____

Co-Supervisor, Dr. Vincent von Tscharner
Faculty of Kinesiology

_____

Dr. Benno Nigg
Faculty of Kinesiology, Engineering, Medicine

_____

Dr. Janet Ronsky
Schulich School of Engineering
Mechanical & Manufacturing Engineering

_____

Dr. Ian Wright
TaylorMade-adidas Golf Company

_____

Date

Abstract

The proximal to distal (P-D) movement pattern has been established as a robust solution for creating efficient, high-speed human movements. The optimal pattern of speed creation in the golf swing is yet unknown. The purpose of this investigation was to develop a basic understanding of speed generation in the golf swing. Motion patterns were explored by looking at the magnitudes and timings of peaks in golfer segment angular kinematics, kinetic energy and angular momentum. Results showed that the timing of peak angular kinematics, kinetic energy and angular momentum did not follow a P-D order. It was speculated that the transfer of angular momentum might be improved by altering the sequence of rotations in the conventional golf swing as well as increasing resistance to frontal plane rotation in the Torso segment. The findings of this study may be of benefit to players, teachers and equipment manufacturers in the game.

Acknowledgements

Thank you to Murray, Diane, Susan, Lauren, Bryan, Aiden and Harris. You mean the world to me. Without Sunday (Monday, Tuesday etc.) dinners and time together, none of this would have been worthwhile.

Thank you to Darren Stefanyshyn for taking me under your wing. You've taught me a great deal about critical thinking and professionalism in science and business. I couldn't have asked for a better supervisor, role model and mentor. I wouldn't be where I am today without you.

Thank you to Benno Nigg, for appearing on my exam committee and for giving me the opportunity to work for your company. Thank you for building the HPL, for creating a research partnership with adidas and for being a founder of the field of biomechanics. I owe you a great deal.

Thank you to Vincent and Michaela von Tscharner for much appreciated helpings of home cooked meals and honest advice. Vincent, you have been a great teacher to me.

Thank you to Janet Ronsky for appearing on my exam committee and for teaching me the finer points of motion analysis in biomechanics.

Thank you to Ian. I've felt like your little brother in the few years we've got to work together. I look forward to our business meetings in Encinitas surf breaks.

Thank you to Ursula, Jyoti, Glenda, Byron, Glen and Andrzej for keeping the HPL upright.

Thank you to Bryan, Sean, Blayne, Jay, Tif, Derek, S.K., Josh, Grant, Spencer, Danny, JP, Dave, Meegan, Aviv, Laurence, Jordan, and the entire HPL grad student entourage for my most memorable, if unmentionable, times at the lab.

Thank you to Kim and Jessica. I was blessed with funny, intelligent and honest office mates, even though I heard more about floral arrangements and bridesmaids' dresses than I'd ever care to remember.

Thank you to Berti and Heiko. Your support and understanding has made this thesis possible. I am proud to be a part of your ait research family.

Finally, thank you to Rosalie, Darren, SK, Jill, Blayne, Jay, Sean and Tif for all of your work with my paper shuffling and making my thesis comprehensible. I owe you all pints and then some.

Table of Contents

List of Tables

List of Figures and Illustrations

List of Symbols, Abbreviations and Nomenclature

2D	Two Dimensional	$KE_{\mathbf{RR}}$	Remote Rotational Kinetic Energy
3D	Three Dimensional	KE_T	Total Kinetic Energy
CHS	Club Head Speed	KE_{TR}	Translational Kinetic Energy
COM	Center of Mass	P-D	Proximal to Distal
g	Acceleration due to gravity	$\vec{r}$	Radius vector
h	Height	$\overline{R}$	Rotation matrix
Hc	Registered Golf Handicap	$\vec{S}_{cm}$	Position of center of mass
$\vec{H}$	Angular Momentum	t	Time
H_{AT}	Absolute Angular Momentum	$\vec{V}_{cm}$	Velocity of center of mass
H_{CP}	Club Plane Angular Momentum	$\vec{V}_{\Delta}$	Differential velocity vector
$\vec{H}_{L}$	Local Angular Momentum	$\vec{V}_{\Delta rad}$	Radial component of differential velocity vector
$\vec{H}_{R}$	Remote Angular Momentum	$\vec{V}_{\Delta tan}$	Tangential component of differential velocity vector
$\vec{H}_{RP}$	Remote Planetary Angular Momentum	x	Global x coordinate
$\vec{H}_{RS}$	Remote Solar Angular Momentum	y	Global y coordinate
$\vec{H}_{T}$	Total Angular Momentum	z	Global z coordinate
$\bar{I}$	Inertial Tensor	$\boldsymbol{\alpha}$	Angular Acceleration
KE	Kinetic Energy	$\boldsymbol{\theta}$	Angular Position
$KE_{\mathbf{LR}}$	Local Rotational Kinetic Energy	$\boldsymbol{\omega}$	Angular Velocity

Chapter One: Introduction

1.1 Background

The comedian Robin Williams (2002) has called golf a masochistic invention of the Scottish, designed to irritate its participants. Williams described golf as a game where funny shaped sticks are used to hit a ball into a hole shaped like a gopher's den. These holes are placed hundreds of yards away from the player, hidden behind trees and bunkers. A little flag is placed next to the hole on the green, to give players "a little shred of hope"; but water holes and sand traps surround the green out of view, for extra frustration. When a golfer finally does manage to bash his ball into the gopher hole with his funny shaped stick, he'll find that he needs to repeat the process 17 more times before the game is complete.

Smacking rocks with sticks has been a pastime of humans for thousands of years. Variants of this form of play have been found in records of history in ancient Rome, China, and Laos. However, historians argue that the characteristic separating stick and rock games from modern golf was the presence of a hole. Heiner Gillmeister (2002) contends that the game of golf originated in the Netherlands in the 14th century. The word *golf* appears to have been derived from the Middle Dutch word *kolve*, meaning shepherd's crook. In 1545, Dutch lecturer Pieter van Afferden included a chapter in a Latin language textbook on the rules of *kolve*. Apparently it was illegal, even in the middle ages, to drive your ball out of turn. Gillmeister (2002) reasons that the game travelled by maritime trading routes from the Netherlands to Scotland, where the

development of 18 holes on the St. Andrews course closely resembles the modern form of the game played today.

Although the game of golf has been played for nearly 700 years, rigorous study of player motion during the golf swing is relatively new. In the mid 1960's, the Spalding Brothers of sporting goods fame took a series of strobo-graphic photographs of touring professional Bobby Jones. This series of photos marked the first biomechanical analysis of the golf swing. Over the past 40 years, the complexity of the method has increased but the aim of the research has remained the same. The role of biomechanics in golf has been to improve performance and reduce injury risk in the game through the application of Newton's Laws of Motion to the golf swing. The following research seeks to fulfill a part of this role.

1.2 Understanding Speed Generation

The game of golf requires that the golf ball travels large distances towards a target, using the least number of strokes, or ball-club contacts, possible. In the case of long holes, golfers must therefore strive to maximise the distance the ball travels when taking their first shot. This is known as a golf drive. While there are many factors that control the success of a golf drive, distance is largely determined by the speed of the club head as it contacts the ball.

Rick Martino is the Director of Instruction for the Professional Golf Association (PGA) tour. Martino (2005) describes *timing* as the relative pattern of movement of the body segments during the swing; while *tempo* is used to describe the combined speed of the swing as a whole. Martino (2005) states that timing is much more important than

tempo in creating a fast swing. Many players of the game may sympathize with this assessment anecdotally. When learning how to hit a driver, experienced players often teach beginners to “swing easy”. Beginner golfers are often surprised to find that “relaxed” swings produce better results than “hard swings”. While the speed of the club is largely determined by the forces and moments applied at the grip, it is the pattern or relative timing of the motion that is key in developing that grip loading.

Golfers interact with the ground via their feet. Through a series of twists and turns of their hips, spine, shoulders and wrists, speed is created at the end of their club. The motion occurs on multiple planes within a three dimensional space. If club head speed was measured by rotating these joints separately, the summed result would be far less than during a normal swing, when all of the joints are allowed to work together in optimal coordination. It is important to understand how the relative timing and magnitudes of body segments interact to generate a fast swing. This information will help golfers to drive the ball further or with greater efficiency. It is the aim of this paper to explore body segment interactions to investigate how speed is generated in the golf swing.

The optimal pattern of motion for human body segments has been studied in a variety of sports other than golf. In activities such as kicking, jumping and overhand throwing, many authors have shown that a proximal to distal progression of motion results in the highest performance. It is possible that this movement pattern is a natural consequence of our mass distribution. Our bodies have evolved in such a manner that our largest muscle groups are located near the body center. This is also the location of our largest concentrations of mass. As we move away from the body center, segment

volumes decrease, segment masses decrease, and the length of long bones also decrease. By the time we reach our hands and feet (our most distal endpoints); segment length, mass and segment volumes have decreased to be a fraction of that near our core. In high-speed movements therefore, it could be logical for humans to have evolved a movement pattern that follows a proximal to distal sequencing, matching that of our segment mass distribution.

In golf however, mass distribution is altered from that of other sports. A club is added to the hands, and because of the handgrip used, this club segment hinges at the wrist joints. The center of gravity of this external implement is located near its distal end. The distance from the wrist joint to the club center of mass creates a large radius of gyration, meaning that the club segment does not follow the progression of mass distributions already found in the human body. For this reason, it is hypothesized that the proximal to distal pattern that has evolved for high-speed human movement will not be suitable for golf. The addition of an external element, with a large radius of gyration, to the distal end of a human chain of linked segments should require a change in movement pattern for optimal performance.

1.3 Purpose

This research will investigate the angular kinematics, energetics, and angular momentum of body segments in the golf swing. The aim of this work is to develop a basic understanding of the pattern of body segment interaction in the generation of speed in the golf swing. The benefits of this research will be both academic and practical. Academically, a basic understanding of the golf swing will aid in future modeling of the

swing, and in understanding optimal motion for sports involving an external implement (such as racket sports, polo, or field hockey). In practical terms, this research work will be of benefit to those interested in improving performance in golf. Teaching pros and club manufacturers may be interested in exploring how body segment interaction can be optimized.

1.4 Hypothesis

H_0: The timing and magnitudes of peaks in angular kinematics, kinetic energy and angular momentum of body segments, progress in a proximal to distal manner during the golf swing.

1.5 Summary

This study aims at investigating speed generation in the golf swing by exploring the patterns of angular kinematics, kinetic energy and angular momentum in golfer segments. The results provide a basis for understanding high performance in the golf swing. The proposed research will use a linked chain framework that is an extension of biomechanical studies that have been performed in other sports. The information gained in this research may be of benefit to golfers wishing to generate more speed in their swing, or by golfers wishing to generate speed more efficiently in their swing.

Chapter Two: Literature Review

The following literature review has been separated into three sections. The first section of this review will look at generalized segmental human motion. The intention of this section is to explore what is known about the general pattern of segment sequencing in human movements such as kicking, jumping and overhand throwing. The second section of this review looks at considerations when using a segment-based framework versus a joint framework when analyzing energetics in human movement. The final section of the review examines the development of golf biomechanics, focusing specifically on studies in optimization of club speed.

2.1 Optimizing Speed in Segmental Human Motion

Movement patterns in segmented human motion have been studied in biomechanics for a variety of motions including kicking, jumping, and overhand throwing. The following section focuses on optimal patterns of motion for a linked system of body segments. This is a topic that has been debated in biomechanics research for the past thirty years. To begin, we will look at a kinematic chain of body segments as generalized link mechanism. Figure 2.1.1 illustrates an example of a 2D, 2 segment linkage-mechanism as described by Vinogradov (2000).

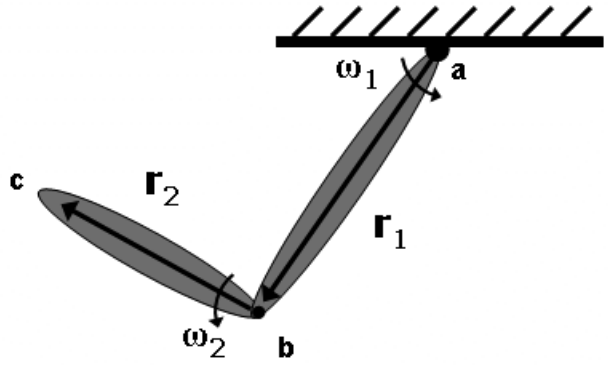

Figure 2.1.1: Example of a 2D, 2 segment linkage. Points *a* and *b* are the proximal and distal joints respectively. *c* represents the linkage distal end point. r_1 and r_2 are the respective lengths of the first and second segments; while ω_1 and ω_2 are the respective angular velocities.

The velocity of point ***b*** relative to a coordinate system fixed to the external reference frame is shown in equation 2.1.1 (Vinogradov, 2000). The velocity of the end point ***c*** is given by equation 2.1.2. For a linked mechanism, the velocity of a segment end point is not only dependent on the angular velocity of that segment, but also on the velocity of the endpoints of all of the segments that precede it. In Figure 2.1.1, the linkage contains only one preceding segment but in human motion it is possible to have many more.

$$\vec{v}_b = \vec{\omega}_1 \times \vec{r}_1 \qquad 2.1.1$$

$$\vec{v}_c = \vec{v}_b + \vec{\omega}_2 \times \vec{r}_2 \qquad 2.1.2$$

2.1.1 Simultaneous Peaking of Body Segment Angular Velocities

Authors have argued over the optimal pattern of timing for joint angular velocities in a linked system. Koniar (1973) has argued for what he called the "*principal of superposition of angular speeds in joints*". In order to achieve maximum performance for a given action, Koniar said that all segments should reach a maximum angular velocity at precisely the same moment. He measured 20 athletes with electro-goniometers and found that subjects jumped highest when segmental angular velocities peaked *simultaneously*. No mention was made as to the sampling frequency or smoothing methods used in this investigation.

Koniar wasn't the only author to describe this "*principle*" of simultaneous segmental speed peaks. Gowitzke and Millner (1988) stated that "*in theory, each joint action should impart maximal linear velocity at the instant of release*". These authors noted that this phenomenon wasn't seen in hitting or throwing sports. They speculated that it would be possible to estimate the degree of coordination for a given performance by comparing peak end point velocity with a theoretical end velocity if all segments were to peak at the same time.

Joris *et al* (1985) described a simultaneous maximality of body segment angular velocities as "*the Hocmuth Optimization Principal*". In a study of over hand throwing in handball, those authors set out to determine if simultaneous peaking of segment angular velocities actually improved performance. They found that this pattern could only be possible in a purely theoretical, *kinematic* sense; that is, if the segments contained no mass. Of course, this constraint does not hold true for real human movement. The authors found that distal segments seemed to go through periods of highest acceleration when the

preceding segments underwent a deceleration. Joris *et al* stated that Newton's third law could likely explain the deceleration of proximal segments. Those authors reasoned that "*for every action on a more distal segment ...*" (i.e. joint torque) "*there is an equal but opposite reaction on the more proximal segment*." In their experiment, they found that optimal performance was found when segmental angular velocities peaked in a proximal to distal (P-D) fashion.

2.1.2 Proximal to Distal Sequencing of Body Segment Motion

Bunn (1972) was the original author to refute the concept of simultaneous peaking of limb angular velocities. In his "*guiding principles of human motion*", he stated that optimum speed of a kinematic chain's distal end point can only be reached when body segment angular velocities peak in a P-D fashion. According to Bunn, *"... movement of each member should start at the moment of greatest velocity, but least acceleration of the preceding member*". He reasoned that proximal joints could attain higher angular velocities if their distal counterparts would remain flexed later in motion. Although he did not provide equations to prove his work, Bunn argued that higher limb angular velocities could be easier to attain if the radius of gyration of the linked system is kept small (ie. when a joint is flexed). He felt it would be possible to capitalize on this increased angular velocity by quickly lengthening the system's radius of gyration pre-impact. He observed that the knee seemed to be flexed until late before ball contact for maximum kicking velocity in human kicking motions.

Figure 2.1.2 shows hypothetical profiles of angular velocity for a planar, multi-segment chain. Figure 2.1.2 *a)* represents the motion pattern that Koniar referred to as the

Superposition of Angular Speeds. Figure 2.1.2 *b)* represents the Summation of Speed Principal as described by Bunn (1972).

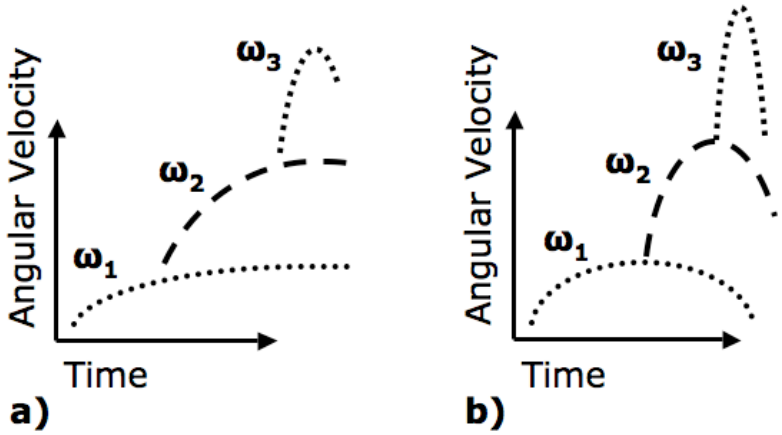

Figure 2.1.2: Hypothetical segmental velocity profiles in a 3 link chain. In part *a)* all segments peak simultaneously. Part *b)* shows a proximal to distal progression of angular velocity peaks.

Putnam (1993) supported what she referred to as Bunn's "*summation of speed principal*". She wrote that striking and throwing motions *must* follow a proximal to distal progression. This is due to what Putnam refers to as "*motion dependent interaction… between links".* In a Lagrangian model of two-link motion, Putnam found that angular kinematics of connected links did not solely depend on external moments applied (ie. muscle torques); but also on resultant joint "*interactive moments"* between links. It is speculated that these so called *moments* are actually due to reaction forces occurring at the joints; and the virtual or inertial forces acting on the segment CG (center of gravity). Putnam noted that the *interactive moments* were dependent on the relative angular position, angular velocity, and angular acceleration of each segment in series. Putnam found that *interactive moments* due to relative angular velocity were greatest when segments were orthogonal. Conversely, interactive moments due to relative angular

acceleration were greatest when segments were co-linear. In both cases, interactive moments caused the proximal segments to slow down while the distal segments sped up. In any case, Putnam showed that the kinematics of inter-segmental movement had an interdependent relationship with the loading of those segments.

Herring and Chapman (1992) carried out a 2D, three segment, over-hand throwing optimization. In the study, relative timing and direction of external joint torques were manipulated to find an optimal strategy for the longest possible throw. They found that a proximal to distal (P-D) sequencing was essential in obtaining the highest overall distal end point velocity. This was not only true of the onset timing of torques, but also in timing and magnitude of segmental angular velocities. The authors also found that negative torques applied to proximal segments can enhance distal end speed if applied just prior to release. Of note, Herring and Chapman found that P-D sequencing was a very robust solution for optimal segmental movement. Their optimization tended towards this type of movement pattern for a wide range of limb lengths, inertial properties, and applied muscle torques. They concluded that the linked, segmental nature of human limbs predisposes our movement systems to P-D sequencing.

Feltner and Dapena (1989) created a 3D, two segment, over-hand throwing model. They attempted to address the "*cause-effect*" interdependent mechanisms that link segment kinematics and kinetics. The purpose of their investigation was to show resultant joint forces and torques as a function of relative segment kinematics. They also showed how segment kinematics can be determined as a function of joint forces / torques in addition to gravity and neighbouring segment kinematics. The authors showed that

kinematics of a double pendulum represent an extremely multifaceted, interdependent system that does not rely solely on external impulses alone.

In summary, there have been two generalized motion patterns introduced that attempt to predict an optimum solution for speed generation in multi-segmented movement. Koniar (1973) introduced the concept of simultaneous peaking of angular velocities between body segments to reach optimum speed generation. Bunn (1972) presented a contrasting solution. He stated that segments should peak in a proximal to distal manner to achieve maximal distal end point velocity. Since these concepts were established, only Koniar's own study has quantitatively supported the concept of simultaneous peaking. The papers of Gowitzke and Millner (1988) and Joris *et al* (1985) supported the concept of simultaneous peaking in theory, but their results showed that humans displayed a pattern of P-D peaking in real movement.

Simulation work has gone on to support the concept of P-D patterning in segmented human movement. Putnam (1993) showed this pattern to be a function of the inertial property of our limbs. Simulation work by Herring and Chapman (1992) showed that a P-D pattern of segmental motion was a robust solution for a wide range of system parameters in their speed optimization study. Finally, the simulation work of Feltner and Dapena (1989) showed that a system involving 3D motion in linked segments is extremely complex and interdependent; and cannot be defined by external loading alone.

It seems that a pattern of P-D peaking in segmental human motion has been established as an optimal solution for speed generation. However, previous studies in the literature have shown that humans seem to have evolved to use this type of patterning in movements such as kicking, jumping and throwing. In these movements, there are no

external implements involved as a part of the dynamic, segmented chain. This is an important distinction. In general, human segments decrease in mass as you move along the body in a proximal to distal manner. In golf, the system may be slightly different. The club is an external implement that is swung as to be another segment in the dynamic linkage. Although the mass of the club is most likely less than that of the arms segment, the length of the club requires a large radius to be created between the club CG and the focus of club rotation. The result of this is a distal segment that may have more inertia than what humans have evolved to move optimally. Therefore, it remains to be seen whether a P-D pattern of segmented motion exists in the golf swing.

2.1.3 Out of Plane Segmental Motion

Marshall (2002) compiled a review article looking specifically at patterns of limb movement in regards to throwing and striking sports. He found that the literature tended to support the P-D sequencing as predicted by Bunn's summation of speed principle. Marshall noted that P-D sequencing was generally a pattern found in flexion and extension of linked segments. In a paper by Marshall and Elliot (2000), it was found that long-axis rotation of segments did not follow a classic P-D pattern. In addition, internal rotation was estimated to have a large end point velocity contribution in throwing and racquet sports. Proximal internal rotation was found to have a contribution of between 46-54% of racquet head speed in tennis, while distal segment internal rotation contributed between 5-12%.

Marshall has shown that P-D sequencing may not be an optimal solution for movement occurring outside of the principal motion plane. The golf swing is a complex,

3D movement that occurs on multiple planes of motion. It is possible that out of plane motions have an effect on overall CHS. Therefore, in addition to angular velocity of golf segments, it would be worthwhile to explore measurements of motion that take out of plane movements into account.

2.2 Joint vs. Segment Energetics

Winter (1987) said that transfer of energy flow in human movement can be analyzed either by a "*segment by segment"* or "*joint by joint"* framework. In joint energetics, mechanical power is calculated using resultant loads at segment end points. Winter set forth the following equations describing joint power calculations. Equation 2.2.1 describes the power at a joint for a given muscle moment M; where ω_j describes the angular velocity of a given segment. In addition to muscular energy, Winter noted that power can enter a joint "*passively"* through reaction forces at segment endpoints. Equation 2.2.2 describes power derived from resultant joint forces; where $\boldsymbol{v}$ is a vector describing the velocity vector of the joint center. Joint power calculations can indicate joint energy generation or absorption; depending on whether the power sign is positive or negative respectively.

$$P_m = \vec{M} \bullet (\vec{\omega}_2 - \vec{\omega}_1) \qquad 2.2.1$$

$$P_{JF} = \vec{F} \circ \vec{v} \qquad 2.2.2$$

These equations describe *sources* of segmental energy, either due to muscle moments or joint contact forces. Their direction implies whether a segment absorbs, or generates energy. Segment energetics on the other hand, are a direct measurement of the quantity of energy a segment *contains*. Stefanyshyn (1996) has described the following equations concerning segmental energy. In equation 2.2.3, a segment's total energy E_T is the sum of its potential E_P, translational kinetic $KE_{\text{translational}}$ and rotational kinetic $KE_{\text{rotational}}$ energies. E_P is found by multiplying a segment's mass by the acceleration of gravity and the height of its center of mass (eq. 2.2.4). Translational kinetic energy is found by multiplying half of a segment's mass by the square of the absolute speed of its CG (eq. 2.2.5). Rotational kinetic energy is described in equation 2.2.6 where matrix $\boldsymbol{I}$ is a segment's inertial tensor and vector $\boldsymbol{\omega}$ is the angular velocity.

$$E_T = E_P + KE_{\text{translational}} + KE_{\text{rotational}} \qquad 2.2.3$$

$$E_P = m \cdot g \cdot h \qquad 2.2.4$$

$$KE_{\text{translational}} = \frac{1}{2} m \cdot \left|\vec{v}\right|^2 \qquad 2.2.5$$

$$KE_{\text{rotational}} = \frac{1}{2} \bar{I} \cdot \vec{\omega}^2 \qquad 2.2.6$$

In studying segments and joints, which framework is utilized is dependent on the question being answered. A joint energetics framework is useful to determine if power is created from muscular work or joint contact work. Joint energetics can also be useful to

calculate a direction of energy flow (Winter, 1987). However, if the goal of the study is to obtain direct measurements of the destinations of energy created, then segmental energetics may be a stronger approach.

There are other variables to consider when choosing between a joint or segmental framework. Winter (1987) stated that joint power calculation accuracy depends on a number of assumptions made in the biomechanical model. This method relies on the assumption of spherical joints between segments. It also assumes that the relative position of the center of mass to the segment origin is consistent. Joint power measurements are also dependent on the estimation of muscle moments applied at the joint. In addition, if a muscle were to span two joints, care must be taken when describing *energy flow* between segments. For these reasons, it may be useful to evaluate the energy calculations in a joint framework against that found studying segment energetics.

If joint energies are a measure of the *sources* of mechanical power, then segment energies are a measure of the *destinations* of this power (Stefanyshyn, 1996). To get an idea of the accuracy of power in a given movement; joint energies and resulting segmental energies should reach a balance. Winter (1987) stated that measurements of joint energetics and segmental energetics have balanced in studies of walking and running. Such a comparison has yet to be made in the golf swing. The joint energy models of Nesbit and Serrano (2005), Sprigings and Neal (2000) and Sprigings and Mackenzie (2002) have all used simulations to determine the profiles of joint torques and joint forces. These profiles come from forward dynamic simulations that are optimized to mimic the kinematics of real swings. These joint power calculations have yet to be compared to segmental energy profiles to estimate the accuracy of their findings.

2.3 Kinetic Energy in Cracking Whips

In an article entitled *Whip Waves*, McMillen and Goriely (2003) explored the mechanics of cracking whips. The authors modelled a leather bullwhip as an elastic rod of decreasing mass and cross-sectional area. One cracks a whip by throwing the handle and creating a forward moving loop known as a buckling discontinuity (see Figure 2.3.1). The loop moves through the whip as a wave. Energy and momentum are conserved after the initial handle throw. Speed increases as the wave moves through whip elements of decreasing mass and decreasing radius. By the time the wave reaches the end of the whip, the tailpiece has undergone an acceleration of up to 50,000 times that of gravity. Krehl *et al* (1998) developed a sophisticated motion capture system to film the end velocity of the distal whip tip. Those authors found that the speed generated in the whip was nearly 2.2 times the speed of sound. McMillen and Goriely (2003) contend that the air pushed at the front of the whip creates a supersonic wave that sounds like a large *crack*.

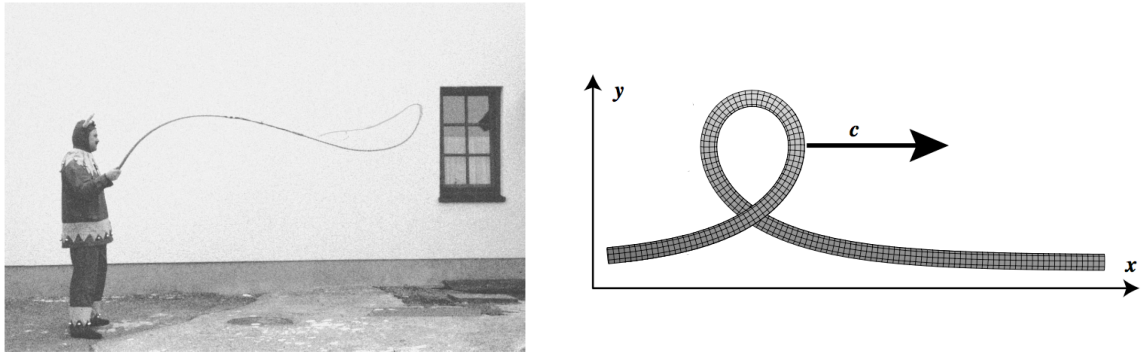

a) b)

Figure 2.3.1: a) Blackforest whip cracker at Shrovetide (from Krehl *et al,* 1998). The photo was taken just prior to cracking. Notice the forward moving loop near the end of the whip. b) 2D whip wave model from McMillen and Goriely (2003). The wave is moving through the whip with forward velocity *c*.

In modelling whip motion as a wave, McMillen and Goriely (2003) found that energy flow in the whip is dependent upon the mass and radius of its elements. If the whip elements became larger along the direction of the wave flow, the wave would slow down and its energy would be stored as potential energy. The wave model slowly reversed and flowed back in the direction of smaller elements.

Whip cracking can be compared to various types of human motion. The elements of a whip, like that of the body, decrease in mass and rotational inertia distally along the system length. Movement is initiated at the proximal root, and the speed created at the distal end is dependent on the efficiency of energy transfer along its elements. However, energy and angular momentum are not conserved in a system of human links. Muscles acting across joints are able to create additional work on distal segments. The question remains: If humans are able to create additional work along our musculo-skeletal chains while the leather whip is limited to the initial throw energy, why do we not achieve movements approaching the speed of sound? The following section will address high-speed motion and efficient energy transfer in musculo-skeletal chains.

2.3.1 Musculo-skeletal Whip Cracking

Researchers at the Royal Tyrrell Museum have studied whether it was possible for certain species of dinosaurs to create sonic booms with their tails (Myhrvold and Currie, 1997). Those authors examined the tail vertebrae of a Sauropod species called *Apatosaurus.* They found that the tail vertebrae were of sufficient number, length, and decreasing inertia to have behaved like a bullwhip. Furthermore, CAT scan studies of the distal vertebrae showed signs of diffuse idiopathic skeletal hyperostosis (ie. bone scars) that the

authors believe stem from using the tail as a noise generator. In a simulated reconstruction of the *Apatosaurus* tail whip, the authors reported that the distal end was able to reach a whipping speed of 540 m/s, roughly 1.5 times the speed of sound. For this species it would have been possible to create supersonic shock waves by wagging its tail. Apparently efficient transfers of kinetic energy may be possible in musculo-skeletal chains.

Whip-like motion is of interest in human movement because of the creation of high speed with a high level of efficiency. However, our bodies do not have the number of segments or the sheer length found in the tail of an *Apatosaurus*. Is it then possible for human movement to resemble that of a whip?

Joris *et al* (1985) studied the motion of body segments in female handball throwers. Those authors noted that the upper arm throw consists of a whip-like, sequential movement of 6 body segments. For the group of athletes studied, the fastest throws came from players whose distal segments peaked in velocity following the proximal segments in a sequential pattern. Interestingly, the segment velocities decreased substantially after peaking. The decrease in a proximal segment velocity occurred simultaneously with large increases in distal segment velocities. In this way, the transfer of energy in human segments during handball throwing resembles that of a whip. It has yet to be determined if this whip-like transfer of kinetic energy is visible in the golf swing.

2.4 Golf Biomechanics

The application of biomechanics in the sport of golf emerged in the mid 1960's when the Spalding Brothers of Byron, Illinois took a series of stroboscopic photographs of a golf swing. Since then, the focus of this field has been in performance improvement or injury reduction by means of furthering the understanding of the mechanics of golf movement. The focus of this review will be on golf biomechanics research that has contributed to performance improvement, specifically the understanding of speed generation in the swing. Table 2.4.1 is an abbreviated list of selected articles in golf biomechanics literature, and their role in developing an understanding of the generation of speed. The relative contribution of these articles will be explained in further detail in the following sections.

Table 2.4.1: Timeline of selected Golf Biomechanics articles and their contribution to the understanding of speed creation in the golf swing.

Year	Author(s)	Contribution
1967	Williams	• Stroboscopic motion analysis; first to propose delay of wrist un-cocking; proposed relative timing more important than muscle torque.
1968	Cochrane and Stobbs	• Search for the perfect swing; Lagrangian double pendulum swing model; proposed maximal shoulder torques & free hinge timing of wrist un-cocking for optimal speed.
1970	Jorgensen	• First mathematical proofs that delay of wrist un-cocking is important in speed creation.
1974	Cooper *et al*	• Qualitative full body kinematics + force plate data; concluded segments follow P-D sequencing; quantified golfer interaction with ground.

1977	Pyne	• Showed that angular velocity of the hands is not constant during the downswing;
1979	Budney and Bellows	• Used double pendulum to study effect of club parameters; found performance enhancement with decreased shaft weight.
1981	Vaughn	• 3D kinematics and kinetics from motion analysis, inverse dynamics; resultant force on grip along shaft of club towards golfer; late slowing of hands increased CHS.
1982	Milburn	• 2D kinematics from motion analysis; 'centrifugal force' responsible for wrist un-cocking; positive acceleration of club came at expense of deceleration of arm.
1985	Neal and Wilson	• 3D kinematics and kinetics from motion analysis; found shoulder joint loads were greater and acted earlier than loads at wrist.
1994	McLaughlin and Wilson	• 3D angular position of segments from motion analysis; used Principal Component Analysis to find that delay of wrist onset important for CHS.
1994	McTeigue	• 3D hip and torso kinematics; large subject group of professional players; quantified '*X-factor*'.
1998	Burden *et al*	• 3D kinematics from motion analysis; results supported P-D sequencing in full body movement.
1999	Pickering and Vickers	• Ran speed optimizations of 2D double pendulum model; found wrist delay and forward ball positioning to improve performance.
2000	Sprigings and Neal	• Three segment simulation model; found greater realism in simulated shoulder torques; linked wrist delay with torso rotation.
2002	Sprigings and Mackenzie	• Three segment simulation model, calculated joint powers; found P-D sequencing of joint power generation.
2005	Coleman and Rankin	• 3D kinematics from motion analysis; reasoned that downswing motion from multiple segments does not fit well into single plane.

2005 Nesbit	• 3D, full body kinematics and kinetics from multi model simulation; found that most work done on club by pulling force exerted on grip by arms segment.
2005 Nesbit and Serrano	• 3D, full body kinematics and kinetics from multi model simulation; calculated full body joint power contribution towards CHS; wrist torques found to be relatively unimportant.

2.4.1 2D Golf Models

One of the first scientific papers dealing with motion analysis in the golf swing was a 1967 study by Williams called *Dynamics of the Golf Swing – with Conclusions of Practical Interest.* In it, Williams took hand and club kinematics measurements from a Spalding Brothers' stroboscopic photograph of touring professional Bobby Jones. Figure 2.4.1 is a copy of the image used.

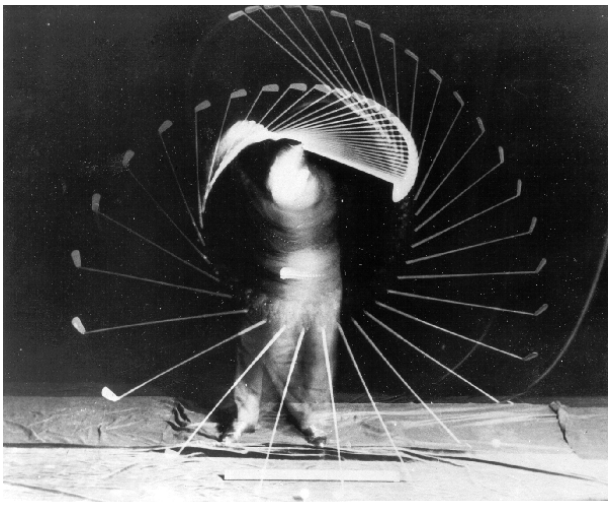

Figure 2.4.1: 100 Hz stroboscopic photograph of Bobby Jones hitting a 2 iron. Adapted from Bunn (1972).

Williams made many assumptions in this early study that have since been disproven. For example, he assumed that the clubs and hands travel in the same plane. He also assumed that the hands travel about a fixed rotation point (i.e. the leading shoulder);

and that angular velocity of the hands stay constant throughout the second half of the downswing. Aside from these postulations, Williams made some insightful conclusions that are still valid in golf science today. For instance, he was the first researcher to propose that delaying un-cocking of the wrists could account for a large increase in CHS. He also reasoned that relative timing between segments, or swing tempo, would be more important than muscular torque in creating a long hit. Because of errors Williams made in his initial assumptions, mathematical and logical proof of these later assertions would have to wait nearly thirty years.

In recent reviews of the current state of golf biomechanics, papers by Farrally *et al* (2003) and Hume *et al* (2005) noted that new studies have not significantly improved on the 2D double pendulum golf swing model proposed by Cochran and Stobbs (1968) in their book entitled: *A Search for the Perfect Swing*. This Langrangian pendulum model put forth in *Perfect Swing* is still revered in review articles today; and for good reason (apart from A.J. Cochran being a co-author of Farrally's review). The double pendulum model can allow for a breadth of complex, inter-dependent solutions that closely mimic real life golf motion. In general, golf swing modeling has since been a collection of tweaks and modifications on this ground breaking work. An illustration of the double pendulum is shown in Figure 2.4.2. The proximal segment represents the motion of the lead arm; while the distal segment represents the motion of the club shaft.

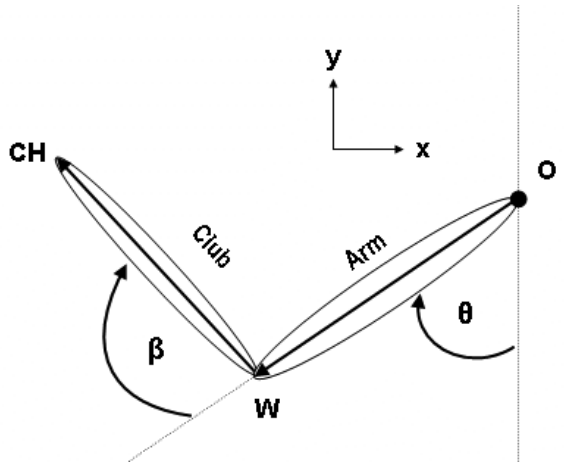

Figure 2.4.2: The golf swing as a double pendulum. Adapted from Jorgensen (1999). *θ* and *β* represent shoulder and wrist angles respectively. Points *CH*, *W,* and *O* represent the positions of the club head, wrist and the system origin respectively.

Early calculations by Cochran and Stobbs (1968) lead them to two general conclusions about optimizing swing speed. First, they found that the arm segment should be '*driven strongly*'. This was interpreted to mean that the external muscle torque operating at the shoulder joint should be maximized. Secondly, they stated that the load applied to the club should happen only "*at the stage of the action when it is trying to fly outwards at its own accord*". This was interpreted to mean that the external muscle torque operating at the wrist should onset correspondingly with the outward, centripetal acceleration of the club shaft. No mention is made as to the direction, magnitude, or profile of this wrist impulse.

Perhaps it was a delay on a journal editor's desk that cost Ted Jorgensen some acclaim in the hallowed history of golf biomechanics. His 1970 paper called *Dynamics of the Golf Swing* was actually submitted in the same year *Perfect Swing* was published. In it, Jorgensen belatedly introduced a 2D double pendulum model of the golf swing. Like the work of Cochrane and Stobbs, his calculations lead him to conclude that maximizing

shoulder torque could improve CHS. But unlike the work in *Perfect Swing,* Jorgensen found that delaying the opening of the wrist beyond the timing of a free hinge opening would lead to a great increase in CHS. Jorgensen was the first author to show mathematical proof that the *active* delay of wrist un-cocking (beyond the timing of a "*natural*", free-hinge release) could improve speed generation in golf. This finding was later repeated by many other authors.

Pyne (1977) expanded on the standard pendulum model by attempting to quantify the effectiveness of the "*wrist snap"*. In the practice of Williams and Cochran and Stobbs, Pyne separated the downswing into two general stages: pre and post wrist un-cocking. Pyne attempted to quantify wrist snap efficiency by creating what he called a "*club head speed coefficient*". This was a ratio of absolute end point velocity comparing CHS just before wrist un-cocking to CHS at impact. Pyne concluded that "*injection speed"* (i.e. wrist contribution) could be improved by adding mass to the arm segment, or by optimizing club length. In addition, Pyne was the first author to show that William's assumption of constant hand angular velocity in the second phase of the down swing was incorrect. He noted that Jimmy Thompson (a "*prodigious hitter"* in his day) was observed to "*stop*" his hands before ball contact.

Milburn (1982) looked at the transfer of speed between a golfer's segments. He studied 2D motion of the lead arm and club segment and noticed a pattern of positive angular acceleration of the club at the expense of angular deceleration of the arm. This finding was in direct support of a P-D sequencing pattern in golf. Milburn stated that this phenomenon was indicative of a free-hinge system. In addition, he felt that the impetus of wrist un-cocking was a "*centrifugal"* or virtual inertial force that was acting on the

double pendulum system. This *force* tended to pull the club head outwards; and straighten out the arm and club links at the wrist joint. Like earlier researchers, Milburn came to the conclusion that if the golfer were to initially delay the onset of the wrist un-cocking, he would be more likely to attain maximum segmental angular velocities.

Budney and Bellow (1979), engineering researchers from the University of Alberta, were the first group to examine changes in club parameters on the double pendulum golf model. The authors are one of few groups to report that delayed wrist snap did not appreciably contribute to CHS. Of note, they were the first group to prove that decreasing club shaft weight could improve energy efficiency for a given swing speed.

Pickering and Vickers (1999) looked at joint energetics in the double pendulum model. They found that it was possible for a golfer to have a successful swing without applying an impulse at the wrist. They deemed that this "*natural release"* was, understandably, the most efficient swing type in lowering muscular energy supplied. Further optimizations were run to determine the timing of wrist release and relative ball position that would allow for greatest impact velocity. It was found that a delayed wrist release coupled with a ball positioning closer towards the lead foot resulted in maximum CHS.

In summary, scientific work in golf using the double pendulum swing model has afforded a basic advancement in the understanding of this complex human motion. The preceding articles have shown that the double pendulum itself can be modeled with a variety of segment parameters and joint load profiles that are able to create realistic golf motion. Understandably, work using a two link model has focused primarily on the joint that connects the segments in enquiry; the wrist. The consensus of this work has shown

that a delay in opening of the wrist joint improves golf performance by generating increased CHS. It is interesting to note that the late onset of wrist un-cocking in golf corresponds to Bunn's original observation of delaying knee extension in maximal ball kicking. It seems that the double pendulum golf model agrees with the optimal motion pattern existing for other sports.

For the two body segments studied in the double pendulum model, a P-D sequencing of motion seems to be ideal for optimal speed generation. It is still unclear however, if the same holds for a real golf swing; a complex motion involving multiple human body segments and an external implement; moving in three dimensions.

2.4.2 3D Golf Models

Insight into 3D kinematics and kinetics in golf first appeared in the work of Vaughan (1981). In his investigation, club markers were filmed with two orthogonal high-speed film cameras. Resultant forces and torques applied at the hands were calculated from club kinematics using a Newtonian-Euler approach. Vaughan noted that Budney and Bellow (1979) predicted that the wrist should undergo a positive torque throughout the downswing. This torque would be positive about an axis pointing up from the club shaft plane, and would tend to rotate the club towards the target. Vaughan's results suggested that this torque was negative for the first half of the downswing; which tended to keep the wrists cocked. The external wrist torque then became positive at wrist un-cocking, and remained positive for the remainder of the downswing. Vaughan cautioned that the external wrist torque should not be confused with the wrist muscle torque since the club grip is in contact with both hands. Two contact points on the grip would therefore

represent a distributed load. According to Vaughan: "*it should be recognized that this normal torque cannot be considered as a valid measure of the … un-cocking action of the wrists.*" This could be a relevant source of error when modeling the wrist as a spherical joint.

In addition to resultant joint moments, Vaughan also examined resultant joint forces. He found that the largest component of the grip force at ball impact was applied along the shaft, pulling towards the golfer. He also found that the positive wrist torque was initiated by applying a force at the hands in the opposing direction of the clubface. Of note, Vaughan observed that a late slowing of the hands before impact coincided with a large increase in CHS.

Neal and Wilson (1985) repeated the work done on 3D club loading by Vaughan. A major difference with their paper was that their results were presented in a global reference frame instead of in a local frame fixed to the club. Their torque results supported the findings of Vaughan. The timing of wrist un-cocking coincided with a change from negative to positive wrist torque about the golfer's frontal axis. The authors also presented results on the resultant joint force acting on the shoulder. When comparing resultant joint loads, peak forces acting on the shoulder joint were of greater magnitude, and occurred earlier in the downswing, than those forces acting at the wrist joint.

McLaughlin *et al* (1994) measured a variety of 3D golf "*kinematic parameters"*; actually body segment angular positions at key time points during the swing. The group performed a linear regression and later a principal component analysis on the data to find which parameters had the highest correlation with CHS. Not surprisingly, they found that delayed wrist onset was important in speed generation.

Coleman and Rankin (2005) investigated the applicability of 2D multi-segment models in representing 3D motion. They measured 3D kinematics of the left shoulder girdle, left arm and club shaft during the downswing. They found that the motions of these segments did not all lie along the same plane. Coleman and Rankin concluded that 2D models do no realistically represent multi-segment movements in a golf swing, which they found not to occur in a single plane. No mention was made as to whether the movement of individual segments could be reliably fit with separate planes.

In summary, these papers exploring 3D motion in golf have contributed to the overall understanding of the swing. Vaughn (1981) was the first author to use inverse dynamics based on optical motion analysis in golf. Neal and Wilson (1985) used a similar method to show that loading in the shoulder preceded loading in the wrist in the downswing, in a P-D manner. These two motion analysis studies have laid a foundation in the understanding of joint loading in the swing. The work by McLaughlin *et al* (1994) and Coleman and Rankin (2005) have repeated the finding of wrist delay and noted that a single 2D plane cannot effectively represent the motion of a golf swing. However, an optimal motion pattern still remains to be determined in golf for 3D full body movement.

2.4.3 Adding the Spine and Hips

In a golf study by Cooper *et al* (1974), P-D sequencing of motion onset was observed qualitatively starting with knee joint movement and transferring superiorly and distally to the hip, spine, shoulder, then wrist. This investigation looked at force plate data under each foot during the swing. The authors referred to free moments about the vertical axes of the force plates as "*rotational forces"*. When viewing a right-handed golfer from

above, these rotational ground reaction *forces* were clockwise at the top of the downswing. They quickly switched to become counter clockwise just prior to ball contact. Although not discussed, their graphs indicated that this phenomenon increased in magnitude and tended to occur later in the swing as the golfer shifted from smaller irons to a driver. This work supports the idea that a golfer interacts with the ground via his feet when creating a golf swing. From this point of view, a golf swing begins with a kinetic interaction at the ground.

Although Cooper *et al* looked at other body segments using qualitative observation; spine and hip rotations had not been quantified in the literature until later. McTeigue (1994) conducted a study on relative spine to hip rotation using large groups of PGA, senior PGA, and amateur players. Kinematic data were collected using a linkage of gyroscopes and potentiometers. His investigation was designed to look at the so called "*X-factor",* or range of torso rotation relative to the hips. He found that spine flexibility did not differ between professional and amateur players (although it was limited in the senior PGA group). An interesting result of this study was that of the "*hip slide*". McTeigue found that both amateur and professional players underwent a lateral transition of the lead shoulder during the downswing. Professional players accomplished this by shifting their weight from their back to front foot and keeping their torsos vertically aligned. Amateur golfers tended to accomplish the shoulder shift by a lateral bending of the spine.

Burden *et al* (1998) explored hip and torso rotations in the context of the summation of speed principle. They measured 3D kinematics in a group of eight golfers using a two-camera motion capture system. They claim that their results supported a P-D

segment sequence as required by Bunn's principle. However, this group did not investigate segment angular velocity or angular impulse. The summation of speed, as described by Bunn (1972) and Putnam (1993) described the relative timing of either sequential angular velocity peaks, or sequential torque onsets. This theory did not refer to relative angular positions specifically, as was reported in this article. Also, measurements of shoulder and hip angular positions were made by connecting bi-lateral bony landmarks; and projecting the resulting vector on the ground plane. As the motion of these segments likely does not coincide with the plane of the ground, these projections may have lead to erroneous results. However, this group did find that players who timed angular position peaks in a P-D fashion were more likely to generate greater swing speed.

The 2D double pendulum model was modified with the simulation work of Sprigings and Neal (2000). The authors added a third segment to the standard double pendulum model. They chose lengths and inertial properties to correspond with segment parameters of real golfers; and for the first time, based applied torques on the force-length, force-velocity and activation parameters of human muscles. They supported the finding by Pickering and Vickers that it was possible to have ball contact with a free-hinge wrist joint. Sprigings and Neal were the first authors to simulate a torso segment in the kinetic golf model. They stated that torso rotations were very important in recreating realistic swings. They found the magnitude of applied torques at the shoulder joint could be lowered to a much more realistic level if a component of the angular impulse could be derived from inter-segmental interaction. Also, the authors reported that the angular position and velocity of the torso seemed to have a direct effect on delaying wrist action, which ultimately lead to higher club speeds.

Sprigings and Mackenzie released a study in 2002 to follow the work done on the triple segment golf simulation. Here the authors used the same 3 segment model to identify the mechanical sources of power in the golf swing. The authors used a forward dynamics approach to optimize muscle model variables with measured kinematics. The authors calculated the power at each joint due to muscle torques or joint contact forces. By integrating this power, they calculated joint energies and the mechanical sources of this energy. Their results indicated a P-D sequence of total work done. The authors also noted that the onset of muscular power at the wrist joint precedes the onset of applied positive wrist torque. This means that some of the energy gained by the wrists is due to the resistive torque acting to keep the wrists cocked. Sprigings and Mackenzie noted that muscular power increased distal segment energy at the expense of decreasing energy in the proximal segment, although no direct measurements of segment energy were reported.

Sprigings and Mackenzie (2002) had applied a high level of realism in the muscle models used for their simulation. However, they did not account for an onset of muscle torque during the backswing. All muscle load profiles started from zero at the beginning of the downswing. It is quite possible that a golfer's muscles are able to develop force before the initiation of downward movement. This potential error in muscle work done on the segments leads to the question of how the resulting joint energetics compare to direct physical measurements of energy contained in the segments.

Perhaps the most comprehensive look at the inter-relationship between motion and loading in 3D golf swing has been in work done by Nesbit (2005). In subsequent articles from the same journal; Nesbit introduced a 3D full-body, multi model, integrative

motion capture / kinetic analysis system. Nesbit used separate models for the human body, the ground, and the club. Kinematics from video motion capture data were used as input. A full body human segments model came from an ADAMS module called ANDROID (MSC Software Corporation; Santa Ana, CA). It consisted of 15 linked rigid body segments interconnected with spherical joints. The resultant joint torque profiles were optimized to match realistic kinematics as measured by the video capture system.

In the first article, Nesbit stated that the resultant forces acting on the club were applied at the grip by the arm segments; while the resultant moments acting on the club where due to muscular work done at the wrists. He compared angular work done by the wrists to linear work done by the arms. His results indicate that better golfers tend to do more work by using their arms to pull on the golf club; than by applying a torque at the wrists. He reasoned that greater club head speed is created by reducing the radius of the path of the hands just prior to impact.

In the second article by Nesbit and Serrano (2005), the authors calculated work done at each joint in the full body model by using a joint power approach. They then determined the locations of the sources of power in the golf swing. They found that the back and the hip joints generated up to 70% of the total work done in the swing, while 26% of the total work was contributed by the arms (mostly by the right elbow). They concluded that the generation of work, and its transference to the club, is mostly a "*bottom-up phenomenon"*; moving upward and outward. Of note, the authors noted that proximal segments tended to slow down to become "*static support*" for their distal counterparts.

Nesbit and Serrano (2005) found that the majority of the joint work performed was used in moving the proximal segments. Very little of the total work was actually transferred to the club. Of the work done on the club at the wrist joint, a linear force applied by the arms generated the majority. Wrists torques showed a comparatively smaller contribution towards an increase in overall CHS.

Interestingly, Nesbit and Serrano showed that total body joint power tended to switch from positive to negative around the time of impact; but only the scratch golfers were able to zero their power generation *exactly* at impact. This would result in maximization of club speed. If power became negative pre impact, the body would work to slow the club. If power were still positive post impact, it would mean usable work was wasted. It seemed precise timing of total joint power application was indicative of player ability.

In summary of the golf research presented in this section, an inter-relationship between loading and motion had begun to be established in full body 3D golf movement. Part of this work has stemmed from optical motion analysis studies. The work by Cooper *et al* (1974) had shown qualitatively that motion in the golf swing should begin at the ground. McTeigue (1994) showed that the torso has a larger range of motion than the hips; and that a difference exists between amateurs and professionals in how the torso rotates at the end of the downswing. The study by Burden *et al* showed that range of motion, and timing of angular position peaks followed a P-D sequence in successful swings.

The latter research papers presented in this section on 3D, full body golf motion have used simulations of various modelling complexity (Sprigings and Neal, 2000;

Sprigings and MacKenzie, 2002; Nesbit, 2005; Nesbit and Serrano, 2005). These studies have given insight into the sources of mechanical power in the golf swing. In their simulations, these authors have used forward dynamic analysis to optimize musculoskeletal models in recreating known kinematics. While the motion of the models has been matched to that of a realistic golf swing, it is currently unknown if the joint loads created by the models are also correct. Therefore, it would be worthwhile to apply a segmental energetics framework to the golf swing to evaluate simulated sources of mechanical energy with direct measurements of the destinations of that energy,.

Chapter Three: Methods

3.1 Subjects

Data from 500 male, right-handed golfers were used in this study. Individual driver swing trials were taken from each subject. The mean height and weight for the subjects was 1.81 m (0.0697 m STDEV) and 87.12 kg (9.73 kg STDEV), respectively. The subjects were chosen based on having a registered Hc of 5 or less. It was speculated that the motion of skilled golfers would be repeatable; and that their swings would result in a successful golf drive. Informed consent was obtained from all subjects.

3.2 Data Collection

Kinematic data were collected using Motion Analysis Technology by TaylorMade (MATT) systems (TaylorMade-adidas Golf, Carlsbad CA) from 5 different locales; Aviara Golf Acadamy, Carlsbad CA; Fancourt Country Club, George SA; PGA of America, Port St. Lucie, FL; Reynolds Plantation, Greensboro GA; and TaylorMade-adidas Golf, Carlsbad CA. Five different locations were used to increase the size of the subject population and to reflect golf motion from a number of respected teaching academies. The MATT system consists of nine high-speed, infrared cameras that collect the positions of retro-reflective markers at 110 Hz. This position data is then collected on a central PC and converted into 3D golfer motion using MATT software jointly developed by TaylorMade-adidas golf and Motion Reality Inc. (MRI, Marietta, GA). The creation of 3D golfer motion will be discussed in further detail below.

Subject motion was tracked using 28 retro-reflective spherical markers. The markers were placed on anatomical landmarks and fixed to the subjects' clothing, as shown in Figure 3.2.1.

a)  b) 

Figure 3.2.1: Retro-reflective marker placement in: *a)* frontal view; and *b)* lateral view. These pictures have been altered to protect the subject's anonymity.

Position data from the markers were used to scale and update a kinematic golf model designed by MRI. Figure 3.2.2 *a)* shows an animation frame of the MRI kinematic model being scaled to fit a subject's body profile. The MRI golf model uses a generic human avatar for swing animations. That avatar has virtual markers attached at key locations, as shown in Figure 3.2.2 *a)*. The model was adjusted in height and width so that the virtual markers fit the positions of the subject's real markers in a least squares sense.

It was not uncommon that noise in marker position data resulted in deviations of fitted golfer movement. Each swing trial was examined to ensure it was free of unnatural movements. Trials with large single frame deviations of golfer movement were removed from the study. In the end, 447 trials from the original subject set were used in the

analysis. Figure 3.2.2 *b)* shows a frame of animated data from the MRI kinematic model of a successful swing trial.

a) 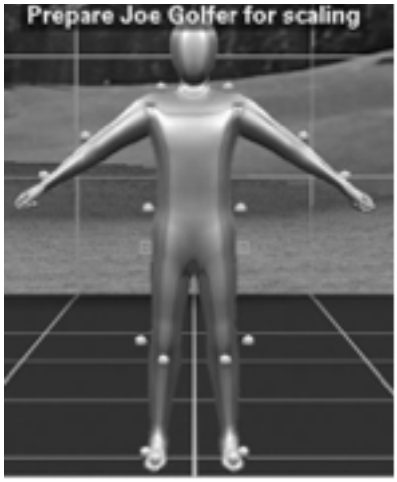

b) 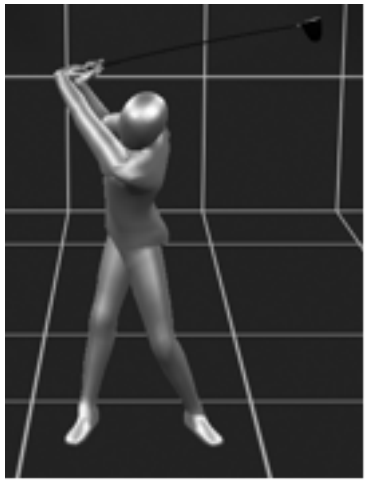

Figure 3.2.2: ***a)*** **Scaling the MRI kinematic model to markers on a subject.** ***b)*** **Animated golf motion from the MRI kinematic golf model.**

3.3 MRI Kinematic Golf Model

Golfer body motion was animated using the MRI kinematic model to give a best-fit approximation of whole body movement to the positions of filmed markers. MRI kinematic modelling is slightly different than classical motion analysis, as outlined by Nigg *et al* (1999). Orientation and position of the subject's rigid bodies are not rigidly defined from the position of any three markers. Instead, the kinematic model uses some constraints specific to the golf swing in order to use a decreased marker set. For example, both hands of the golfer are constrained to attach to the grip of the golf club throughout the swing. Also, the golfer is constrained to have his entire body face the ball at the address position. By using this information, the MRI model is able to use a best-fit approximation of the recorded maker positions to the expected marker positions of a generic golf swing. In doing so, the MATT golf analysis system is able to substantially

decrease the number of markers used and decrease the reliance on the repeatability of marker placement.

Figure 3.3.1 illustrates the conceptual difference between classical motion analysis and the MATT kinematic model. In this drawing, rigid body motion is represented by a dark coloured ellipse. The small grey circles represent retro-reflective marker placements. In classical motion analysis, a rigid body is anchored to a set of tracked markers. This set can be no less than three for tracking 3D movement (Cappozzo *et al*, 1996). In comparison, motion of a rigid body in the MRI kinematic model is not rigidly fixed to the tracked markers. The relative contribution of a marker's position on the motion of a rigid body is determined by a weighting function for that marker. This can be conceptualized as tracking a rigid body by markers on springs. The 'stiffness' of the springs coincides with the weighting attributed to the markers. Reliable marker placements, like welded club attachments, receive a higher marker weighting. Markers attached by relatively loose fitting clothing on top of moving soft tissue (such as the player's back) would receive lower marker weighting. As a result, the motion created by the MRI kinematic model is a generic kinematic chain that has been altered to fit the motion of tracked markers in a least-squares sense. The most reliable marker positions (ie welded markers), are given preference in this optimization.

Classical 3D Motion Analysis **MATT Kinematic Model**

Figure 3.3.1: A conceptual comparison of classical motion analysis with the MRI kinematic golf model.

Although the MRI kinematic model differs substantially from the classical method, it shares some commonalities with other motion analysis models in current literature. In 1993, Soderkvist and Wedin published an article that outlines a biomechanics analysis method dealing with marker noise reduction. This method is known as singular value decomposition (SVD). In essence, rigid body motion is defined by a least squares approximation to recorded marker positions. The use of this SVD step is widely accepted in current motion analysis research. The calculation method used in the MRI kinematic model also employs a least squares analysis. This step should be seen as a continuation of the smoothing method introduced by Soderkvist and Wedin. In addition, commonly used motion models including the Conventional Gait Model and the Cleveland Clinic Gait Model (Baker, 2006) use generalized gait assumptions to constrain systems of equations and decrease their marker sets. Gait models of this nature are widely used in biomechanical analysis today (Baker, 2006). The MRI kinematic golf model is

not unlike these types of gait models in the analysis steps taken to decrease marker sets. The use of this model falls within accepted practices of current biomechanical analysis. The kinematic data obtained from the MRI golf model include position and orientation for all of the golfer's tracked rigid bodies.

3.4 Data Filtering

Kinematic data were filtered using a fourth order Wavelet Low Pass filter (von Tscharner, 2002). Filtering was necessary to decrease noise in the rigid body transform data. It is speculated that a Wavelet filter is not prone to aliasing errors found in using many filter shapes such as a Butterworth. The Wavelet filter uses wavelet decay in the frequency space filter shape. This shape allows a smoother separation between frequencies neighbouring a cut-off threshold. The cut off frequency was chosen to remove high frequency noise data as signal content diminished using a power spectral density analysis (Wood, 1992).

3.5 Golfer Segments

The kinematic golf model was split into four segments to explore the possibility of proximal to distal peak energy sequencing. Each of the segments contained a number of rigid bodies. The Hips segment contained the feet, lower legs, thighs and the pelvis. The Torso segment included seven independent sections of the thorax, two sections of the neck, and the head. The Arms segment consisted of the shoulders, arms, hands, and fingers. The club segment consisted of a grip, 8 shaft sections, and the club head. Calculation of the mass and moments of inertia of these rigid club bodies were measured

directly previously. Calculation of the mass and moment of inertia of the player's body segments will be discussed in section 3.7.1.

3.6 Swing Plane Kinematics Calculations

In order to analyze angular kinematics of the golf swing, a plane of movement was needed to project the motion of complex, 3D joint rotations into 2 dimensions. The work of Coleman and Rankin (2005) showed that the motion of the shoulder girdle, lead arm and club could not be reliably fit into a single plane. It was speculated, that the rotations of these body segments needed to be defined by individually fit swing planes.

Separate planes of motion were found for the club, the arms, the torso, and the hips during the downswing of a golf drive. For the club and arms segments, a least squares regression was used to fit sequential end point positions into a plane. For the torso and hips segments, a helical axes method was used to find a primary axis of rotation that was normal to the movement plane. The latter method was used to find torso and hips planes as the former method seemed to be more sensitive to noise for these segments. It is speculated that slower rotation speeds and the non-rigid behaviour of the hips and torso segments made them especially susceptible to noise in this respect.

Once movement planes were defined for each of the four segments, angular kinematics were found within each plane. Angular position, angular velocity, and angular acceleration were found by tracking the motion of each segment with respect to their individual movement plane. The following sections discuss the calculation of individual segment motion planes in further detail.

3.6.1 Club Swing Plane

A swing plane was found to fit the movement of the club segment during the downswing. Initially, a 3D position vector was calculated for the club head at each sampled time point during the downswing. Figure 3.6.1 shows the positions of the club head during a single trial. All sampled positions during the downswing are marked with an *X*. Because the club is moving slower during the beginning of the downswing, there are many more sampled position points at the top of the swing. In order to avoid biasing the plane orientation on points from the top of the swing, a mean point gapping method was employed. The mean distance between neighbouring points was found for a swing. Any two neighbouring points that had a distance equal or greater to the mean point gap distance were included in the plane regression calculation. In Figure 3.6.1, all included points are marked with a circle.

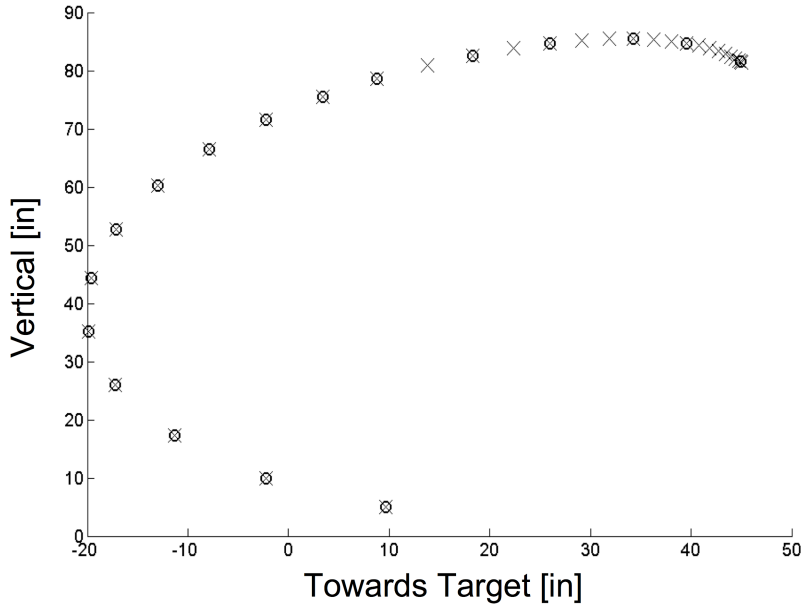

Figure 3.6.1: Positions of the club head during the down swing for a single trial. All sampled

positions are marked with an *X*. Circled positions show points used in swing plane regressions. Vertical direction is positive up. The horizontal direction is positive towards the target.

To calculate the orientation of the club swing plane, a least squares regression method was used. The equation for a general plane is given in eq. 3.6.1 (Kwon, 1998).

$$z = c_1 \cdot x + c_2 \cdot y + c_3 \qquad 3.6.1$$

This can be rearranged in matrix form in order to solve for the plane constants (see eq. 3.6.2). In this equation, $\boldsymbol{C}$ is a vector containing the three constants from the plane equation. $\boldsymbol{X}$ is a matrix containing the x and y coordinates of the selected points in addition to a column of ones. $\boldsymbol{Z}$ is a vector containing the z coordinates of the selected points. Gaussian Elimination was used to solve for the regression constants in $\boldsymbol{C}$ (Hoffman, 2001).

$$\hat{X} \cdot \vec{C} = \vec{Z} \qquad 3.6.2$$

Figure 3.6.2 shows the orientation of the club head plane in relation to the club head positions used for a single trial. Note that this solution method can become unstable if the vector normal to the plane becomes closely aligned with any of the 3 orthogonal lab axes. This did not occur for the hands or club planes found during this investigation.

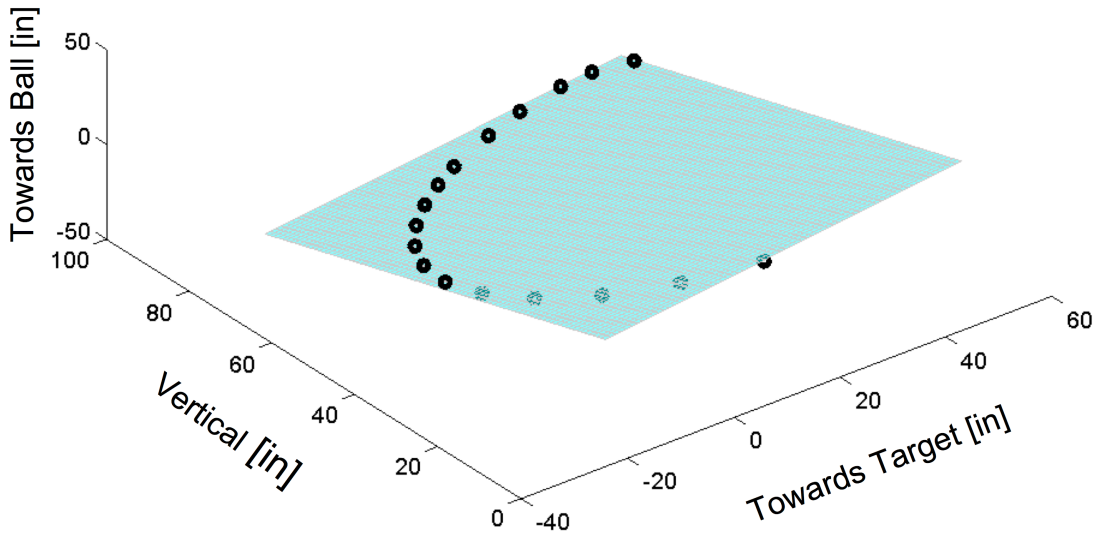

Figure 3.6.2: Relative orientation of the club plane in the global reference frame during downswing for a single trial. Club head positions used for the calculation are depicted by black circles.

Once the best-fit orientation of the club swing plane was calculated, the angular position of the club shaft along this plane could be examined. The club shaft was taken to be a vector that connected the grip of the club to the hosel; i.e. the distal end of the club shaft. The shaft vector was projected onto the surface of the club plane using the plane matrix projection method described by Kwon (1998). The plane was then rotated into a 2D coordinate space so that the projected vector angular position could be calculated. Figure 3.6.3 shows the resulting angular position calculation for a single golf drive trial.

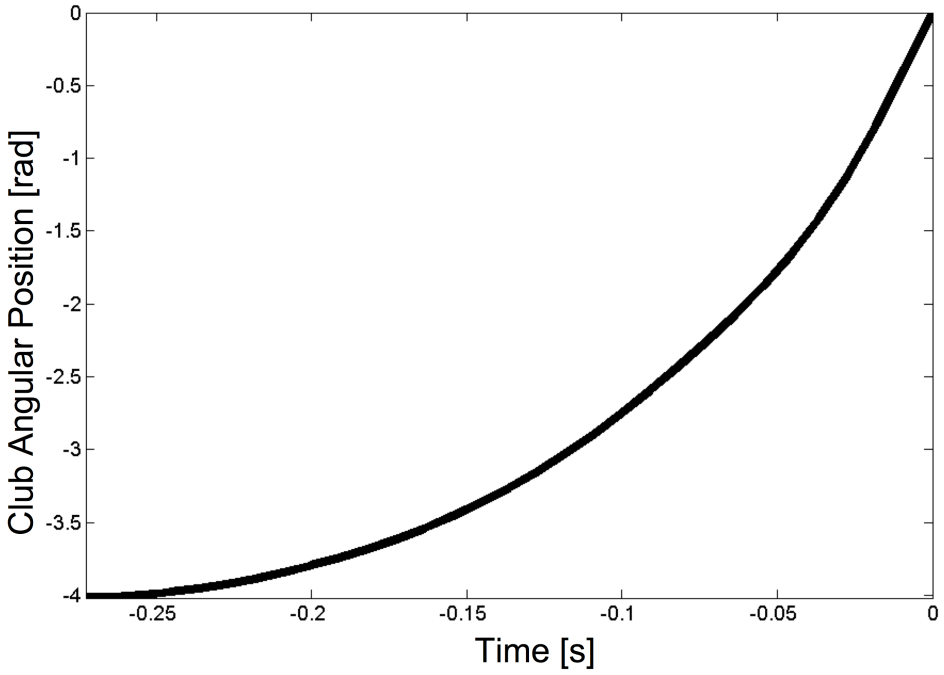

Figure 3.6.3: Angular position [rad] of the club shaft during the downswing for a single trial. Ball impact occurs at time = 0 sec.

To calculate derivatives of angular position of the club segment in the swing plane, club angular position data were first filtered using a Wavelet Low Pass filter (von Tscharner, 2002). The cut off frequency was chosen to remove high frequency noise data as signal content diminished using a power spectral density analysis (Wood, 1992). Once angular position data were filtered, first and second derivatives were calculated using a 2^{nd} order finite difference method (Hoffman, 2001).

3.6.2 Arms Swing Plane

The arms segment swing plane was fit to the downswing motion of the left arm. Arm swing plane kinematics were calculated using the same approach outlined for the club. A virtual marker was created to be the distal point of the arms segment. This point was the

midpoint between the two hand rigid bodies as projected along the grip vector. The positions of this mid-hands point used in the plane regression were chosen using a mean gap method so as not to bias the arm plane calculation on the beginning of the downswing. The arm swing plane was calculated using a least-squares approach as outlined above. A vector connecting the left shoulder to the mid-hands virtual marker was projected onto the arms swing plane. The angular position of the arm direction vector was measured in relation to the arms swing plane. Angular velocity and angular acceleration of the arms segment was calculated using the methodology described above for the club.

3.6.3 Torso Swing Plane

The orientation of the torso segment swing plane was based on the rotation of the shoulder girdle. The methodology outlined above did not seem to provide a stable solution when applied to shoulder girdle or pelvis rotation. These segments have a smaller range of motion, lower angular velocity, and smaller radius of gyration than the club or arms segments. In order to define planes describing the average rotation path for these segments, a modified instantaneous helical axes (IHA) approach was used.

To find the plane of the shoulder girdle, virtual markers were created that were fixed to the kinematic model. Markers were created to approximate the model's sternum, C7 vertebrae, and external scapular angles. Movement of these markers were measured during the downswing. Relative marker motion between successive frame recordings was used to create a 3x3 rotation matrix describing the orientation of the shoulder girdle segment as a quasi-rigid entity. This is a least-squares methodology that utilizes the

singular value decomposition (SVD) method as outlined by Soderkvist and Wedin (1993).

Equation3.7.9 defines local angular velocity as found from the rotation matrix (Berme *et al*, 1990). Local angular velocity was then rotated into global coordinates. Torso global angular velocity was a 3D vector describing a primary axes about which the shoulder girdle turned relative to the lab.

$$\omega_i^{\angle} = \frac{d\overline{R_i}}{dt}\overline{R_i^t} \qquad 3.6.3$$

A unit vector was found with the direction of the mean torso segment angular velocity vector during the downswing. This direction vector was used as the normal vector describing the orientation of the torso segment swing plane. A line connecting the spine virtual marker with the left shoulder marker was projected onto this plane. The 2D orientation of this line in relation to the shoulder plane was calculated to determine angular position of the torso segment during the swing. First and second derivatives of torso angular position were calculated using the methodology outlined for the arm and club segments. Figure 3.6.4 illustrates the shoulder girdle with relative approximations of marker placements.

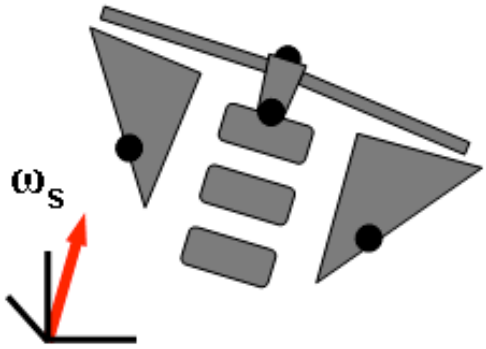

Figure 3.6.4: Skeletal shoulder girdle illustration with approximated relative marker positions. 3D torso segment angular velocity vector ω_s was used as the directional vector for the torso plane norm.

3.6.4 Hips Swing Plane

The orientation of the hips was based on the average rotation of the pelvis during the downswing. The hip segment swing plane was calculated using the same helical method used for the shoulder girdle. Virtual markers were attached to the sacrum and left and right hips of the kinematic model. Rotation matrices were calculated between frames from the positions of these markers using the SVD method described above. Rotation matrices were used to calculate the local angular velocity vectors using equation 3.6.3. Rotating local angular velocity into the global coordinate system then gave the direction of the normal vector describing the orientation of the mean hip swing plane. A direction vector connecting the spine and the left hip was projected onto this plane and its relative angular position was calculated. First and second time derivatives were calculated from the angular position data using the methodology outlined above.

3.6.5 Swing Plane Statistics

Timing and magnitude of peaks were compared for angular position, angular velocity, and angular acceleration of the segment swing plane data. Inter segment differences in these timings and peaks were compared using paired t-tests. An α level of 0.05 was used to indicate statistical significance.

3.7 Kinetic Energy Calculations

3.7.1 Rigid Body Mass and Inertial Properties

Truncated cones and ellipsoids were the generic geometric shapes fitted to the golf model geometries, to allow for estimations of human mass distribution. These shapes were modeled to be homogenous, and of known volume and inertial properties. An example of the geometric shapes applied to model the human golfer can be seen in Figure 3.7.1. The shapes were given a density of 1.03×10^3 kg/m^3, as reported to be the mean density of the human body, by Clauser, McConville and Young (1969).

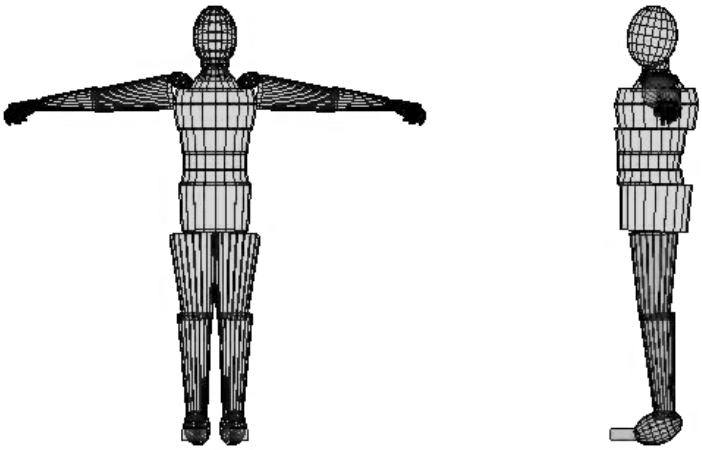

Figure 3.7.1: Example of the rigid body geometries applied to the kinematic golf model.

3.7.1.1 Validating Calculated Body Mass

The self-reported body masses (BM) of a subset of 21 subjects were used to evaluate the calculated BM. The self-reported mass was on average 2.1% lower than the mass calculated by the model with a standard deviation of 8.2% body mass. In order to ensure that our calculated mass was not statistically different from our reported whole body mass, a student t-test was employed to test if the difference found was significantly different than zero. A p-value of 0.8819 showed that the differences between the measured and modeled body masses were not significantly different.

3.7.2 Kinetic Energy Equations

The total KE for each segment was calculated as the sum of the rotational and translational kinetic energies of those segments (eq. 3.7.1). The translational KE was found about the center of mass of each segment as a whole (eq. 3.7.2). The mass of the segment was found as the sum of masses of the rigid bodies comprising the segment (eq. 3.7.3). The velocity of the segment center of mass was calculated as the first time derivative of the segment centroid position vector (eq. 3.7.4). The segment center of mass position vector was a mass normalized sum of all positions of all the segment's rigid bodies (eq. 3.7.5, see Figure 3.7.2a).

$$KE_{\text{total}} = KE_{\text{translational}} + KE_{\text{rotational}} \qquad 3.7.1$$

$$KE_{\text{translational}} = \frac{1}{2} m_{cm} \vec{V}_{cm}^{\,2} \qquad 3.7.2$$

$$m_{\text{segment}} = \sum_{i=1}^{n} m_i \qquad 3.7.3$$

$$\vec{V}_{cm} = \frac{d\vec{S}_{cm}}{dt} \qquad 3.7.4$$

$$\vec{S}_{cm} = \frac{\sum_{i=1}^{n} m_i \vec{S}_i}{m_{cm}} \qquad 3.7.5$$

Rotational KE was calculated as the sum of local rotational energy of the rigid bodies about their own center of mass, and remote rotational energy of the rigid bodies about each segment center (eq. 3.7.6). Local rotational KE of the individual bodies was calculated using the angular velocity vectors and moment of inertia tensors for each body (eq. 3.7.7, see Figure 3.7.2). The inertial properties of each body were derived from their geometry and the angular velocities of each body were obtained from the skew-symmetric angular velocity matrix (eq. 3.7.8). This matrix was calculated by finding the first derivative of the 3x3 rotation transform at each time step and multiplying by the transpose of that rotation transform (eq. 3.7.9) (Berme *et al*, 1990).

$$KE_{\text{rotational}} = KE_{\text{body rotation}} + KE_{\text{segment rotation}} \qquad 3.7.6$$

$$KE_{\text{body rotation}} = \frac{1}{2}\vec{\omega}_i^{\,t}\overline{I}_i\vec{\omega}_i \qquad 3.7.7$$

$$\vec{\omega}_i = \begin{pmatrix} \omega_i^{\angle}(3,2) \\ \omega_i^{\angle}(1,3) \\ \omega_i^{\angle}(2,1) \end{pmatrix} \qquad 3.7.8$$

$$\omega_i^{\angle} = \frac{d\overline{R_i}}{dt}\overline{R_i^{\,t}} \qquad 3.7.9$$

Remote rotational KE was found by calculating the tangential velocity of each body *i* about the segment center of mass (see Figure 3.7.2c). The difference velocity vector V_Δ is the velocity vector of a rigid body minus the velocity of the segment center of mass (eq. 3.7.11). A radius vector *r*, from the segment center of mass position to the body center of mass position was found at each time interval. The component of the difference velocity along the radius vector ($V_{\Delta\text{rad}}$) was found as the projection of the velocity on the radius (eq. 3.7.13). The tangential component was then found by vector subtraction (eq 3.7.12). This difference velocity tangential component vector was then used to calculate remote rotational KE (eq. 3.7.10).

$$KE_{\text{segment rotation}} = \sum_{i=1}^{n} \frac{1}{2} m_i \left(\vec{v}_{\Delta\tan_i} \right)^2 \qquad 3.7.10$$

$$\vec{V}_{\Delta i} = \frac{d\vec{P}_i}{dt} - \frac{d\vec{P}_{cm}}{dt} \qquad 3.7.11$$

$$\vec{V}_{\Delta\tan_i} = \vec{V}_{\Delta_i} - \vec{V}_{\Delta\text{rad}_i} \qquad 3.7.12$$

$$\vec{V}_{\Delta\text{rad}_i} = \vec{r}_{\text{u}_i} \left(\vec{r}_{\text{u}_i} \bullet \vec{V}_{\Delta_i} \right) \qquad 3.7.13$$

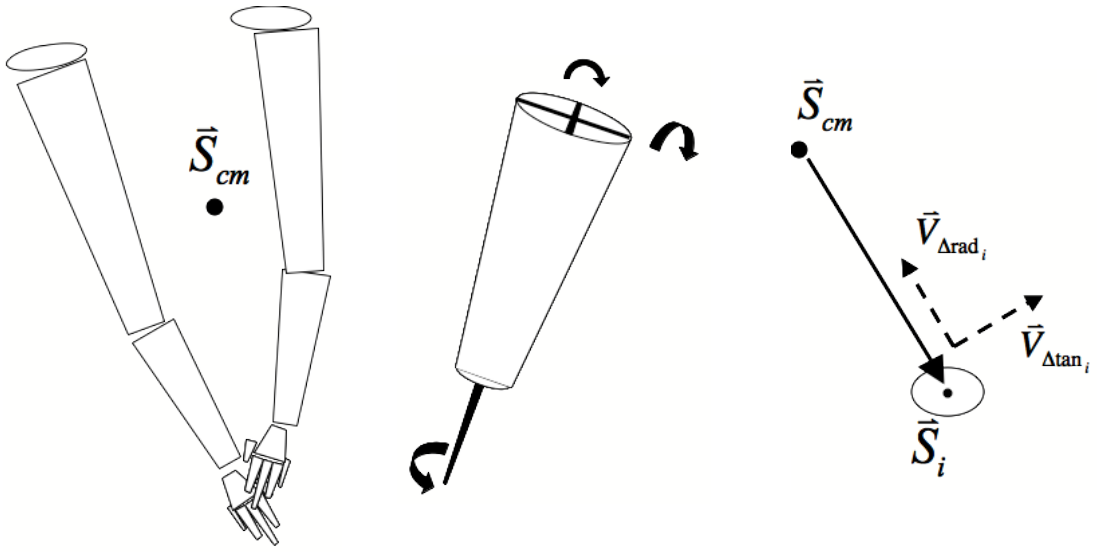

a) b) c)

Figure 3.7.2: Kinetic energy calculations. 3.7.2.a) shows the position of segment center of mass S_{cm} as a function of rigid body positions for the calculation of translational kinetic energy. 3.7.2.b) shows the three axes of rotation about a hypothetical rigid body for the calculation of local rotational kinetic energy. 3.7.2c) shows remote rotational kinetic energy or the energy due to a rigid body (S_{cm}) rotating about the segment center of mass (S_{cm}). V_{rad} and V_{tan} are the respective radial and tangential components of the vector describing the differential velocity between the rigid body and the segment (V).

Total KE traces were filtered using a 4th order low pass Wavelet filter at a cut-off frequency of 20 Hz. Statistical comparisons were made between timing and peak magnitudes of segmental KE using a multi-factorial one-way ANOVA test at a significance level α=.05; with a Tukey *post hoc* analysis.

3.8 Angular Momentum Calculations

The mass and inertial properties of rigid bodies in the kinematic model were found using the method outlined in section 3.7.1. The rigid bodies of the kinematic model were divided into the Club, Arms, Torso, and Hips segments as described in section 3.5 Golfer Segments.

Golf swing angular momentum $\boldsymbol{H}$ was calculated using a method adapted from Bahamonde (2000) who described $\boldsymbol{H}$ in the tennis serve. According to Bahamonde, a segment can have two types of angular momentum during a sports movement. The first type he called Local Angular Momentum or $\boldsymbol{H}_{\text{L}}$. This vector describes the momentum of a rigid body due to the rotation of that body about its own center of mass (CG). The second type of momentum described by Bahamonde was called Remote Angular Momentum, or $\boldsymbol{H}_{\text{R}}$. This vector describes the momentum of a rigid body rotating about the system CG. This framework was slightly modified for the purposes of this study. The organizational level of *segments* was added to our body framework. The same calculation

for Local Angular Momentum as described by Bahamonde was used; but the Remote Angular Momentum calculation was split into two parts. The first part described the momentum caused by rigid bodies rotating about the segment CG. This component will be referred to as Planetary Remote Angular Momentum or $\boldsymbol{H}_{\mathrm{PR}}$. The second part describes the momentum caused by the segment CG rotating about the system CG. This component will be referred to as the Solar Remote Angular Momentum or $\boldsymbol{H}_{\mathrm{SR}}$.

Figure 3.8.1 illustrates the vectors used to calculate $\boldsymbol{H}$ in this study. A hypothetical segment with CG $\boldsymbol{B_0}$ is rotating about system CG $\boldsymbol{A}$. This segment is broken up into 4 rigid bodies with local CG's $\boldsymbol{B_1}$ through $\boldsymbol{B_4}$. These rigid bodies rotate about the segment CG as well as about their own. Rigid body $\boldsymbol{B_1}$ illustrates local angular momentum $\boldsymbol{H}_{\mathrm{L}}$ in this diagram. This rigid body is rotating about its own center of mass with angular velocity vector $\boldsymbol{\omega}_{\mathbf{local}}$ shown as a dashed line. Planetary remote angular momentum $\boldsymbol{H_{PR}}$ is illustrated using the small dotted and solid vectors. Here the rigid body marked $\boldsymbol{B_4}$ is shown to be rotating about the segment CG marked $\boldsymbol{B_0}$. Solar remote angular momentum $\boldsymbol{H_{SR}}$ is illustrated using the larger dotted and solid vectors. The segment CG marked $\boldsymbol{B_0}$ is shown to be rotating about the system CG marked $\boldsymbol{A}$. The calculation of these momenta will be discussed in further detail below.

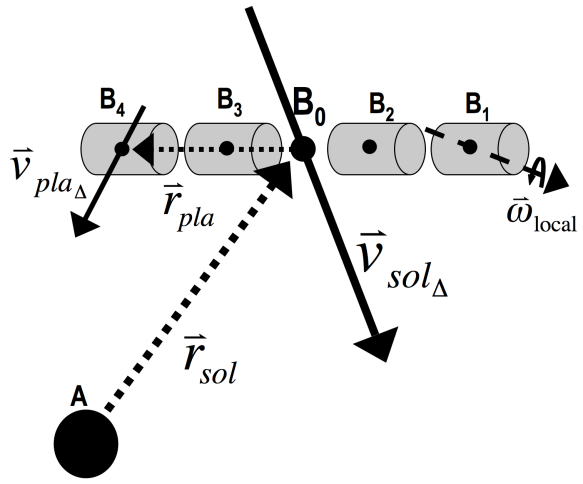

Figure 3.8.1: Body segment angular momentum. Point A represents the system CG. The truncated cylinders represent rigid bodies within a segment. Point B_0 is the segment CG. H_{SR} is determined by vectors v_{sol} and r_{sol}. $H_{PR\,4}$ is determined by vectors v_{pla} and r_{pla}. $H_{L\,1}$ is determined by the product of the inertial tensor of rigid body B_1 and the vector ω_{local} shown in green.

3.8.1 Local Angular Momentum

Local angular momentum $\boldsymbol{H}_{\text{L}}$ is due to the rotational inertia of a segment spinning about its own center of mass. Figure 3.8.1 shows rigid body B_1 spinning about its own mass center. The equation for $\boldsymbol{H}_{\text{L}}$ is given in equation 3.8.1. Matrix $\boldsymbol{I}_{\text{i}}$ is the inertial tensor of rigid body $\boldsymbol{i}$. Vector $\boldsymbol{\omega}_{\textbf{local i}}$ is the local angular velocity attributed to rigid body $\boldsymbol{i}$. Matrix $\boldsymbol{R}_{\text{i}}$ is the rotational transform for rigid body $\boldsymbol{i}$, and is used to convert the angular momentum from the local rigid body coordinate system into components used in the global lab reference frame. The sigma symbol signifies that $\boldsymbol{H}_{\text{L}}$ is summed for all rigid bodies $\boldsymbol{i}$ in a given segment.

$$\vec{H}_{\text{L}} = \sum_{i=1}^{n} \hat{R}_i \left(\hat{I}_i \cdot \vec{\omega}_{\text{local}\,i} \right) \qquad 3.8.1$$

3.8.2 Remote Angular Momentum

Remote angular momentum (***H_R***) is described by the cross product of a linear momentum vector of a moving mass and a radius vector connecting that moving mass with a reference point (Bahamonde, 2000. See eq. 3.8.2). This linear momentum vector incorporates a velocity of the moving mass relative to the reference point. As mentioned previously, remote angular momentum has been organized into 2 levels for this investigation. The first level of remote angular momentum describes rigid bodies rotating about the segment CG and has been referred to here as planetary remote (***H_PR***). The second level of remote angular momentum describes segments rotating about the system CG and has been referred to as solar remote (***H_SR***).

$$\vec{H}_R = m \cdot \left(\vec{r} \times \vec{v}_\Delta \right) \qquad 3.8.2$$

3.8.3 Planetary Remote Angular Momentum

Planetary remote angular momentum (***H_PR***) describes the momentum of a rigid body's CG rotating about a segment's CG. Equation 3.8.3 describes ***H_PR*** as calculated for this study. m_i describes the mass of a rigid body ***i***. Planetary radius of gyration $r_{\text{pla } i}$ is a vector connecting rigid body ***i*** with the segment CG. Planetary difference velocity vector $v_{\text{pla}\Delta i}$ is the difference velocity between the rigid body and the segment. The sigma symbolizes that these calculations are summed for rigid bodies ***i*** through ***n*** for a given segment.

$$\vec{H}_{PR} = \sum_{i=1}^{n} m_i \cdot \left(\vec{r}_{\text{pla } i} \times \vec{v}_{\text{pla } \Delta_i} \right) \qquad 3.8.3$$

3.8.4 Solar Remote Angular Momentum

Solar remote angular momentum ($\boldsymbol{H_{SR}}$) describes the momentum of a segment rotating about the system CG. Equation 3.8.4 describes solar remote $\boldsymbol{H}$ as calculated for this study. $\boldsymbol{m_{seg}}$ describes the mass of a segment. Solar radius of gyration $\boldsymbol{r_{sol}}$ is a vector connecting the segment CG with the system CG. Solar difference velocity vector $\boldsymbol{v_{sol_\Delta}}$ is the difference velocity between the segment and the system.

$$\vec{H}_{SR} = m_{seg} \cdot \left(\vec{r}_{sol} \times \vec{v}_{sol_\Delta} \right) \qquad 3.8.4$$

3.8.5 Angular Momentum Statistics

Total angular momentum ($\boldsymbol{H}_T$) for each segment about the system's center of mass was found by summing $\boldsymbol{H}_L$, $\boldsymbol{H}_{RP}$ and $\boldsymbol{H}_{SP}$ for that segment (eq. 3.8.5). $\boldsymbol{H}_T$ was presented using the orthogonal components of the lab coordinate system (as by Bahamonde). $\boldsymbol{H}_T$ was also presented being projected in the club swing plane (as calculated in section 3.6.1). The purpose of this projection was to simplify the interpretation of body segment momentum. The club swing plane is a direction line that contains the portion of angular momentum directly affecting the collision impulse on the golf ball. The timing and magnitudes of angular momentum peaks were compared for each segment across all subjects. Statistical comparisons were made between timing and peak magnitudes of segmental $\boldsymbol{H}_T$ using a multi-factorial one-way ANOVA test at a significance level α=.05; with a Tukey *post hoc* analysis.

$$\vec{H}_T = \vec{H}_L + \vec{H}_{PR} + \vec{H}_{SR} \qquad 3.8.5$$

Chapter Four: Angular Kinematics Results

4.1 Angular Position of Golfer Segments

The mean angular positions ($\boldsymbol{\theta}$) of the Hips, Torso, Arms and Club segments for 447 players during a golf swing are shown in Figure 4.1.1. $\boldsymbol{\theta}$ are measured in radians, in the swing planes of their respective segments. $\boldsymbol{\theta}$ are measured relative to the segment starting positions at takeaway. Negative values represent rotational displacement in the direction of the backswing. In Figure 4.1.1, time has been normalized relative to total Movement Time (MT) for the backswing and downswing respectively. It must be noted that the average time for the backswing and downswing are not equal although normalizing them in this fashion may give that impression. As such, the abscissa represents normalized time as a percentage of backswing or downswing. The reader should note that the backswing is approximately 3.5 times longer than the downswing. The mean time taken for the backswing was 0.89s (0.16s SD) while the mean time for downswing was 0.25s (0.04s SD).

In Figure 4.1.1, positive angular displacement is defined as counter-clockwise when observing a right-handed player in the frontal plane. In all cases, the segments undergo a negative angular displacement from the takeaway position. The time to peak for all segments occurs near MT 0%, or top of backswing. The magnitude of the angular displacement peaks increases from Hips out to Club in a proximal to distal manner. The timing and magnitude of the peaks will be examined in further detail below.

In Figure 4.1.1, the downswing is represented from MT 0% to MT 100%. During this time, the proximal segments are generally shown to have a more positive angular

displacement as compared to their distal neighbours. In other words, within a segment's swing plane, proximal segments are closer to their impact position than their distal neighbours for the majority of the downswing. There is a very interesting exception to this point at approximately MT 80% where the Arms segment θ crosses the θ of the Torso.

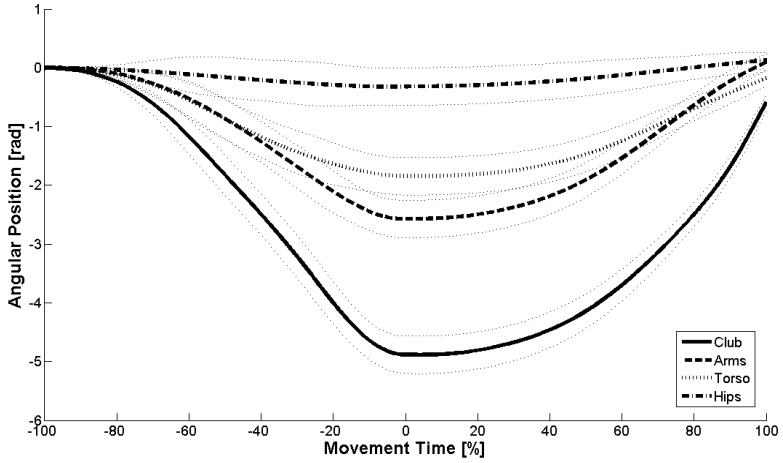

Figure 4.1.1: θ of body segments during the golf swing. Movement Time (MT) is measured along the abscissa. MT-100 = takeaway; MT 0 = top of backswing; and MT 100 = ball contact. Angular position is measured in radians along the ordinate, relative to position at takeaway. Golfer segment mean angular positions are shown in thick lines. Standard deviation is shown in smaller dotted lines above and below the means.

The time to peak θ for golfer segments during a swing is shown graphically in Figure 4.1.2. The bars represent mean time to peak as a percentage of MT. The vertical dashed black bars show standard deviation. Horizontal bars represent significant difference in pair wise comparisons. Asterisks represent significant difference from all other segments.

The Hips segment reached a maximum deviation in angular range of motion earlier in the swing than all three other segments. This was at -4.06 % MT, just prior to the top of backswing. This was found to be significantly different from other segments.

The Arms segment was the second segment to reach its peak $\boldsymbol{\theta}$. This was also found to be significantly different than the other segments. The Torso and Club segments were the last to reach their peak angular range of motion. These were not at significantly different times from one another. The pattern in which golfers reach a maximum angular range of motion in the golf swing is: Hips, Arms, and then Torso/Club.

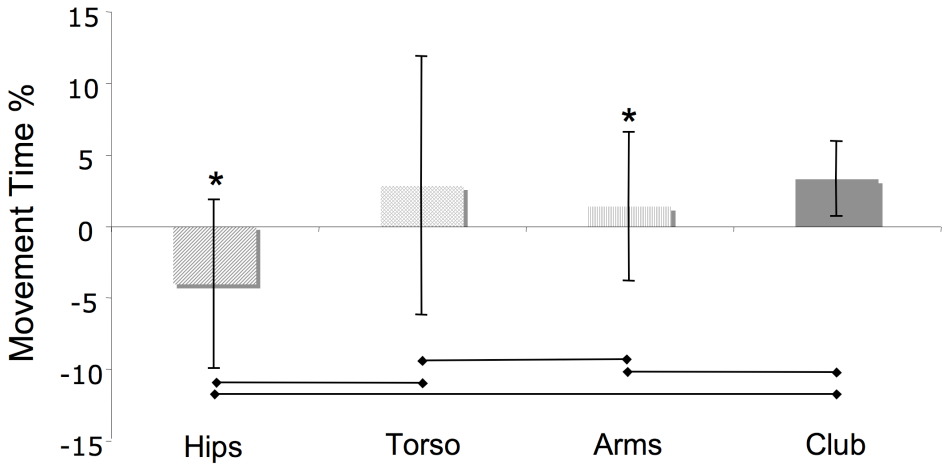

Figure 4.1.2: Time to peak of angular position. Time has been expressed as a percentage of MT; where -100 = takeaway, 0 = top of backswing, and 100 = ball contact. Standard deviation is shown using vertical black bars. Asterisks represent significant difference from all other segments. Pair wise differences are shown with black horizontal bars.

In Figure 4.1.3, the mean $\boldsymbol{\theta}$ peaks for the four golfer segments are plotted. $\boldsymbol{\theta}$ is expressed in radians and measured relative to position at takeaway. The dashed bars represent standard deviation. The peak $\boldsymbol{\theta}$ of the four segments were found to increase in magnitude in a proximal to distal manner from the Hips segment out to the Club. The difference in magnitudes between segments was found to be significant for all pair wise comparisons.

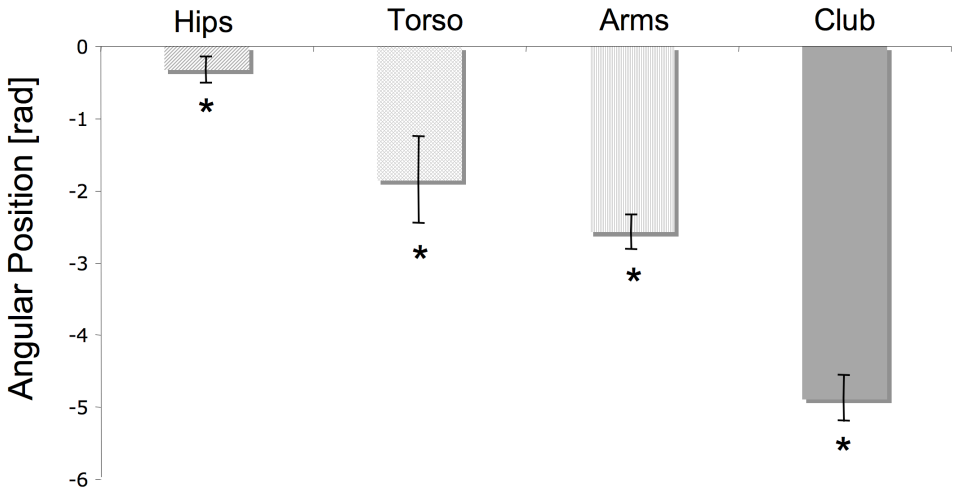

Figure 4.1.3: Peak angular position. Angular position has been expressed in radians. Standard deviation is shown using vertical black bars. All segments were found to be significantly different from one another (indicated by the asterisks).

4.1.1 Angular Position Summary

Not surprisingly, all segments reached a peak angular displacement near top of backswing, around 0% MT. The Hips were the first segment to reach this peak, followed by the Arms, then the Club and Torso together. The magnitude of this peak increased in a proximal to distal manner from the Hips to the Club.

4.2 Angular Velocity of Golfer Segments

Mean angular velocities (ω) of golfer segments in their respective swing planes are shown in Figure 4.2.1 during a golf swing. Positive ω is in the direction of the downswing, while negative ω represents rotational velocity away from the ball. Angular velocity is expressed in radians/second. The abscissa measures normalized time expressed as a percentage of MT. All segments showed a negative ω during the backswing. At MT 0%, or top of backswing, segments went through a reversal of ω to

move in a positive direction towards ball contact. Club ω undergoes a large increase near the end of the down swing. The time to peak and peak magnitudes of the golf segments will be discussed for the downswing below.

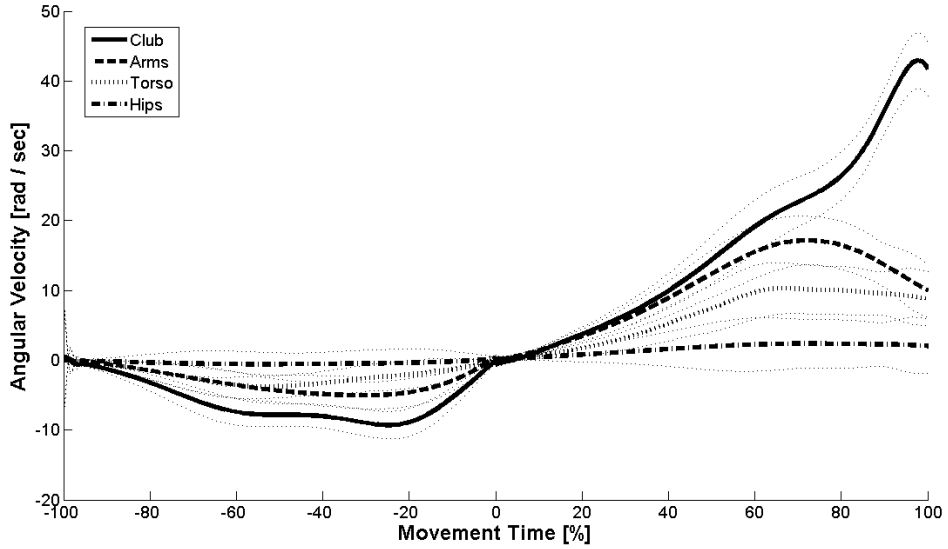

Figure 4.2.1: Angular Velocity of body segments during the golf swing. Angular Velocity is measured in the swing plane and expressed in radians/s. The X-axis represents normalized time. Golfer segment mean angular velocities are shown in thick lines. Standard deviation is shown in smaller dotted lines above and below the means.

Figure 4.2.2 shows the time to peak for segment angular velocities during the downswing. The Torso and Arms segments' angular velocities were found to peak first, followed by the Hips and then the Club segments. The Club and Hips segments' time to peak were significantly different from all other segments. There was little timing difference between the three body segments; Hips, Torso, and Arms all peaked near 70% MT. The Club segment peaked much later at 98% MT, or just prior to impact. It is interesting to note that all human based golf segments seemed to peak together, while the non-human segment, or most distal segment showed a delay before peaking.

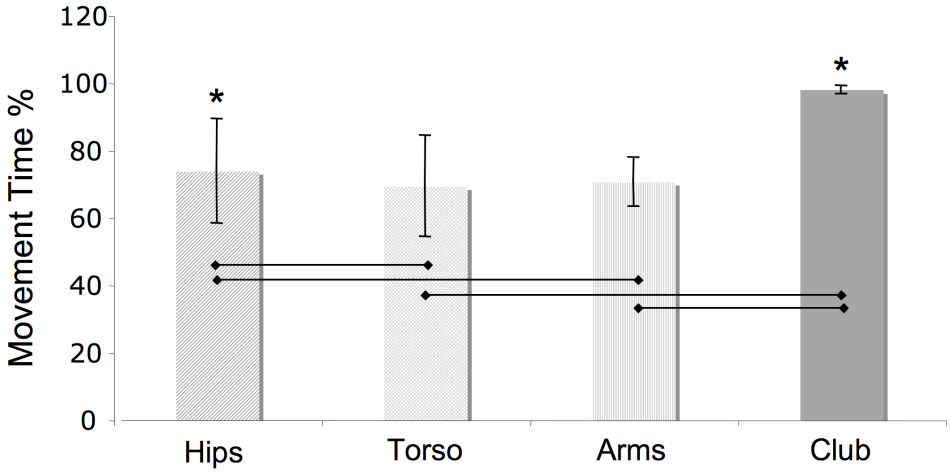

Figure 4.2.2: Time to peak angular velocity during the downswing. Time has been expressed as a percentage of MT. Standard deviation is shown using vertical black bars. Horizontal bars represent pair wise significant difference while asterisks represent significant difference from all other segments.

The magnitudes of angular velocity peaks during the downswing are shown in Figure 4.2.3. These peaks increased in a proximal to distal manner from the Hips segment up and out to the Club segment. The largest change in angular velocity between adjacent segments was found between the Arms and Club segment. Specifically, an increase of 25.3 rad/s, or approximately 58.6% of the Club mean peak angular velocity, was recorded.

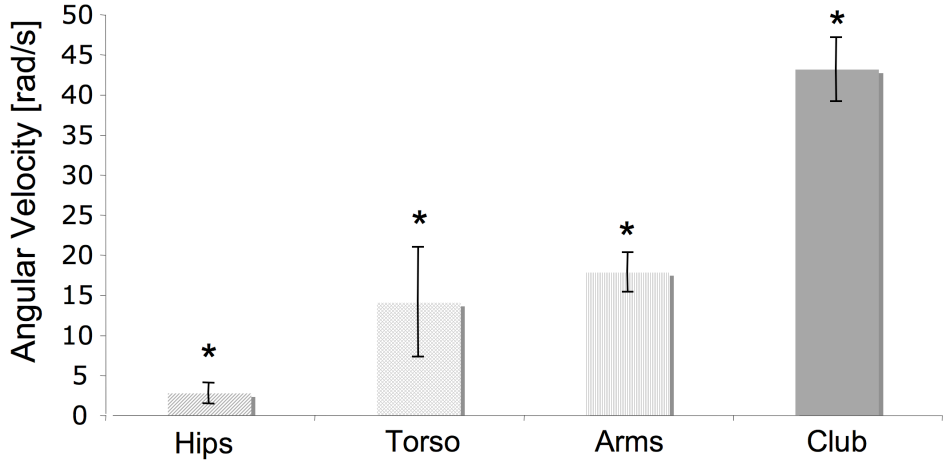

Figure 4.2.3: Peak angular velocity during the downswing. Angular velocity has been expressed in rad/s. Standard deviation is shown using vertical black bars. All body segments were found to be significantly different from one another (indicated by the asterisks).

4.2.1 Angular Velocity Summary

During the backswing, all golfer segments showed a negative angular velocity. The Hips and Torso reached a peak negative velocity before the Arms and Club segments. The magnitudes of peak negative angular velocity were found to increase in a proximal to distal manner. The largest changes of angular velocities from adjacent segments came from the connection point between the Hips and Torso segments, and the connection between the Arms and Club segments.

In the downswing, the Arms and Torso segments were found to have the shortest mean time to peak, near 65% MT. The Hips, and then the Club segment followed them. The Club segment peaked much later than the other three segments, at 98% MT. The magnitude of mean positive angular velocity peaked in a proximal to distal manner during the downswing. The largest difference between adjacent segments came at the connection between the Arms and Club. This was a difference of 25.3 rad/s or 58.6% of Club $\boldsymbol{\omega}$.

4.3 Angular Acceleration of Body Segments

Mean golfer segment angular acceleration ($\boldsymbol{\alpha}$) traces are found in Figure 4.3.1. Positive $\boldsymbol{\alpha}$ represents rotational acceleration in the direction of the downswing. Negative $\boldsymbol{\alpha}$ is in the direction moving away from the ball. As can be seen in the graph, the initial start of the traces contains noise due to error in the differentiation. For this reason, magnitudes and

timing of positive angular acceleration peaks were analyzed from -80% MT to ball contact. All segments had a positive increase in angular acceleration prior to ball contact. Timing and magnitudes of $\boldsymbol{\alpha}$ peaks are described in detail below.

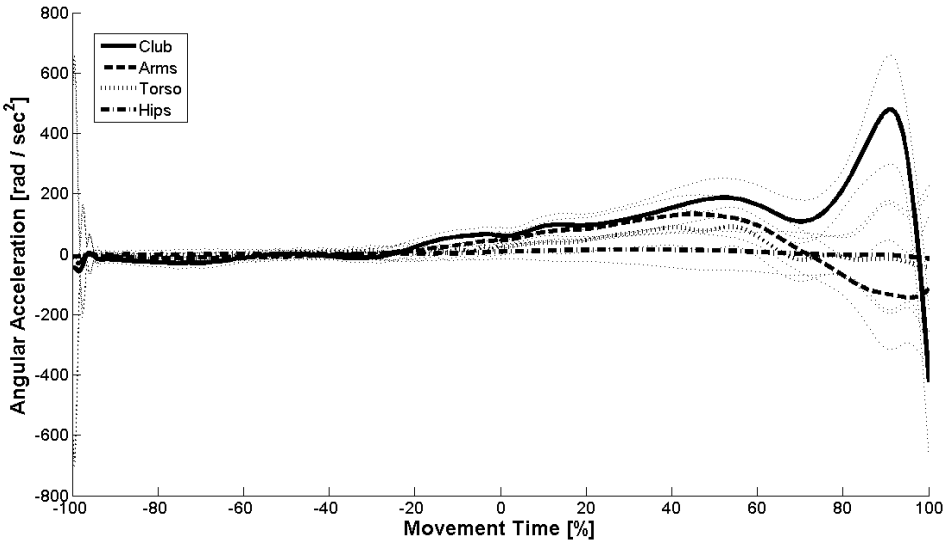

Figure 4.3.1: Angular acceleration of body segments during the golf swing. The abscissa has been normalized to a percentage of MT. The ordinate depicts angular acceleration in rad/s^2. Golfer segment mean angular accelerations are shown in thick lines. Standard deviation is shown in smaller dotted lines above and below the means.

Mean angular acceleration time to peak is shown in Figure 4.3.2 for the four golfer segments. All segments reached a positive $\boldsymbol{\alpha}$ peak sometime during the downswing. The Arms segment was the first to peak, followed by the Hips segment, then the Torso segment. Although significantly different, all three body segments peaked at approximately 50% of the downswing. The Club segment $\boldsymbol{\alpha}$ peaked at 89.9% MT, much later than the other three.

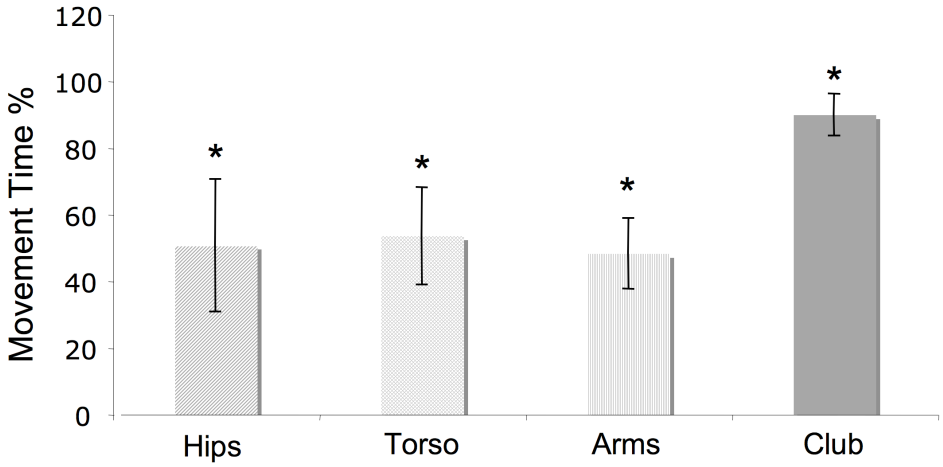

Figure 4.3.2: Time to peak angular acceleration during the golf swing. Time to peak has been expressed as a percentage of MT. Standard deviation is shown using vertical black bars. All body segments were found to be significantly different from one another (indicated by the asterisks).

The peak angular acceleration, shown in Figure 4.3.3, is expressed in rad/s^2. All segments were found to be significantly different. At 502 rad/s^2, the Club segment had the highest mean peak $\boldsymbol{\alpha}$, followed by the Torso, then the Arms and finally the Hips segment. The largest change in $\boldsymbol{\alpha}$ between adjacent segments happened between the Hips and the Torso segment, amounting to 69.3% of Club peak $\boldsymbol{\alpha}$. Interestingly, there was a decrease in $\boldsymbol{\alpha}$ between the Torso and Arms segments.

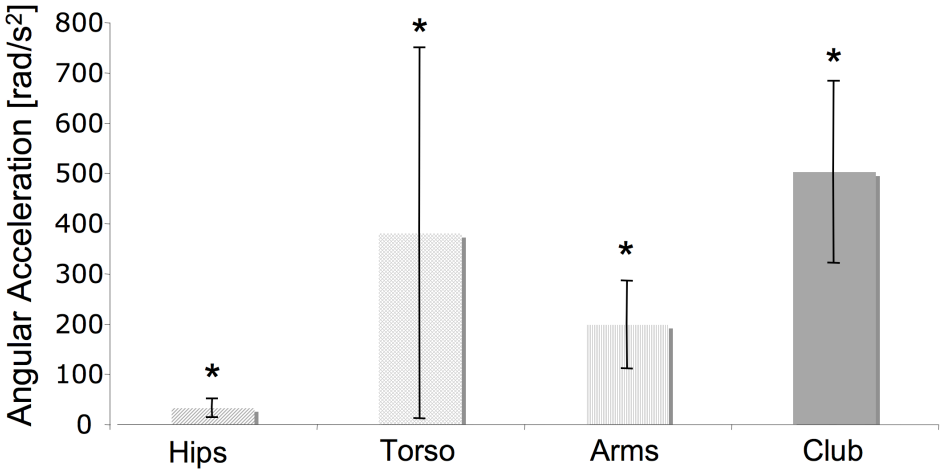

Figure 4.3.3: Peak angular acceleration during the golf swing. Angular acceleration has been measured in rad/s^2. Standard deviation is shown using vertical black bars. All body segments were found to be significantly different from one another (indicated by the asterisks).

4.3.1 Angular Acceleration Summary

Angular acceleration increased during the downswing for all four golfer segments. The time to peak angular acceleration was much later for the club (89.9% MT) as compared to the other three segments (~50% MT). The magnitudes of the peaks did not occur in a proximal to distal fashion. The largest increase in $\boldsymbol{\alpha}$ between adjacent segments (69.3% of peak Club $\boldsymbol{\alpha}$) occurred at the connection point between the Hips and Torso segments. There was a decrease in $\boldsymbol{\alpha}$ found to occur between the Torso and Arms segments.

Chapter Five: Kinetic Energy Results

5.1 Total Kinetic Energy of Golfer Segments

The mean total kinetic energy (KE_T) of the Hips, Torso, Arms and Club segments for 447 players during a golf swing are shown in Figure 5.1.1. KE_T was measured in joules as a summation of rotational and translational KE for each segment. In Figure 5.1.1, time has been normalized relative to total Movement Time (MT) for the backswing and downswing respectively. It must be noted that the average time for the backswing and downswing are not equal, although normalizing them in this fashion may give that impression. As such, the abscissa represents normalized time as a percentage of backswing or downswing. In Figure 5.1.1, all segments go through a small peak of KE_T during the backswing, then a larger peak during the downswing. The timing and magnitude of the peaks will be examined in further detail below.

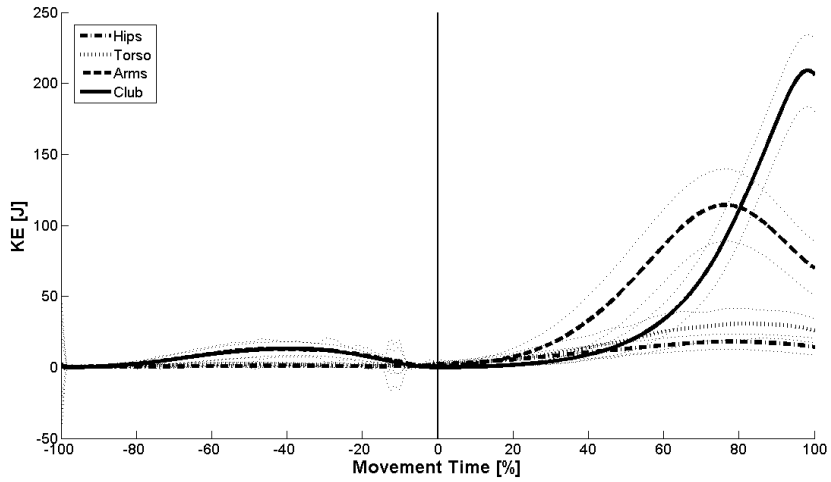

Figure 5.1.1: Total kinetic energy during the golf swing. Movement Time (MT) is measured along the abscissa. MT-100 = takeaway; MT 0 = top of backswing; and MT 100 = ball contact. Total kinetic energy is measured in joules along the ordinate. Golfer segment mean KE_T are shown in thick lines. Standard deviation is shown in smaller dotted lines above and below the means.

The timing of the KE_T peaks is shown in Figure 5.1.2. Only the Club segment was found to peak at a significantly different time from any other segment. The Hips, Torso and Arms segments all peaked in KE_T around 75% MT. The Club segment peaked much later at 98.3% MT, just prior to ball contact.

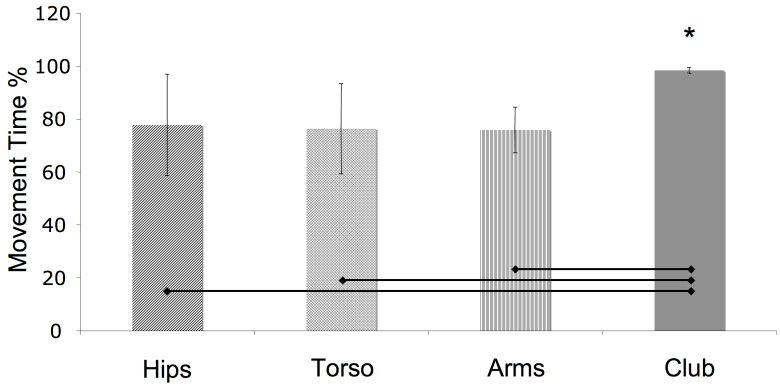

Figure 5.1.2: Total kinetic energy time to peak during the golf swing. Time has been expressed as a percentage of MT; where -100 = takeaway, 0 = top of backswing, and 100 = ball contact. Standard deviation is shown using vertical black bars. Asterisks represent significant difference from all other segments. Pair wise differences are shown with a black horizontal bar.

The magnitudes of the mean KE_T peaks are shown in Figure 5.1.3 for the four golfer segments. The peaks increased in a proximal to distal (P-D) manner starting at the Hips segment and moving up and out towards the Club segment. All differences were significant. The difference in KE_T between adjacent segments also increased in a P-D manner. The segment connection between the Hips and the Torso showed a difference of 18.5 J or 8.8% of the Club KE_T. The connection point between the Torso segment with the Arms showed an increase of 78.9 J or 37.5% of Club KE_T. The largest increase between adjacent segments came at the connection point between the Arms and Club segment. This segment interface showed an increase of 91.6 J or 43.6% of the peak Club KE_T.

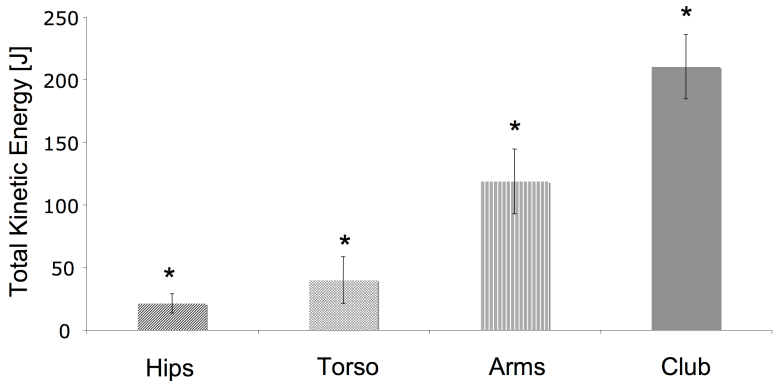

Figure 5.1.3: Peak total kinetic energy. KE_T **has been expressed in joules. Standard deviation is shown using vertical black bars. All segments were found to be significantly different from one another (as represented by asterisks).**

As previously mentioned, total kinetic energy (KE_T) has been found by summing the translational kinetic energy (KE_{TR}) and rotational kinetic energy for each segment. The rotational KE was found as the sum of local rotational kinetic energy (KE_{LR}) and the remote rotational kinetic energy (KE_{RR}). Figure 5.1.4 shows the KE_T for each segment as the sum of its components. The relative contribution of KE_{TR} , KE_{LR} and KE_{RR} changes for each segment. The Club energy is largely made up of KE_{TR} , while the Torso energy is largely composed of KE_{LR}. The KE_T of the Hips and Arms segments are made up of a combination of two or three components that are closer in peak magnitudes. The relative magnitudes and timings of the translational and rotational kinetic energy peaks will be discussed in further detail in the sections to follow.

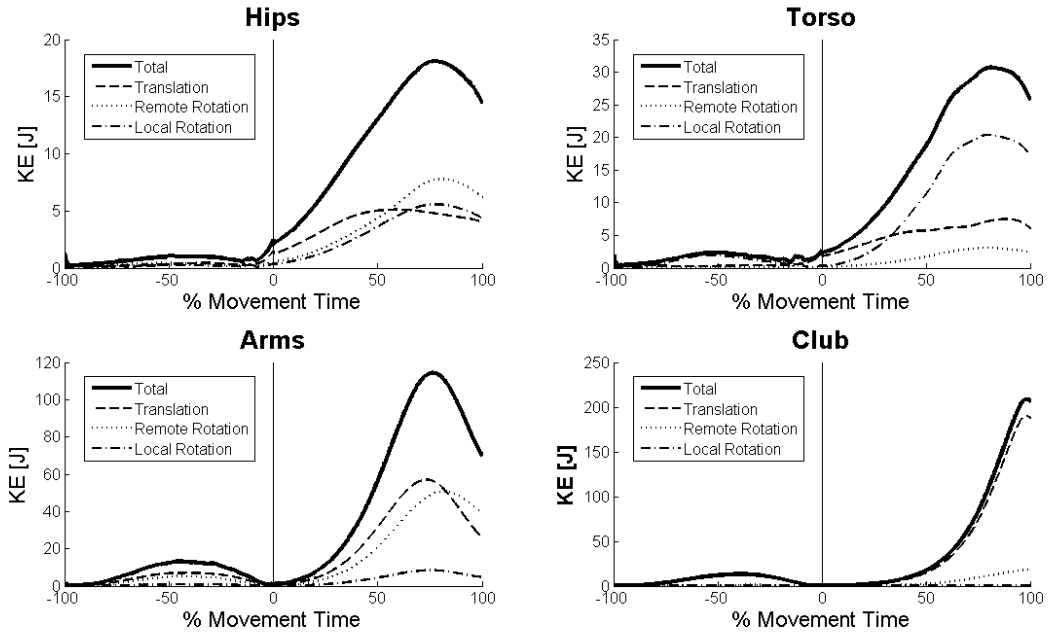

Figure 5.1.4: Total kinetic energy as the summation of its components. Kinetic energy is measured along the ordinate in joules. The abscissa represents normalized time. The mean KE_T for each segment is shown in a thick solid black line. KE_{TR} is shown in a smaller, dashed line. KE_{RR} is shown in a dotted line and KE_{LR} is shown as a dash-dot line. Note that all segment graphs are shown in different scale upon the ordinate.

5.1.1 Total Kinetic Energy Summary

Total kinetic energy KE_T was found to show a small peak during the backswing and a larger peak during the downswing for all golfer segments. The downswing mean KE_T traces did not peak in a P-D fashion. All human based segments (the Hips, Torso and Arms) peaked at approximately 75 MT. The Club peaked in KE_T just prior to impact. The magnitudes of the mean KE_T peaks increased in a P-D manner. In addition, the difference in magnitudes between adjacent peaks also increased in a P-D manner. The largest increase in KE_T came at the connection point between the Arms and Club segment, which amounted to roughly 44% of the final Club peak. The Club segment KE_T was largely composed of KE_{TR} while the Torso segment KE_T was chiefly made up of KE_{LR}. The Hips and Arms segments' KE_T were composed of a mix of kinetic energy types.

5.2 Translational Kinetic Energy

Translational kinetic energy (KE_{TR}) traces of golfer segments during a swing are shown in Figure 5.2.1. All segments showed a slight increase in KE_{TR} during the backswing. The increase in KE_{TR} was much more pronounced in the downswing. Mean Club segment KE_{TR} underwent a large increase just prior to ball contact. The time to peak and peak magnitudes of mean KE_{TR} in the four golf segments will be discussed below.

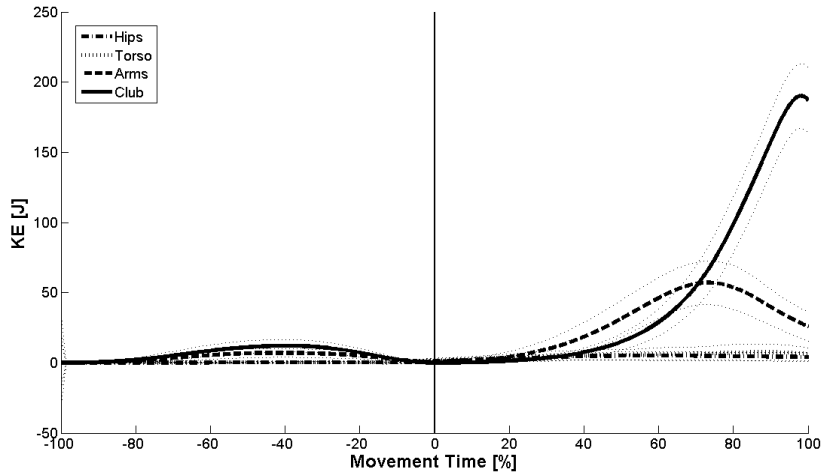

Figure 5.2.1: Translational kinetic energy during the golf swing. KE_{TR} **is measured along the ordinate and expressed in joules. The abscissa represents normalized time. Golfer segment mean** KE_{TR} **are shown in thick lines. Standard deviation is shown in smaller dotted lines above and below the means.**

The time to peak KE_{TR} is shown below in Figure 5.2.2. The Hips and Torso segments were the first to peak at approximately 68% MT. The Arms KE_{TR} peaked soon after (73.1% MT), followed by the Club KE_{TR}, which peaked just prior to impact (98.1% MT). The general timing trend was in a P-D manner, however the largest delay between adjacent segments occurred at the connection point between the Arms and the Club segment. This delay accounted for nearly 25 % MT.

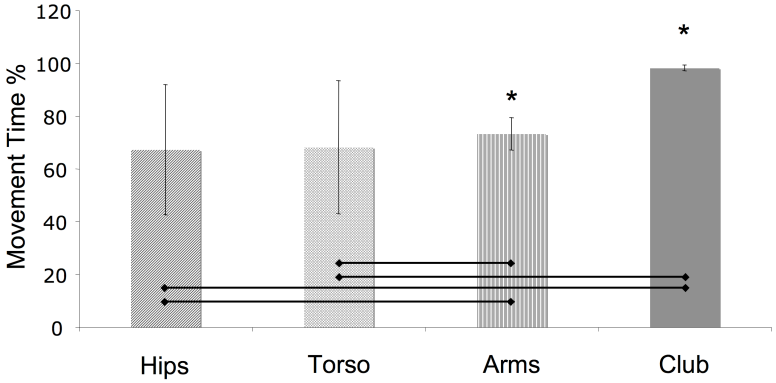

Figure 5.2.2: Translational kinetic energy time to peak. Time measurements have been normalized as a % MT. Standard deviation is shown using vertical black bars. Asterisks represent significant difference from all other segments. Pair wise differences are shown with a black horizontal bar.

The mean peak KE_{TR} values for the four golfer segments are shown in Figure 5.2.3. The peak magnitudes increased in a P-D manner from the Hips segment to the Club. All differences between segments were significant. The difference in peak KE_{TR} between adjacent segments also increased P-D. The largest increase in KE_{TR} came at the connection point between the Arms and Club segment. This amounted to 131 J or 68.8% of the Club segment peak KE_{TR}.

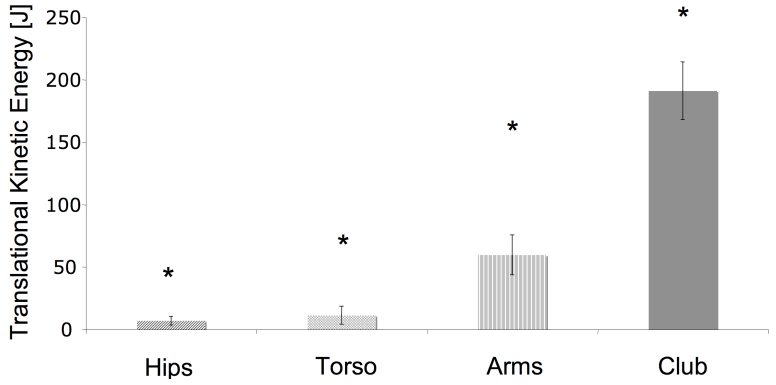

Figure 5.2.3: Peak translational kinetic energy. KE_{TR} has been expressed in joules. Standard deviation is shown using vertical black bars. All segments were found to be significantly different from one another (as shown by asterisks).

5.2.1 Translational Kinetic Energy Summary

The mean translational kinetic energy traces were dominated by the behaviour of the Club segment. The timing of the mean peaks happened in a more or less P-D manner starting with the Hips and Torso segments and moving sequentially to the Arms then Club segments. The delay between the body-based segments was minimal. All body segments peaked at approximately 70 % MT, while the Club segment peaked just prior to impact. The delay from the Arms peak to the Club was 25% MT. The magnitudes of the mean KE_{TR} peaks also followed a P-D manner. The largest increase in KE_{TR} between adjacent segments happened at the connection point between the Arms and the Club. This accounted for 68.8 % of the Club KE_{TR}.

5.3 Local Rotational Kinetic Energy

Local rotational kinetic energy (KE_{LR}) traces of golfer segments during a swing are shown in Figure 5.3.1. KE_{LR} is the amount of rotational kinetic energy created by rigid bodies rotating about their own respective center of masses. The standard deviation traces were relatively larger for all segments in KE_{LR} than for other measurements of kinetic energy. Also, the magnitudes of KE_{LR} peaks were low compared to KE_{TR}. All segments had a slight increase in KE_{LR} during the backswing but peaked in KE_{LR} during the downswing.

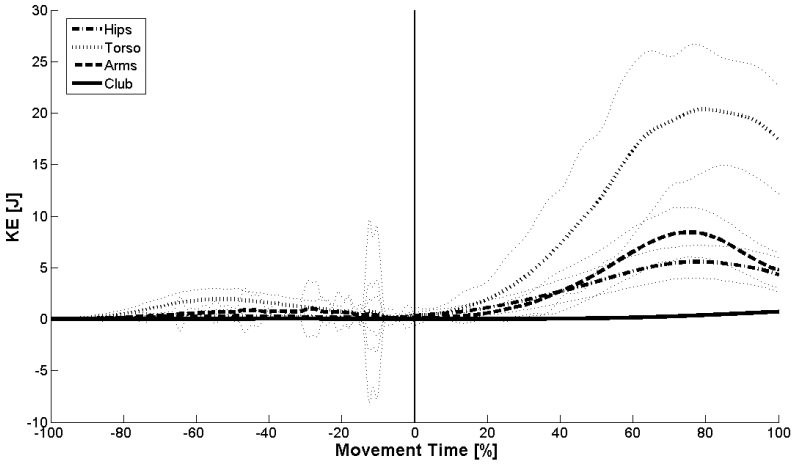

Figure 5.3.1: Local rotational kinetic energy during the golf swing. KE_{LR} **is measured along the ordinate and expressed in joules. The abscissa represents normalized time. Standard deviation is shown with small dotted lines above and below the means.**

The times to peak during the downswing for segments' mean KE_{LR} are shown in Figure 5.3.2. The Arms segment was the first to peak at 68.6% MT. This was significantly different from the other segments. The Club time was the last to peak at 99.4% MT. This was also significant. The Hips and the Torso segments peaked at a time in between (~77% MT). The largest delay between adjacent segments came at the connection point between the Arms and the Club segments. This delay was 30.8 % MT. Interestingly, both of the Hips and Torso segments peaked in local rotational kinetic energy after the Arms segment.

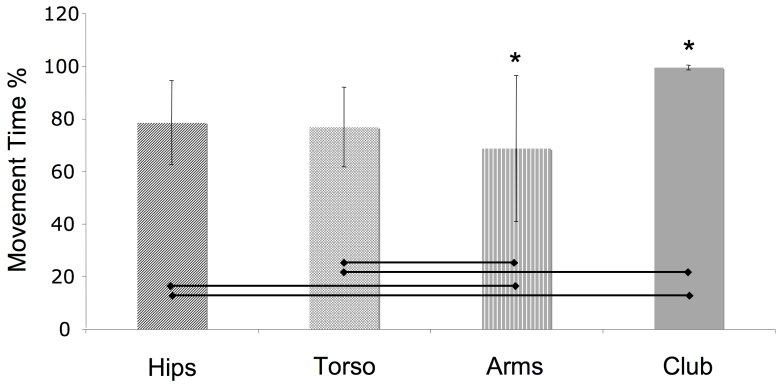

Figure 5.3.2: Local rotational kinetic energy time to peak. Time measurements have been normalized as a % MT. Standard deviation is shown using vertical black bars. Asterisks represent significant difference from all other segments. Pair wise differences are shown with a black horizontal bar.

Mean KE_{LR} peak magnitudes are shown in Figure 5.3.3 for the four golfer segments. All peaks were found to be significantly different. The pattern found was not P-D. The Torso segment had the largest KE_{LR} peak at 26.7 J. This peak was followed in magnitude by the Arms segment, then the Hips segment, then the Club. The Club had virtually no KE_{LR} compared to the other three segments (0.7 J). The largest change between adjacent segments came between the Hips and the Torso segment, for an increase of 20.3 J.

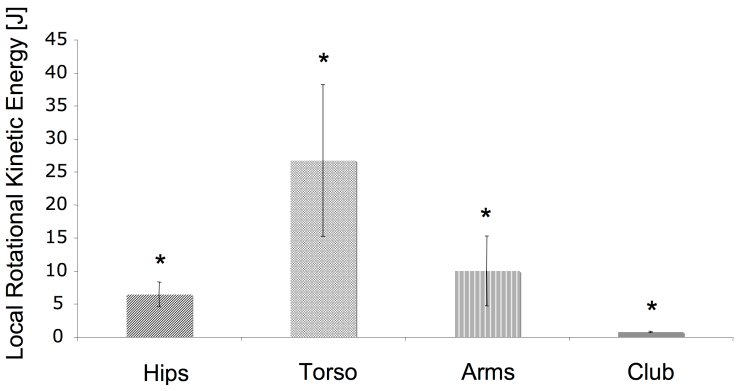

Figure 5.3.3: Peak local rotational kinetic energy. Standard deviation is shown using vertical error bars. All segments were found to be significantly different from one another (as represented by asterisks).

5.3.1 Local Rotational Kinetic Energy Summary

In general, the mean local rotational kinetic energy traces had lower magnitudes, but larger standard deviations than the kinetic energy measures previously discussed. The timing of peaks did not follow a P-D order. The Arms segment was the first to peak (68.6% MT), followed by the Hips and Torso segments together (~77% MT), and the

Club segment was the last to peak (99.4% MT). The Torso segment had the largest KE_{LR} magnitude (26.7 J). The Club segment showed virtually none of this type of energy (0.7 J).

5.4 Remote Rotational Kinetic Energy

Traces of mean remote rotational kinetic energy (KE_{RR}) for the four golfer segments are shown in Figure 5.4.1. KE_{RR} is the amount of rotational kinetic energy created by rigid bodies rotating about the segment center of mass. All segments showed an increase in mean KE_{RR} during the backswing; however, the peak KE_{RR} occurred during the downswing for all four segments. The relative standard deviation was smaller in the KE_{RR} measurements than in the KE_{LR}. The magnitude and timing of the KE_{RR} peaks will be discussed in further detail below.

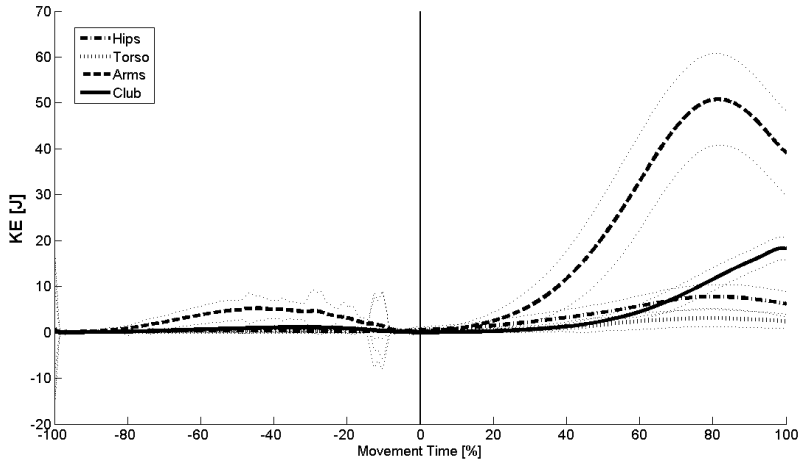

Figure 5.4.1: Remote rotational kinetic energy during the golf swing. KE_{RR} **is measured along the ordinate and expressed in joules. The abscissa represents normalized time. Mean** KE_{RR} **traces are shown as thick lines. Standard deviation is shown with small dotted lines above and below the means.**

The time to peak for KE_{RR} is shown in Figure 5.4.2. All segments peaked during the later stage of the downswing. The Torso segment was the first to peak (73.8% MT), followed by the Hips and Arms segments (~80% MT), then followed by the Club (99.0% MT). The largest delay in peaks between adjacent segments happened at the connection point between the Arms segment and the Club. This delay amounted to 19 % MT of the downswing.

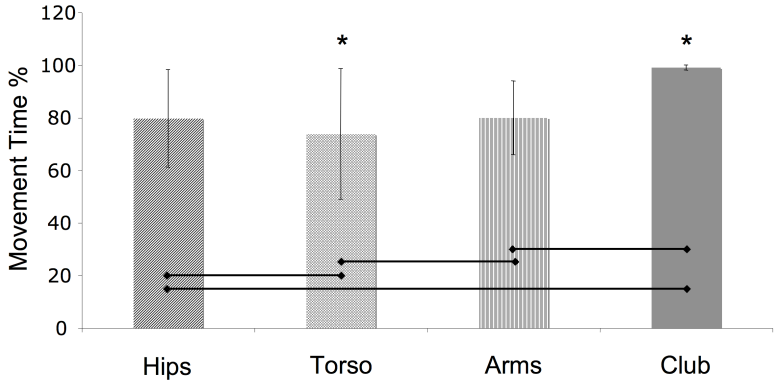

Figure 5.4.2: Remote rotational kinetic energy time to peak. Standard deviation is shown using vertical error bars. Pair-wise statistical difference is shown using the black horizontal bars. The asterisks signify statistical difference from all other segments.

The peak magnitudes of KE_{RR} for the four golf segments are shown in Figure 5.4.3. The pattern is distinctly not P-D. All differences between segments were significant. The Arms segment showed the largest peak at 52.7 J. The largest difference between adjacent segments happened at the connection point between the Torso and the Arms. This increase in energy amounted to 48.5 J, which was 2.6 times larger than the amount of peak KE_{RR} contained in the club (18.5 J).

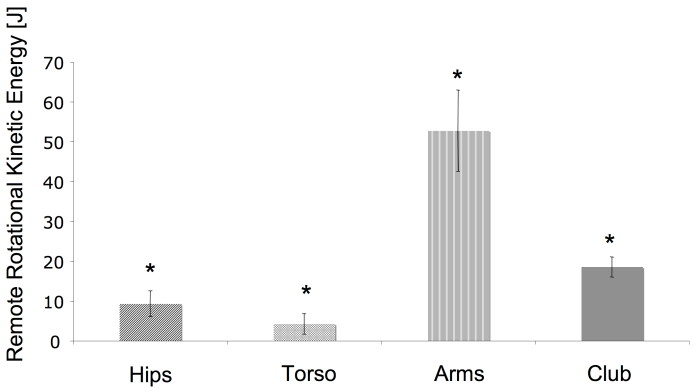

Figure 5.4.3: Peak remote rotational kinetic energy in the golf swing. Standard deviation is represented by the vertical error bars. Asterisks represent significant difference from all other segments.

5.4.1 Remote Rotational Kinetic Energy Summary

The magnitudes of the KE_{RR} peaks were larger than those of KE_{LR} while the relative standard deviations were smaller. All segments peaked during the downswing. The Torso segment was the first to peak (73.8% MT) while the Club segment was the last (99.0% MT). The largest delay between adjacent segments happened at the connection point between the Arms and the Club (a delay of 19.1% MT). The magnitudes of the KE_{RR} peaks did not display a P-D pattern. The Arms showed the largest peak at 52.7 J. The largest increase between adjacent segments came at the connection point between the Torso and the Arms (an increase of 48.5 J). Interestingly, the Club showed a large decrease in peak KE_{RR} magnitude compared to the Arms (a decrease of 34.2 J).

Chapter Six: Angular Momentum Results

6.1 Total Angular Momentum

Total angular momentum ($\boldsymbol{H}_{\mathbf{T}}$) was measured in *kg* m^2/s and was calculated as the summation of local angular momentum ($\boldsymbol{H}_{\mathbf{L}}$), remote planetary angular momentum ($\boldsymbol{H}_{\mathbf{RP}}$) and remote solar angular momentum ($\boldsymbol{H}_{\mathbf{RS}}$). $\boldsymbol{H}_{\mathbf{T}}$ is a three dimensional vector that has been described below in terms of the laboratory coordinates. The laboratory X-axis is a vector that points towards the target of the golf drive. The lab Y-axis points vertically upward. The lab Z-axis points anteriorly from the golfer towards the ball at takeaway.

Figure 6.1.1 describes total angular momentum about an axis pointing in the direction of the driving target ($\boldsymbol{H}_{\mathbf{T\text{-}X}}$). The reader will find that line graphs of this type will show normalized time as a percentage of movement time (MT). It must be noted that the average time for the backswing and downswing are not equal, although normalizing them in this fashion may give that impression. As such, the abscissa represents normalized time as a percentage of backswing or downswing. The reader will note that there is a slight discontinuity at MT 0%. This is because the backswing and downswing were time normalized separately.

The Hips, Arms and Club segments went through a negative peak in $\boldsymbol{H}_{\mathbf{T\text{-}X}}$ during the backswing, and positive peaks in $\boldsymbol{H}_{\mathbf{T\text{-}X}}$ during the downswing. This pattern was reversed in the Torso segment, which underwent a positive peak in $\boldsymbol{H}_{\mathbf{T\text{-}X}}$ during the backswing and a negative peak during downswing. The timing and magnitudes of these peaks will be described in further detail below.

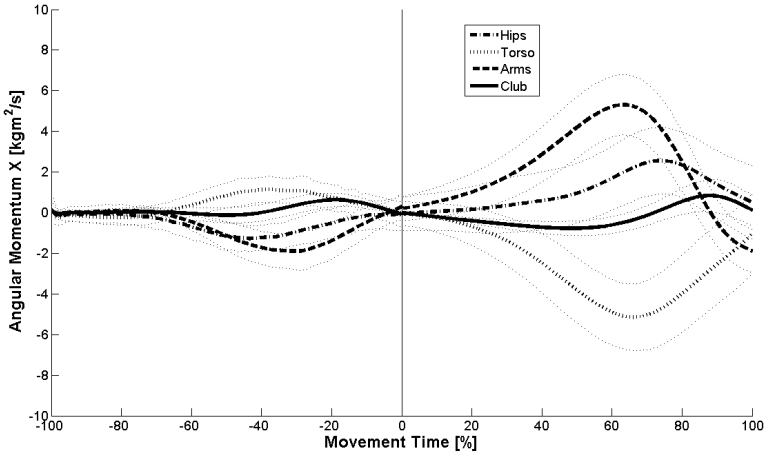

Figure 6.1.1: Total angular momentum towards target (lab X). These are mean traces of H_T in the laboratory X direction. Angular momentum is measured along the ordinate. Normalized time is shown along the abscissa. MT 0 = top of backswing. Thick traces represent the mean $H_{T\text{-}X}$ for each golf segment. The small dotted lines above and below the means show the respective standard deviations.

Total angular momentum in the vertical up direction ($\boldsymbol{H}_{\mathbf{T\text{-}Y}}$) is shown in Figure 6.1.2. Segments go through a negative peak in $\boldsymbol{H}_{\mathbf{T\text{-}Y}}$ during the backswing and a positive peak during the downswing. The peak Club $\boldsymbol{H}_{\mathbf{T\text{-}Y}}$ during the downswing seems to coincide with a decrease in the Arms segment $\boldsymbol{H}_{\mathbf{T\text{-}Y}}$.

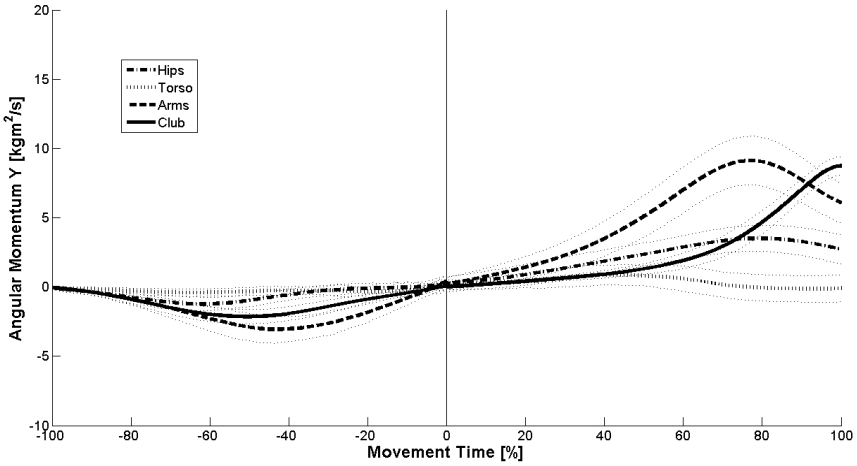

Figure 6.1.2: Total angular momentum in vertical up (lab Y). $H_{T\text{-}Y}$ is measured along the ordinate in *kg m²/s*. The abscissa measures normalized time. Means are shown using thick traces. Standard deviations are shown above and below their respective means using small dotted lines.

Total angular momentum towards the ball at takeaway ($\boldsymbol{H}_{\mathbf{T\text{-}Z}}$) is shown in Figure 6.1.3. Segments underwent a negative peak in $\boldsymbol{H}_{\mathbf{T\text{-}Z}}$ during the backswing and a positive peak during the downswing. The Arms segment was late to peak during the backswing, but first to peak during the downswing. The Club and Torso $\boldsymbol{H}_{\mathbf{T\text{-}Z}}$ peaks during the downswing coincide with a large decrease in Arms $\boldsymbol{H}_{\mathbf{T\text{-}Z}}$.

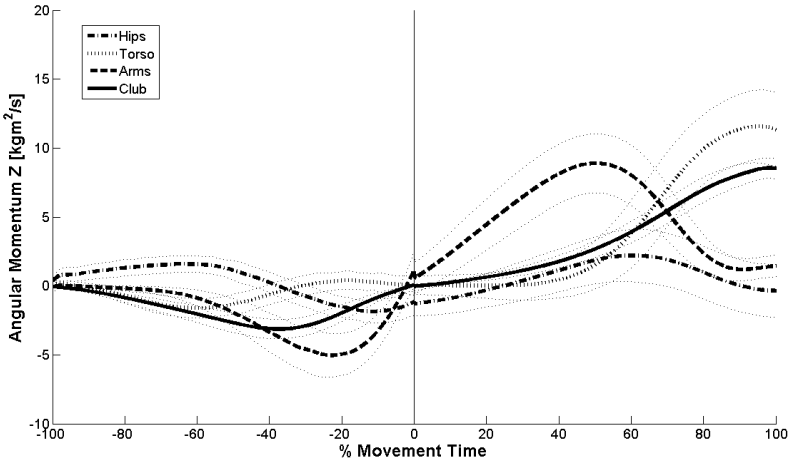

Figure 6.1.3: Total angular momentum towards ball (lab Z). $H_{T\text{-}Z}$ is measured along the ordinate in *kg m²/s*. The abscissa measures normalized time. Means are shown using thick traces. Standard deviations are shown above and below their respective means using small dotted lines.

The peak timings for $\boldsymbol{H}_{\mathbf{T}}$ in the three lab coordinates are described in Figure 6.1.4. All peaks described are in the positive direction about their respective axis. In the direction towards the driving target (lab X), the Torso segment reached a positive peak during the backswing. All other segments peaked during the downswing. The Club segment peaked significantly earlier than the Hips and Arms segments, which peaked around MT 64%. In the direction pointing vertical upward (lab Y), the Torso was the first to peak at MT 42.5%. The Club segment peaked last at MT 99.6%, just prior to contact.

In the direction towards the ball at takeaway (lab Z), the Hips segment was the first to peak at MT 24.0%. This was followed by the Arms segment which peaked at MT 50.4%, and finally by the Torso and Club segments, which peaked just prior to impact. There was not a proximal to distal (P-D) timing of peaks in $\boldsymbol{H}_{\mathbf{T}}$ for any of the three lab coordinates.

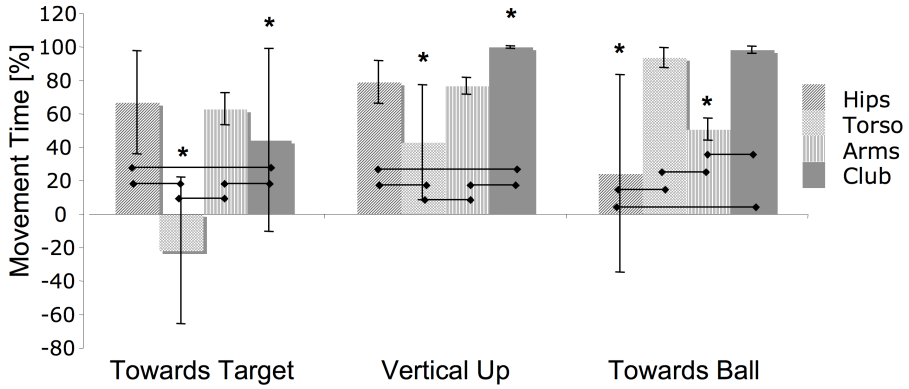

Figure 6.1.4: Total Angular Momentum time to peak. Time has been expressed as a percentage of MT. Standard deviation is shown using vertical error bars. Asterisks represent significant difference from all other segments. Time to peak has been analyzed in the 3 directions of the lab coordinate system separately.

Peak magnitudes of $\boldsymbol{H}_{\mathbf{T}}$ expressed in the 3 lab coordinates are shown in Figure 6.1.5. In the direction towards the driving target (lab X), the Club segment had the smallest peak at 1.1 $kg\ m^2/s$ and the Arms segment showed the largest peak at 5.6 $kg\ m^2/s$. Interestingly, the largest change between adjacent segments was a decrease in $\boldsymbol{H}_{\mathbf{T\text{-}X}}$ at the connection point between the Arms and the Club (a change of -4.5 $kg\ m^2/s$). In the vertical up direction (lab Y), the Arms had the largest peak at 9.4 $kg\ m^2/s$. The largest increase in $\boldsymbol{H}_{\mathbf{T\text{-}Y}}$ between adjacent segments happened at the connection point between the Torso and Arms segments. This accounted for 7.8 $kg\ m^2/s$, or 89% of peak Club $\boldsymbol{H}_{\mathbf{T\text{-}Y}}$. In the direction towards the ball at takeaway (lab Z), the Torso segment showed the

highest $\boldsymbol{H_{T\text{-}Z}}$ peak (11.9 *kg* m^2/s). The largest increase between adjacent segments happened at the connection point between the Hips and Torso segment. This accounted for 8.6 *kg* m^2/s or roughly the same amount of $\boldsymbol{H_{T\text{-}Z}}$ as seen in the Club peak.

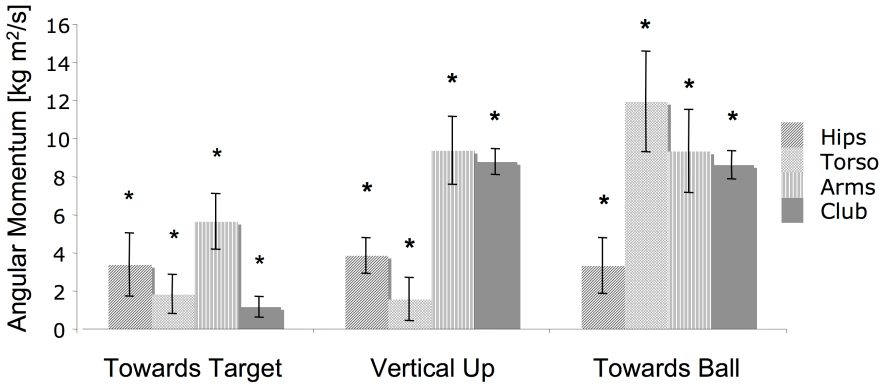

Figure 6.1.5: Peak total angular momentum. H_T is measured in kg m^2/s. Vertical error bars represent standard deviation. Asterisks show statistical difference from all other segments. H_T has been analyzed in the 3 directions of the lab coordinate system separately.

6.1.1 Total Angular Momentum Summary

Total angular momentum ($\boldsymbol{H_T}$) is a three component vector describing the sum of local angular momentum ($\boldsymbol{H_L}$), remote planetary angular momentum ($\boldsymbol{H_{RP}}$) and remote solar angular momentum ($\boldsymbol{H_{RS}}$). About the axis pointing toward the driving target, the torso showed a reverse pattern of $\boldsymbol{H_{T\text{-}X}}$ peaks compared to the other segments. About the direction pointing vertically upward, the peak Club segment $\boldsymbol{H_{T\text{-}Y}}$ peak coincided with a decrease in Arms segment $\boldsymbol{H_{T\text{-}Y}}$. In the direction pointing towards the ball at takeaway, the Arms segment was late to peak during the backswing but first to peak during the downswing. The Arms segment then underwent a large decrease in $\boldsymbol{H_{T\text{-}Z}}$ that seemed to coincide with peaks in the Torso and Club segments' $\boldsymbol{H_{T\text{-}Z}}$.

The $\boldsymbol{H_T}$ time to peak did not follow a P-D pattern in any of the 3 lab coordinate axis. In the direction towards target, the Hips and the Arms segments were the last to

peak (~MT 64%). In the direction pointing vertically upward, the Club was the last to peak (MT 99.6%) following the Arms and Hips segments (~MT 77%). In the direction pointing toward the ball at takeaway, the Hips and the Arms segments were the first to peak (MT 24.0% and MT 50.4% respectively). The Torso and the Club segments then peaked after, closer to ball contact (MT 93.3% and MT 97.9% respectively).

The magnitudes of the $\boldsymbol{H}_{\mathbf{T}}$ peaks did not follow a P-D pattern in any of the 3 lab coordinate axis. In the direction towards the driving target, the Arms showed the highest $\boldsymbol{H}_{\mathbf{T\text{-}X}}$ peak at 5.6 $kg\ m^2/s$. The largest change between adjacent segments came at the connection point between the Arms and the Club segments, which accounted for a decrease of 4.5 $kg\ m^2/s$. In the direction pointing vertically upward, the Arms again showed the largest peak $\boldsymbol{H}_{\mathbf{T}}$ with a value of 9.4 $kg\ m^2/s$. The largest increase between adjacent segments occurred at the connection point between the Torso and Arms segments. This accounted for 7.8 $kg\ m^2/s$, or 89% of peak Club $\boldsymbol{H}_{\mathbf{T\text{-}Y}}$. In the direction pointing towards the ball at takeaway, the Torso showed the largest peak in $\boldsymbol{H}_{\mathbf{T\text{-}Z}}$ at 11.9 $kg\ m^2/s$.

6.2 Local Angular Momentum

Local angular momentum ($\boldsymbol{H}_{\mathbf{L}}$) is a 3 component vector measuring the momentum caused by the rotation of a rigid body about its own center of gravity. This value has been summed for all rigid bodies within a given golf segment. $\boldsymbol{H}_{\mathbf{L}}$ has been expressed in $kg\ m^2/s$ along the 3 directions of the lab coordinate axes. $\boldsymbol{H}_{\mathbf{L}}$ is shown about the direction pointing towards the driving target in Figure 6.2.1. The magnitudes of the $\boldsymbol{H}_{\mathbf{L\text{-}X}}$ peaks are

lower compared to other measurements of $\boldsymbol{H}$ yet the standard deviations are relatively higher. In addition, only the Torso has any substantial $\boldsymbol{H}_{\mathbf{L}}$ peaks in the lab X direction.

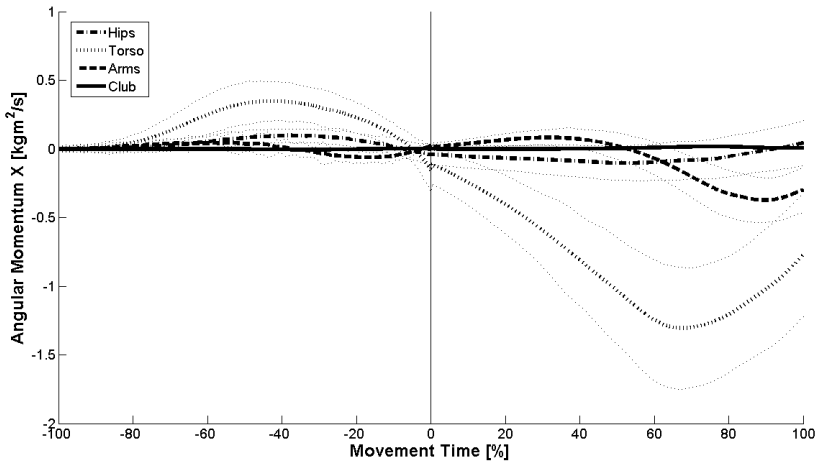

Figure 6.2.1: Local angular momentum towards target (lab X). $H_{L\text{-}X}$ is measured along the ordinate in *kg m²/s*. The abscissa measures normalized time. Means are shown using thick traces. Standard deviations are shown above and below their respective means using small dotted lines.

Local angular momentum in the direction pointing vertically upward ($\boldsymbol{H}_{\mathbf{L\text{-}Y}}$) is shown in Figure 6.2.2. Again, the magnitudes of the $\boldsymbol{H}_{\mathbf{L}}$ peaks are low but the relative sizes of the standard deviations are large. The magnitude of the Torso segment dominates the mean traces of $\boldsymbol{H}_{\mathbf{L\text{-}Y}}$.

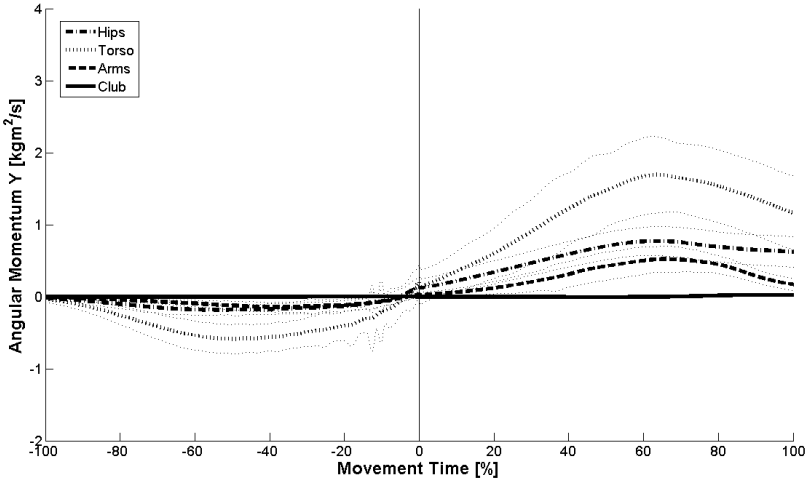

Figure 6.2.2: Local angular momentum vertical up (lab Y). $H_{L\text{-}Y}$ is measured along the ordinate in *kg m²/s*. The abscissa measures normalized time. Means are shown using thick traces. Standard deviations are shown above and below their respective means using small dotted lines.

Local angular momentum in the direction pointing towards the ball at takeaway ($\boldsymbol{H}_{\mathbf{L\text{-}Z}}$) is shown in Figure 6.2.3. The magnitude of the Torso segment $\boldsymbol{H}_{\mathbf{L\text{-}Z}}$ again dominates the mean traces in this graph. The Club segment shows virtually zero $\boldsymbol{H}_{\mathbf{L\text{-}Z}}$.

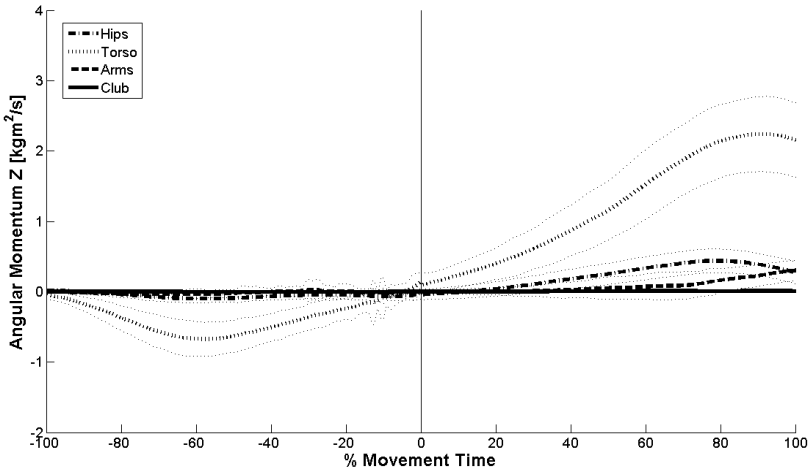

Figure 6.2.3: Local angular momentum towards ball (lab Z). $H_{L\text{-}Z}$ is measured along the ordinate in *kg m²/s*. The abscissa measures normalized time. Means are shown using thick traces. Standard deviations are shown above and below their respective means using small dotted lines.

Time to peak for $\boldsymbol{H}_{\mathbf{L}}$ is shown for the 3 lab coordinate directions in Figure 6.2.4. In all directions, peak $\boldsymbol{H}_{\mathbf{L}}$ timings have not occurred in a P-D progression. For the most part, all positive $\boldsymbol{H}_{\mathbf{L}}$ peaks have occurred in the downswing; except for the Club segment in the direction towards the driving target (MT -22.0%).

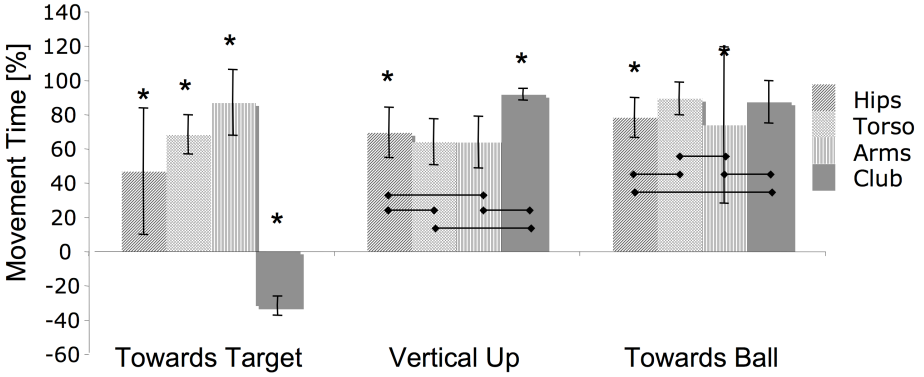

Figure 6.2.4: Local angular momentum time to peak. Time has been expressed as a percentage of MT. Standard deviation is shown using vertical error bars. Horizontal bars represent statistical difference in pair wise comparisons. Asterisks represent significant difference from all other segments. Time to peak has been analyzed in the 3 directions of the lab coordinate system separately.

Peak $\boldsymbol{H}_{\mathbf{L}}$ magnitudes are shown in Figure 6.2.5 for the 3 directions of the lab coordinate system. In the direction pointing towards the driving target, all segment peaks were negative. All segment peaks were positive for the vertical upward and towards ball at takeaway directions. In all cases, the Torso segment had the largest $\boldsymbol{H}_{\mathbf{L}}$. None of the directions analyzed showed a P-D pattern of $\boldsymbol{H}_{\mathbf{L}}$ peak increase. The Club segment showed virtually no $\boldsymbol{H}_{\mathbf{L}}$ magnitude for all directions analyzed.

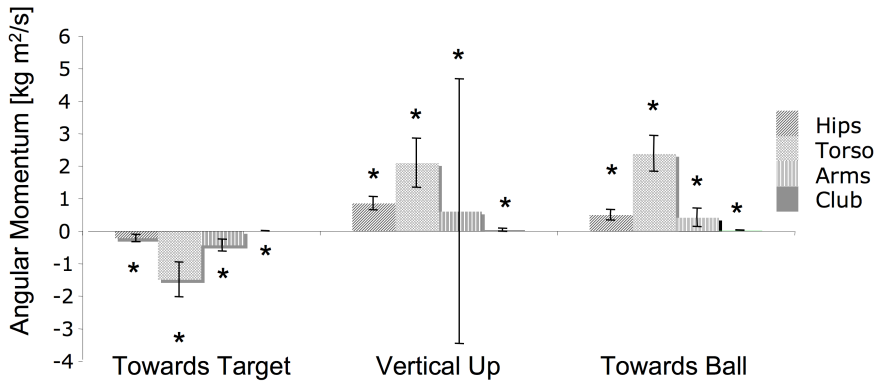

Figure 6.2.5: Local angular momentum peak magnitudes. H_L is measured in kg m^2/s. Vertical error bars represent standard deviation. Asterisks show statistical difference from all other segments. H_L has been analyzed in the 3 directions of the lab coordinate system separately.

6.2.1 Local Angular Momentum Summary

Local angular momentum ($\boldsymbol{H}_{\mathbf{L}}$) is the momentum caused by the rotation of rigid bodies about their own center of gravities. The Torso was the only segment to show a magnitude of $\boldsymbol{H}_{\mathbf{L}}$ that was comparable to other $\boldsymbol{H}$ measurements. The Club segment had virtually no $\boldsymbol{H}_{\mathbf{L}}$ in all directions. The towards target direction showed negative $\boldsymbol{H}_{\mathbf{L}}$ peaks. The magnitudes of the $\boldsymbol{H}_{\mathbf{L}}$ peaks were positive for the vertical upward and towards ball at takeaway directions. The timing and magnitudes of $\boldsymbol{H}_{\mathbf{L}}$ peaks did not progress in a P-D fashion in any of the lab coordinate directions.

6.3 Remote Planetary Angular Momentum

Remote planetary angular momentum ($\boldsymbol{H}_{\mathbf{RP}}$) is the term used here to describe the momentum caused by the rotation of a segment's rigid bodies about the segment center of gravity. $\boldsymbol{H}_{\mathbf{RP}}$ is measured in $kg\ m^2/s$ and has been expressed in terms of the laboratory coordinate axes. Mean $\boldsymbol{H}_{\mathbf{RP}}$ measured in the direction of the driving target ($\boldsymbol{H}_{\mathbf{RP\text{-}X}}$) is shown in Figure 6.3.1. The peak magnitudes are slightly higher than those found for $\boldsymbol{H}_{\mathbf{L}}$ but the standard deviation traces are relatively large compared to other measurements of $\boldsymbol{H}$. The timing and magnitudes of the $\boldsymbol{H}_{\mathbf{RP\text{-}X}}$ will be discussed in further detail below.

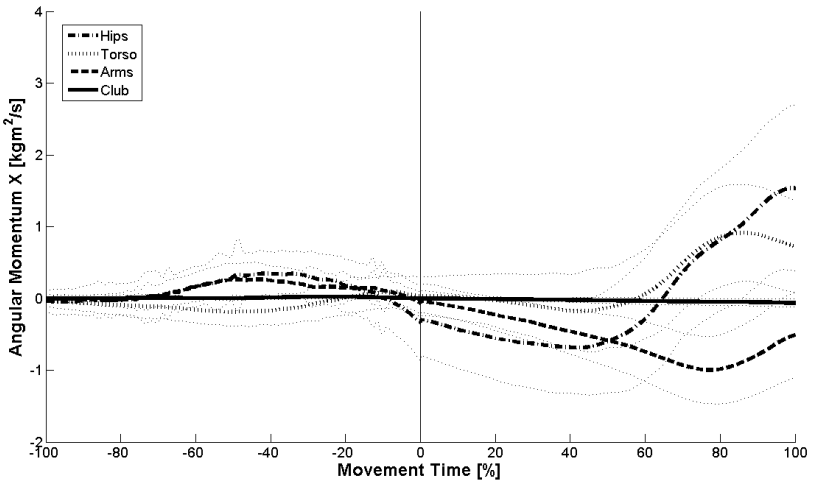

Figure 6.3.1: Remote planetary angular momentum towards target (lab X). $H_{RP\text{-}X}$ is measured along the ordinate in *kg m²/s*. The abscissa measures normalized time. Means are shown using thick traces. Standard deviations are shown above and below their respective means using small dotted lines.

Remote planetary angular momentum about a vertical axis pointing upward ($\boldsymbol{H}_{\mathbf{RP\text{-}Y}}$) is shown in Figure 6.3.2. The relative standard deviation traces are lower than those in $\boldsymbol{H}_{\mathbf{RP\text{-}X}}$. All segments underwent a negative $\boldsymbol{H}_{\mathbf{RP\text{-}Y}}$ peak during the backswing, and a positive $\boldsymbol{H}_{\mathbf{RP\text{-}Y}}$ during the downswing. The magnitudes and timing of the $\boldsymbol{H}_{\mathbf{RP\text{-}Y}}$ peaks will be discussed in further detail below.

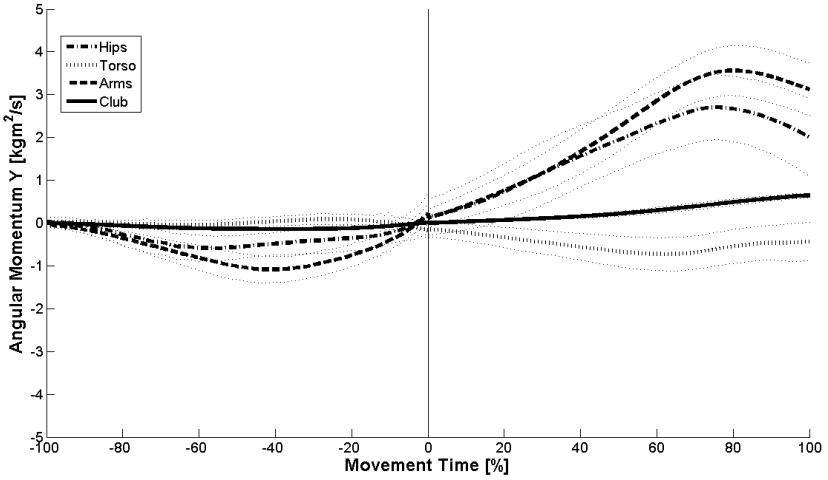

Figure 6.3.2: Remote planetary angular momentum vertical up (lab Y). $H_{RP\text{-}Y}$ is measured along the ordinate in *kg m²/s*. The abscissa measures normalized time. Means are shown using thick traces. Standard deviations are shown above and below their respective means using small dotted lines.

Remote planetary angular momentum about the axis pointing towards the ball at takeaway ($\boldsymbol{H}_{\mathbf{RP\text{-}Z}}$) is shown in Figure 6.3.3. To be looking down this axis is to be looking directly at the golfer in the frontal plane. The traces of $\boldsymbol{H}_{\mathbf{RP\text{-}Z}}$ are dominated by the behaviour of the Arms segment. The Club shows virtually none of this type of momentum. The magnitudes and timing of the $\boldsymbol{H}_{\mathbf{RP\text{-}Z}}$ peaks will be discussed in further detail below.

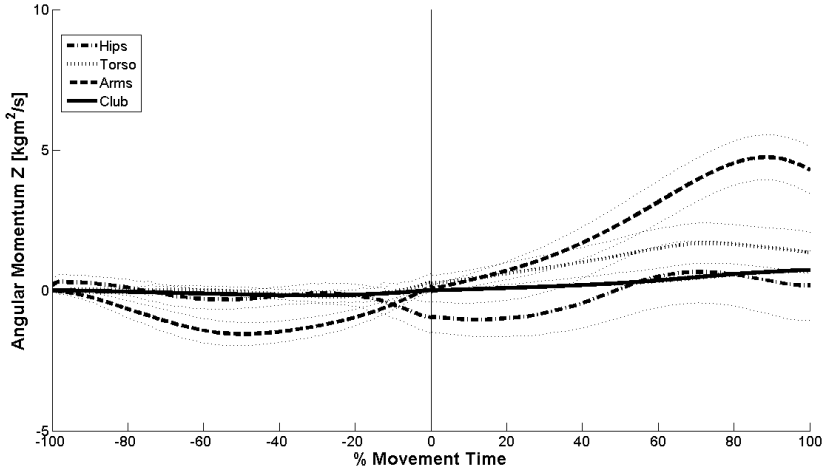

Figure 6.3.3: Remote planetary angular momentum towards ball (lab Z). $H_{RP\text{-}Z}$ is measured along the ordinate in *kg m²/s*. The abscissa measures normalized time. Means are shown using thick traces. Standard deviations are shown above and below their respective means using small dotted lines.

The peak timings of mean $\boldsymbol{H}_{\mathbf{RP}}$ are shown in Figure 6.3.4 for the 3 directions of the lab coordinate axes. In the direction pointing towards the driving target, the Arms and the Club segments reached a positive peak during the backswing (MT -29.5% and MT -11.5% respectively). The Hips and Torso segments did not peak until around MT 75%.

About the axis pointing vertically upward, the Torso peaked during the backswing (MT -16.1%), the Hips and Arms segments peaked around MT 79% and the Club segment peaked just before impact (MT 99.1%). In the direction pointing towards the ball at takeaway, a P-D pattern was found. The timing of the peaks increased sequentially in the downswing starting with the Hips segment (MT 43.6%) moving upwards and outwards to the Club segment (MT 98.9%). The largest delay between segments' peaks occurred between the Hips and the Torso segment. This represented a delay of MT 31.2%.

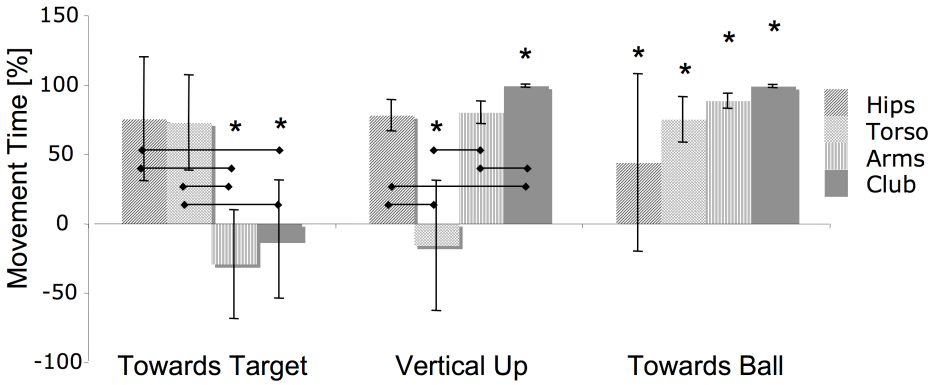

Figure 6.3.4: Remote planetary angular momentum time to peak. Time has been expressed as a percentage of MT. Standard deviation is shown using vertical error bars. Horizontal bars represent statistical difference in pair wise comparisons. Asterisks represent significant difference from all other segments. Time to peak has been analyzed in the 3 directions of the lab coordinate system separately.

The magnitudes of the $\boldsymbol{H}_{\mathbf{RP}}$ peaks are shown in Figure 6.3.5 for the directions of the lab coordinate system. The relative size of the peak magnitudes were approximately double that seen in the $\boldsymbol{H}_{\mathbf{L}}$ peaks. The Hips and Arms segments dominated the size of the peaks for this type of momentum. In the direction pointing towards the driving target, the sizes of the peaks decrease in a P-D fashion. About the axis pointing vertically upward, the Arms and Hips segments have the greatest $\boldsymbol{H}_{\mathbf{RP}}$ (3.7 $kg\ m^2/s$ and 3.0 $kg\ m^2/s$

respectively). In the direction pointing towards the ball at takeaway, the Arms showed the highest peak at 3.7 *kg m²/s*. Interestingly, the largest change between adjacent segments was a decrease of 3.0 *kg m²* at the connection point between the Arms and Club segments.

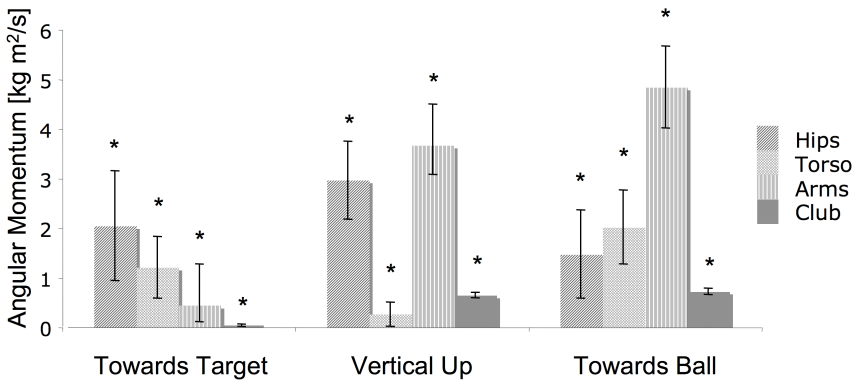

Figure 6.3.5: Remote planetary angular momentum peak magnitudes. H_{RP} is measured in kg m²/s. Vertical error bars represent standard deviation. Asterisks show statistical difference from all other segments. H_{RP} has been analyzed in the 3 directions of the lab coordinate system separately.

6.3.1 Remote Planetary Angular Momentum Summary

Remote planetary angular momentum ($\boldsymbol{H}_{\mathbf{RP}}$) is the term used here to describe the momentum caused by the rotation of a segment's rigid bodies about that segment's center of gravity. $\boldsymbol{H}_{\mathbf{RP}}$ is a 3-component vector that has been described in terms of the lab coordinate axes. About the axis pointing towards the driving target, $\boldsymbol{H}_{\mathbf{RP\text{-}X}}$ showed relatively larger standard deviations than other measurements of $\boldsymbol{H}_{\mathbf{RP}}$.

6.4 Remote Solar Angular Momentum

Remote solar angular momentum ($\boldsymbol{H}_{\mathbf{RS}}$) is the term that has been used to describe the momentum caused by a segment's center of gravity rotating about the golfer's center of gravity. $\boldsymbol{H}_{\mathbf{RS}}$ is a three dimensional vector that has been measured in *kg m²/s* and

expressed along the axes of the lab coordinate system. Figure 6.4.1 shows the segments' mean traces of $\boldsymbol{H}_{\mathbf{RS}}$, pointing in the direction towards the driving target (lab X). Of the components of $\boldsymbol{H}_{\mathbf{T}}$ observed ($\boldsymbol{H}_{\mathbf{L}}$, $\boldsymbol{H}_{\mathbf{RP}}$, and $\boldsymbol{H}_{\mathbf{RS}}$), $\boldsymbol{H}_{\mathbf{RS}}$ shows peaks of the largest magnitudes. In addition, the traces from other segments show paths that are quite distinct from one another. In Figure 6.4.1, the Club section has a small positive peak in both the backswing and the downswing, while the other segments tend to peak in opposite directions. Also, the Torso segment showed a negative peak in the downswing, while the other segments show positive peaks.

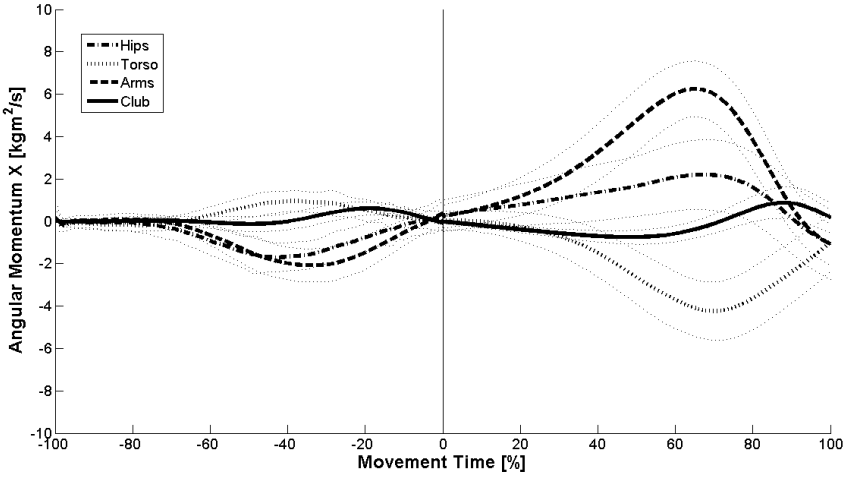

Figure 6.4.1: Remote solar angular momentum towards target (lab X). $H_{SP\text{-}X}$ is measured along the ordinate in *kg m²/s*. The abscissa measures normalized time. Means are shown using thick traces. Standard deviations are shown above and below their respective means using small dotted lines.

Remote solar angular momentum about the axis pointing vertically upward ($\boldsymbol{H}_{\mathbf{RS\text{-}Y}}$) is shown in Figure 6.4.2. The magnitude of the Club and Arm segments' peaks are much higher in $\boldsymbol{H}_{\mathbf{RS\text{-}Y}}$ than other components observed. In Figure 6.4.2, the Club segment is observed to undergo a positive peak in the downswing proceeded by a decrease in the Arms segment before it. Similarly, the Arms segment is observed to

undergo an increase in $\boldsymbol{H}_{\mathbf{RS\text{-}Y}}$ after a decrease in the Torso segment preceding it. In addition, the Hips segment is observed to undergo a decrease in $\boldsymbol{H}_{\mathbf{RS\text{-}Y}}$ preceding the Torso.

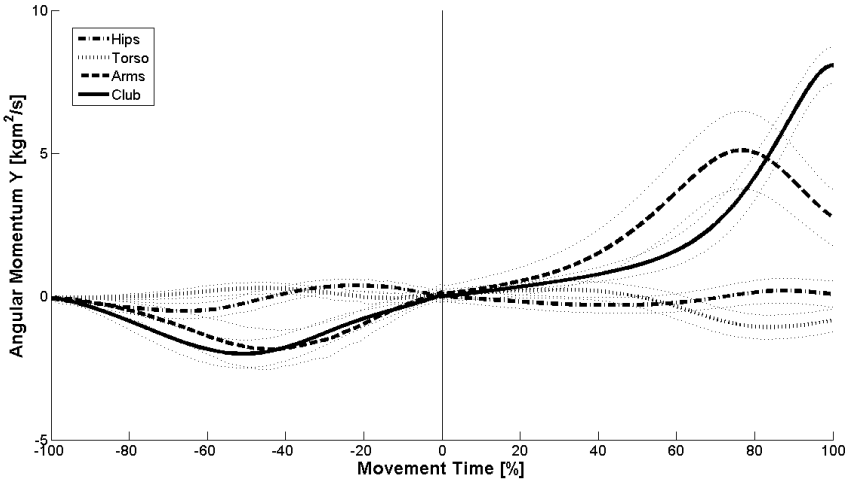

Figure 6.4.2: Remote solar angular momentum vertical up (lab Y). $H_{SP\text{-}Y}$ is measured along the ordinate in *kg m²/s*. The abscissa measures normalized time. Means are shown using thick traces. Standard deviations are shown above and below their respective means using small dotted lines.

Remote solar angular momentum about the axis pointing towards the ball at takeaway ($\boldsymbol{H}_{\mathbf{RS\text{-}Z}}$) is shown in Figure 6.4.3. The axis describes momentum rotating about the golfer's frontal plane. The traces of $\boldsymbol{H}_{\mathbf{RS\text{-}Z}}$ are quite distinct from other components of $\boldsymbol{H}$ observed. In the downswing section of Figure 6.4.3, the Hips and Arms sections peak early. These segments peak and begin to decrease again, meanwhile the Club and Torso sections between to quickly increase in $\boldsymbol{H}_{\mathbf{RS\text{-}Z}}$. Interestingly, the peaks and valleys of adjacent segments are related in Figure 6.4.3 as they were in Figure 6.4.2. It is observed in Figure 6.4.2, when the Club segment shows a positive peak, the adjacent distal segment (the Arms), undergoes a local minimum or valley. Similarly, when the Arms

segment peaks, the Torso segment shows a valley. And when the Torso segment is at a local maximum in the downswing, the Hips segment undergoes a valley. Figure 6.4.3 shows the same phenomenon. When the Club undergoes a positive peak during the downswing, the Arms undergo a valley. When the Arms peak, the Toro valleys. And finally, earlier in the backswing, when the Torso undergoes a positive peak, the Hips show a valley. What is different about the $\boldsymbol{H}_{\mathbf{RS\text{-}Z}}$ traces in Figure 6.4.3 is that the Torso segment does not plateau after its valley as it does in the $\boldsymbol{H}_{\mathbf{RS\text{-}Y}}$ trace of Figure 6.4.2. The Torso undergoes a large, positive increase in $\boldsymbol{H}_{\mathbf{RS\text{-}Z}}$ after the valley.

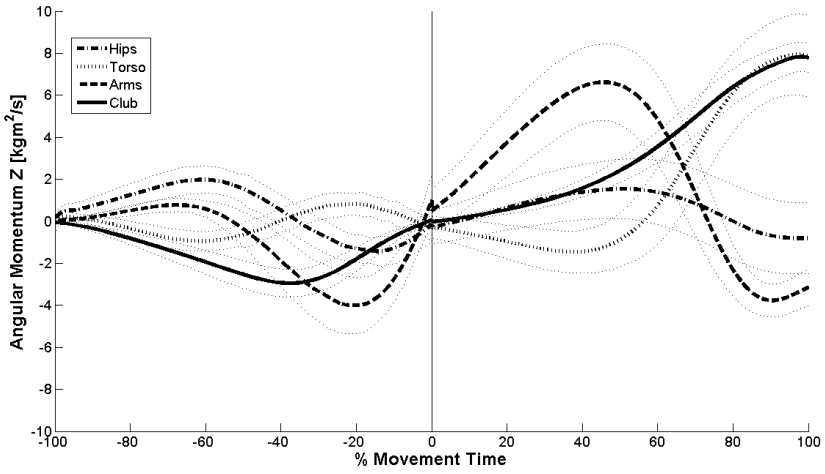

Figure 6.4.3: Remote solar angular momentum towards ball (lab Z). $H_{SP\text{-}Z}$ is measured along the ordinate in $kg\ m^2/s$. The abscissa measures normalized time. Means are shown using thick traces. Standard deviations are shown above and below their respective means using small dotted lines.

The relative timings of the $\boldsymbol{H}_{\mathbf{RS}}$ peaks are shown in Figure 6.4.4. Each bar measures the mean timing of the positive maximum peak. About the axis pointing towards the target, the segment timings do not seem to follow a P-D progression. The Torso shows the first maximum peak during the backswing (MT -25.7%), and the Arms segment shows the latest positive peak during the downswing (MT 64.4%). Looking at

the progression of $\boldsymbol{H}_{\mathbf{RS\text{-}X}}$ peaks in Figure 6.4.1 tells a different story. Here the Club segment undergoes a local maximum right before impact. This occurs when the Arms segment decreases following an Arms peak. The Arms segment itself undergoes a peak as the Torso segment displays a negative valley. And further, the Torso segment peaks during the backswing during a decrease in Hips $\boldsymbol{H}_{\mathbf{RS\text{-}X}}$. This hasn't been represented in the bar graph of Figure 6.4.4.

About the axis pointing vertically upward, the peaks show a positive to distal progression except for the Torso segment. This segment peaked in the downswing. Looking back at Figure 6.4.2, the Torso segment underwent a positive peak around MT 35%, although this peak was not as large as it's previous positive peak during the backswing.

About the axes pointing towards the ball at takeaway, a P-D pattern was not seen. The Torso segment peaked near ball contact (MT 95.5%). Also, the Hips segment has not peaked here as early in the backswing as what was shown in Figure 6.4.3.

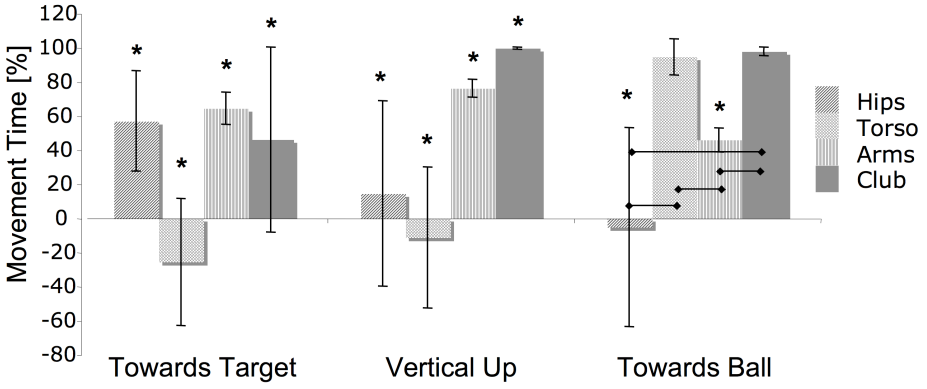

Figure 6.4.4: Remote solar angular momentum time to peak. Time has been expressed as a percentage of MT. Standard deviation is shown using vertical error bars. Horizontal bars represent statistical difference in pair wise comparisons. Asterisks represent significant difference from all other segments. Time to peak has been analyzed in the 3 directions of the lab coordinate system separately.

The mean magnitudes of the $\boldsymbol{H}_{\mathbf{RS}}$ peaks are shown in Figure 6.4.5. In the direction pointing towards the target, the Club segment showed the least angular momentum (1.1 *kg* m^2/s) while the Arms segment showed the most (6.6 *kg* m^2/s). The largest change in $\boldsymbol{H}_{\mathbf{RS\text{-}X}}$ between adjacent segments came at the connection point between the Arms and the Club. This showed a decrease of 5.4 *kg* m^2/s. About the axis pointing vertically upward, the magnitude of the segment peaks proceeded in a P-D manner. The Club segment showed the largest $\boldsymbol{H}_{\mathbf{RS}}$ (8.1 *kg* m^2/s). This was preceded by the Arms segment (5.3 *kg* m^2/s), and the Torso and Hips segments (~0.5 *kg* m^2/s). About the axis pointing towards the ball at takeaway, the peaks again did not follow a P-D progression. The Hips segment was the lowest at 2.8 *kg* m^2/s, followed by the Arms segment at 7.0 *kg* m^2/s, then the Club segment at 7.8 *kg* m^2/s. The Torso segment was found to have the highest peak in $\boldsymbol{H}_{\mathbf{RS\text{-}Z}}$ at 8.2 *kg* m^2/s.

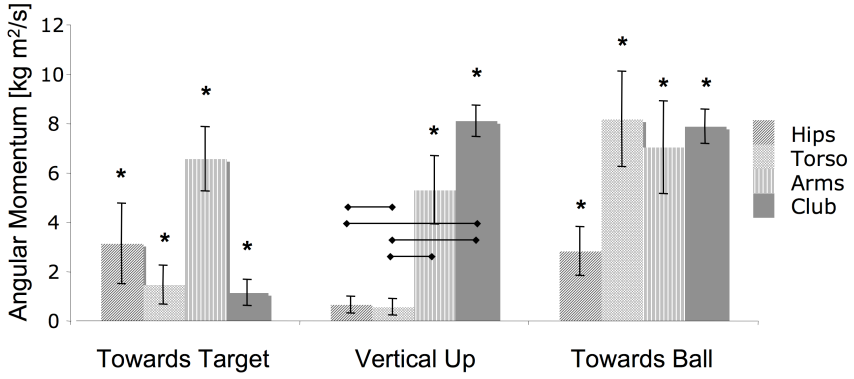

Figure 6.4.5: Remote solar angular momentum peak magnitudes. H_{RS} is measured in kg m^2/s. Vertical error bars represent standard deviation. Asterisks show statistical difference from all other segments. Horizontal bars represent statistical difference in pair wise comparisons. H_{RS} has been analyzed in the 3 directions of the lab coordinate system separately.

6.4.1 *Remote Solar Angular Momentum Summary*

Remote solar angular momentum ($\boldsymbol{H}_{\mathbf{RS}}$) is the term that has been used to describe the apparent momentum of the segment center of gravities rotating about the golfer system center of gravity. In the 3 line graphs describing $\boldsymbol{H}_{\mathbf{RS}}$ about the axes of the lab coordinate system, a pattern is found. When a distal segment goes through a local positive maximum, its proximal neighbour is shown to go through a local negative minimum. In other words, distal peaks have occurred at the same time as proximal valleys. Furthermore, positive peaks of proximal segments precede the local peaks of their respective distal neighbours. This pattern is seen in Figure 6.4.1 through Figure 6.4.3.

From this pattern it would be expected that the bar graphs in Figure 6.4.4 should also reflect a P-D progression of timing. This was not the case. The P-D pattern found of the timing of peaks in mean $\boldsymbol{H}_{\mathbf{RS}}$ was not found to match the pattern of mean timing of $\boldsymbol{H}_{\mathbf{RS}}$ peaks.

The magnitudes of the peaks in $\boldsymbol{H}_{\mathbf{RS}}$ did not follow a clear P-D progression. In the plane normal to the driving target, the Club segment had the lowest $\boldsymbol{H}_{\mathbf{RS}}$ (1.1 $kg\ m^2/s$). About the frontal plane, the Torso segment had the highest $\boldsymbol{H}_{\mathbf{RS}}$ (8.2 $kg\ m^2/s$). Apart from these observations, a P-D progression of magnitude was generally followed.

6.5 Club Plane Angular Momentum

The mean club plane angular momentum ($\boldsymbol{H}_{\mathbf{CP}}$) of the Hips, Torso, Arms and Club segments are shown in Figure 6.5.1. $\boldsymbol{H}_{\mathbf{CP}}$ is a projection of the segments' total angular momentum ($\boldsymbol{H}_{\mathbf{T}}$) along the plane of the Club head in the downswing. It is an expression of a segment's angular momentum in the direction relative to the club-ball collision.

All segments went through a small negative peak of $\boldsymbol{H_{CP}}$ during the backswing, then a larger positive peak in $\boldsymbol{H_{CP}}$ during the downswing. The Arms segment was late to peak in $\boldsymbol{H_{CP}}$ during the backswing but the first to peak during the downswing. Interestingly, the final peak in magnitude for the Torso and Club segments seem to coincide with decreases in the Hips and Arms segments. The timing and magnitude of the peaks will be examined in further detail below.

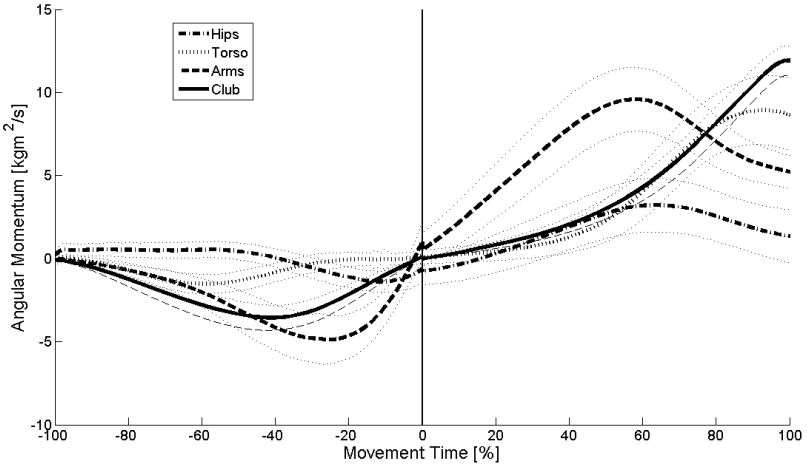

Figure 6.5.1: Club Plane Angular Momentum during the golf swing. Normalized movement time (MT) is measured along the abscissa. MT-100 = takeaway; MT 0 = top of backswing; and MT 100 = ball contact. Angular momentum is measured in *kg m^2/s* along the ordinate. Golfer segment mean angular momentum traces are shown in thick lines. Standard deviation is shown in smaller dotted lines above and below the means.

The timing of the $\boldsymbol{H_{CP}}$ peaks is shown in Figure 6.5.2. The backswing and downswing have been analyzed separately. In both the backswing and the downswing, all segments' peak timings were found to be statistically different from one another. In the backswing, the Torso and Club segments were the first to peak at MT -53.4% and MT -41.0% respectively. The Arms and Hips segments were the last to peak during the backswing at MT -26.8% and MT -11.7% respectively. In the downswing, we saw a reversal of this pattern. The Arms and Hips segments were now the first to peak, at MT

57.8% and MT 66.1% respectively. The Torso and Club were then the last segments to peak at MT 91.5% and MT 99.2% respectively.

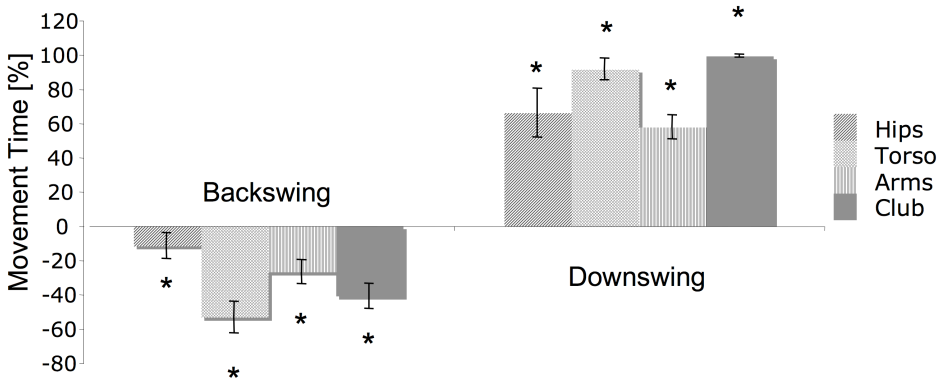

Figure 6.5.2: Time to peak club plane angular momentum during the golf swing. Peak timing has been analyzed in the backswing and downswing separately. Time has been expressed as a percentage of MT; where -100 = takeaway, 0 = top of backswing, and 100 = ball contact. Standard deviation is shown using vertical error bars. Asterisks represent significant difference from all other segments.

The peak magnitudes of $\boldsymbol{H_{CP}}$ are shown in Figure 6.5.3. In the backswing, the Arms segment had the largest negative $\boldsymbol{H_{CP}}$ peak at -5.2 $kg\ m^2/s$. The backswing $\boldsymbol{H_{CP}}$ magnitude did not follow a P-D pattern. However, $\boldsymbol{H_{CP}}$ magnitude clearly followed a P-D sequence in the downswing. $\boldsymbol{H_{CP}}$ increased in magnitude from the Hips segment out to the Club segment, which showed a peak of 12.0 $kg\ m^2/s$. The largest increase between adjacent segments came at the connection point between the Hips and Torso segment. This amounted to 5.4 $kg\ m^2/s$ or 45% of the peak Club $\boldsymbol{H_{CP}}$.

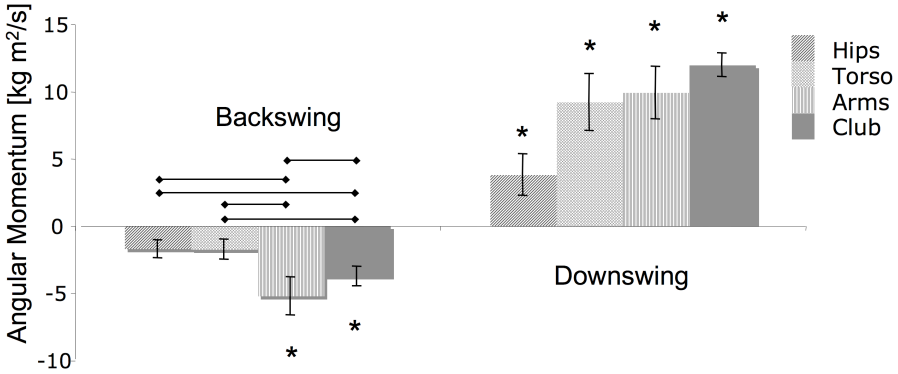

Figure 6.5.3: Peak club plane angular momentum during the golf swing. The downswing and backswing peaks have been analyzed separately. H_{CP} is measured in kg m²/s. Vertical error bars represent standard deviation. Asterisks show statistical difference from all other segments. Horizontal bars represent pair-wise statistical difference.

6.5.1 Club Plane Angular Momentum Summary

The traces of mean segment $\boldsymbol{H_{CP}}$ were negative in the backswing and positive during the downswing. The Arms segment was late to peak during the backswing (MT -26.8%) but the first to peak during the downswing (MT 57.8%). The final peaks of the Club and Torso segments during the downswing coincided with a decrease in $\boldsymbol{H_{CP}}$ in the Arms and Hips segments. During the backswing, the Torso and the Club segments were the first to peak (MT -53.4% and MT -41.0% respectively). However, these segments were the last to peak in $\boldsymbol{H_{CP}}$ during the downswing (MT 91.5% and MT 99.2% respectively). The magnitude of $\boldsymbol{H_{CP}}$ peaks did not follow a P-D pattern during the backswing. The Arms showed the largest magnitude of peak during the backswing at -5.2 $kg\ m^2/s$. In the downswing, $\boldsymbol{H_{CP}}$ peaks increased in magnitude in a P-D pattern starting at the Hips segment (3.8 $kg\ m^2/s$) and moving sequentially out to the Club segment (12.0 $kg\ m^2/s$). The largest increase between adjacent segments occurred at the connection point between

the Hips and Torso segments. This accounted for 5.4 *kg* m^2/s or 45% of the peak Club $\boldsymbol{H}_{\mathbf{CP}}$.

6.6 Absolute Angular Momentum

Absolute angular momentum ($\boldsymbol{H}_{\mathbf{AT}}$) is the term that has been used here to describe an absolute, scalar measurement of the three-dimensional total angular momentum ($\boldsymbol{H}_{\mathbf{T}}$) vector. Mean $\boldsymbol{H}_{\mathbf{AT}}$ has been calculated for each segment in Figure 6.6.1. The four golfer segments undergo a small peak in $\boldsymbol{H}_{\mathbf{AT}}$ during the backswing, and a larger peak again during the downswing. In the downswing the magnitude and relative timing of the peaks do not occur in a P-D pattern. The specific magnitudes and timings of these peaks will be discussed in detail below.

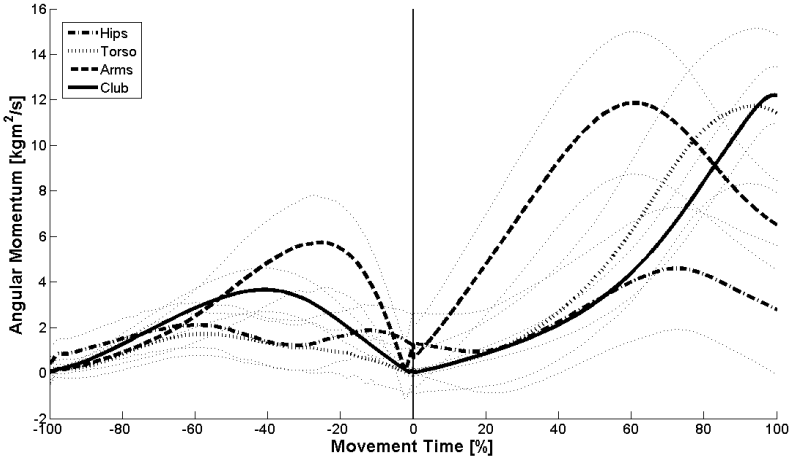

Figure 6.6.1: Absolute total angular momentum in the golf swing. H_{AT} is measured along the ordinate in *kg* m^2/s. The abscissa measures normalized time. Means are shown using thick traces. Standard deviations are shown above and below their respective means using small dotted lines.

The relative timings of the $\boldsymbol{H}_{\mathbf{AT}}$ peaks are shown in Figure 6.6.2 for the backswing and downswing separately. In the backswing, the Torso segment was the first to peak at MT -46.1%. The Hips and the Clubs segments, which peaked at around MT -39%, followed that. The last segment to peak in $\boldsymbol{H}_{\mathbf{AT}}$ in the backswing was the Arms segment (MT -20.7%). In the downswing, the Arms segment was the first to peak MT 60.6%. The Club segment peaked last, just prior to impact at MT 99.1%. The largest delay between adjacent segments occurred at the connection point between the Arms and the Club segments. This accounted for MT 38.6%.

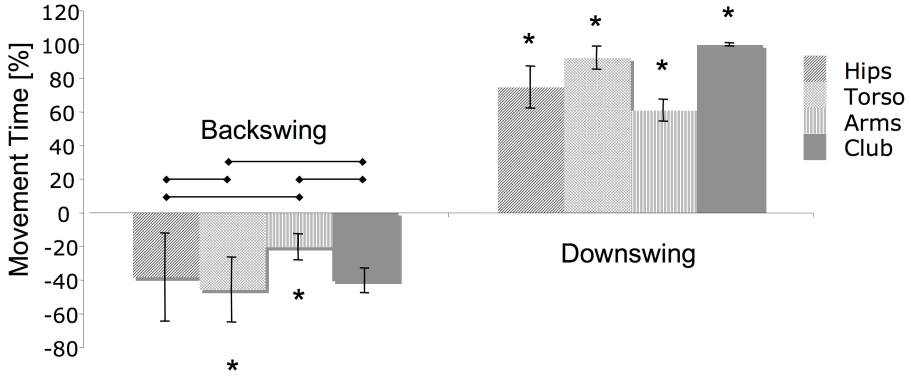

Figure 6.6.2: Absolute total angular momentum time to peak during the golf swing. The backswing and the downswing have been analyzed separately. Time has been expressed as a percentage of MT. Standard deviation is shown using vertical error bars. Asterisks represent significant difference from all other segments.

The mean magnitudes of the $\boldsymbol{H}_{\mathbf{AT}}$ peaks are shown in Figure 6.6.3 for the backswing and downswing separately. In the backswing, the Arms segment had the highest peak at 6.3 $kg\ m^2/s$. This was approximately double the $\boldsymbol{H}_{\mathbf{AT}}$ seen in other segments in the backswing. In the downswing, the Hips segment showed the least amount of $\boldsymbol{H}_{\mathbf{AT}}$ at 5.6 $kg\ m^2/s$. Interestingly, the Torso, Arms and Club segments all had

approximately the same amount of absolute, total angular momentum in the downswing. This value was approximately 12.3 $kg\ m^2/s$.

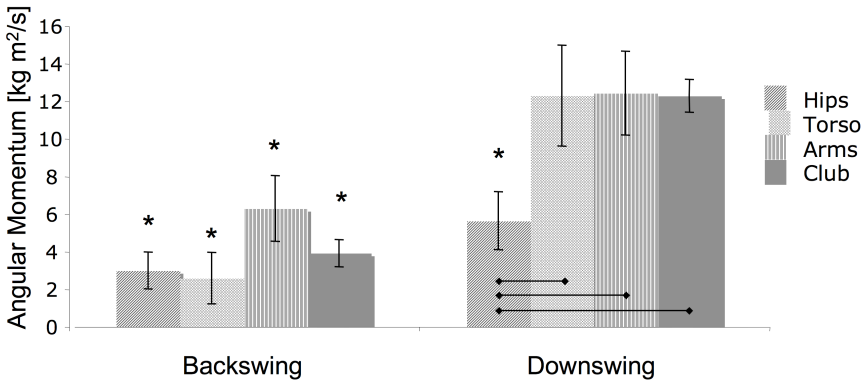

Figure 6.6.3: Absolute total angular momentum peak during the golf swing. The backswing and the downswing have been analyzed separately. Error bars signify standard deviation. Horizontal bars show pair-wise significant difference. Asterisks signify statistical difference from all other segments.

Figure 6.6.4 describes the $\boldsymbol{H}_{\mathbf{AT}}$ of each golfer segment broken up into its constitutive components. The Hips segment contained much less momentum than the other segments. The Arms segment was the first to peak during the downswing. This segment contained primarily $\boldsymbol{H}_{\mathbf{RP}}$ and $\boldsymbol{H}_{\mathbf{RS}}$. The Torso segment was the next to peak. Approximately two-thirds of this segment's $\boldsymbol{H}_{\mathbf{AT}}$ was $\boldsymbol{H}_{\mathbf{RS}}$. The Club segment was the last to peak. This segment contained primarily $\boldsymbol{H}_{\mathbf{RS}}$.

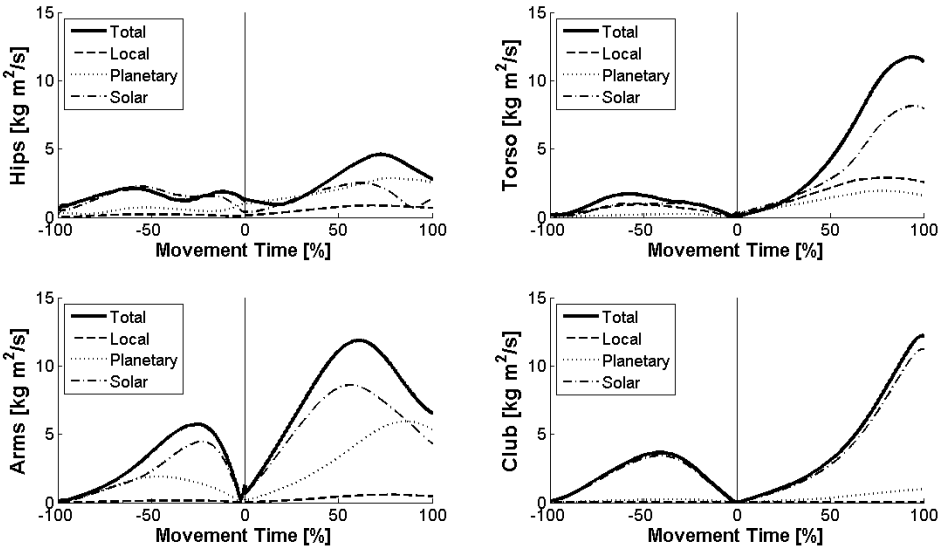

Figure 6.6.4: Absolute angular momentum and its components for the four golfer segments. Absolute values of total, local, remote planetary and remote solar angular momentum have been shown for each segment. Time is shown along the abscissa and has been normalized as a percentage of movement. The ordinate measures angular momentum in *kg m²/s*.

6.6.1 Absolute Angular Momentum Summary

Absolute angular momentum ($\boldsymbol{H}_{\mathbf{AT}}$) is a scalar expression of total angular momentum ($\boldsymbol{H}_{\mathbf{T}}$) vector. It gives a directionless interpretation of overall angular momentum contained within a segment during the golf swing. The timings of $\boldsymbol{H}_{\mathbf{AT}}$ peaks were calculated separately for the backswing and downswing to see if a P-D pattern was visible. In the backswing, the Torso and the Club were the first segments to peak, followed by the Hips and Arms segments. This pattern was reversed during the downswing, where the Torso and Club segments were found to be the last segments to peak. In the downswing, the largest delay between adjacent segments occurred at the connection point between the Arms and Club segments. This accounted for MT 38.6%. There was no evidence for sequential timing in the backswing or the downswing. The magnitudes of $\boldsymbol{H}_{\mathbf{AT}}$ peaks were also analyzed. In the backswing, the Arms segment

contained approximately double the amount of angular momentum of the other segments (6.3 $kg\ m^2/s$). In the downswing, the Hips segment contained about half the angular momentum of the other segments (5.6 $kg\ m^2/s$). Interestingly, the Torso, Arms and Club segments all contained approximately the same amount of angular momentum in the downswing (~12.3 $kg\ m^2/s$).

Chapter Seven: Discussion

7.1 Introduction

The purpose of this study was to develop a basic understanding of segment interaction in generating speed in the golf swing. The preceding results have examined angular kinematics, kinetic energy and angular momentum in the golf swing. These variables have been characterized by describing the timing and magnitude of their peaks. The objective of this analysis was to compare the observed patterns of peak timing and magnitudes with a whip-like proximal to distal (P-D) order that has been observed to be optimal for speed production in other sports (Bunn, 1972; Joris *et al*, 1985; Herring and Chapman, 1992).

It has been previously stated that highly skilled golf subjects have been used to decrease variability and ensure repeatability in our measurements. In addition to this benefit, skilled golfers are of interest because they are, *de facto*, skilled. Any player who has achieved a registered handicap of +5 or better has, by definition, honed a successful swing. The pattern of player segments peak timings and magnitudes that have been presented can be thought of as a successful solution set; producing a swing that satisfies the criteria of par on registered courses.

There is an underlying paradox in this discussion of motion patterns of skilled golfers. It is assumed that the swing patterns presented are those of "pre-optimized" players, whose swings are highly accurate, fast and presumably highly efficient. At the same time, the results are being viewed in a framework that inherently presumes the

motion pattern may still be improved. The purpose of viewing the patterns of peak timing and magnitudes is to garner information for the improvement of maximum speed or efficiency of the swing. It is with a certain level of humility that we suggest that golf swings of touring professionals need improvement. The results presented here are in regards to speed or efficiency of speed creation, which is only one ingredient of a successful swing. By comparing the pattern of motion seen in the golf swing to the predominant pattern seen in other sports, this discussion aims to show how skilled golfers may be able to swing faster.

7.2 Angular Kinematics

Coleman and Rankin (2005) have noted that the golf swing is a complex, three-dimensional movement that cannot fit reasonably in a single plane. However, it is speculated that the motion of the individual segments are highly planar, and that two dimensional simplifications of the golf swing can be made by looking at the movement of the golfer segments within their respective swing planes. In the following section, relative patterns of segment kinematics are explored using a simplified, planar approach.

7.2.1 Angular Position

The timings of the segment angular position (θ) peaks are descriptors of when the segments change direction during the backswing and move toward their respective impact θ. The first peak occurred with the Hips segment, followed by the Arms, Torso and Club segments, respectively. The Hips and Arms rotate in the downswing prior to the

Torso segment. It may be possible that energy transfer through the torso is inefficient; this sequence is not common in other human motions.

The magnitudes of peak $\boldsymbol{\theta}$ increased in a P-D manner. However, the relative angular displacements at each connection point did not increase in a distal fashion. The largest relative angular displacements were at the wrist, or the connection point between the Arms and Club segments and the connection point between Hips and Torso segments. Relative angular displacement between the Torso and Arms segment is likely geometrically constrained at the left shoulder (or the connection point between the Torso and Arms segments) as the left arm is forced to swing in front of the chest. It is speculated that large relative angular displacements between segments allow for larger gains in relative $\boldsymbol{\omega}$ between those segments. The relative difference in $\boldsymbol{\omega}$ will be described in section 7.2.2 below.

In a whip-like, P-D motion pattern, one would expect that the $\boldsymbol{\theta}$ of a proximal segment should continually precede the $\boldsymbol{\theta}$ of that segment's distal neighbour throughout a movement. In the golf swing, if motion were to follow the optimal pattern of other sports, we would expect the $\boldsymbol{\theta}$ of a proximal segment to be closer to impact position than the $\boldsymbol{\theta}$ of its distal neighbours throughout the downswing. However, at approximately MT 80%, the $\boldsymbol{\theta}$ of the Arms segment passes and then leads the $\boldsymbol{\theta}$ of the Torso segment. This does not follow the optimal P-D pattern seen in other sports. If a proximal segment lags in $\boldsymbol{\theta}$ behind its distal neighbour, rotational energy may be transferred proximally toward the core.

Solving for the loading of joints between segments is a complex problem that involves the relative $\boldsymbol{\theta}$, $\boldsymbol{\omega}$ and relative momentums of the attached links (Felter and

Dapena, 1989). It is not within the intended scope of this project to provide a mathematical proof showing why segment θ should precede P-D to effectively transfer energy in a distal direction. It has been shown that P-D motion is a robust solution for speed creation (Herring and Chapman, 1992). It is unknown if simulation research has been performed to explain why θ should proceed P-D. However, a more straightforward explanation will be provided. If a segment is closer to its position at impact during the downswing, the profile of its ω must decrease before impact (or else the impact position will be passed). Conversely, segments lagging further away from their final impact θ must increase in ω before impact (or else the impact position will not be reached).

The distal endpoint velocity is the defining speed measurement of the system. It is more efficient to increase ω progressively from core to club. Increasing ω in segments proximally uses kinetic energy that may otherwise be transferred to the club. Angular velocity and kinetic energy of the segments are discussed further in sections 7.2.2 and 7.4.1 below.

7.2.2 Angular Velocity

During the downswing, the magnitudes of ω peaks increased in a distal fashion. The increase in relative ω of the player segments was proportional to the relative angular displacement of these segments at the top of the backswing. The largest increase in ω between adjacent links happened at the wrist, followed by the connection point between the Torso and Hips. These joints showed the largest relative angular displacements at the top of backswing. There was a small increase in ω at the shoulder connection point. This may be evidence that the amount of ω created in any segment may have as much to do

with its relative angular displacement during the backswing as with optimizing the relative tempo between player segments.

The peak magnitude of the Torso and Arms ω both occurred at approximately MT 75%. It is interesting what occurred to the ω in each segment after this point. The ω of the Arms segment decreased sharply, the ω of the Club segment began to rise sharply, and the ω of the Torso section maintained a plateau until impact. It is unknown what the benefit of maintaining such a high Torso ω carries, if any. It may be argued that the velocity of the Club segment may directly benefit in an additive sense from a high velocity of the Torso by means of the "*superpositioning*" principal (Koniar, 1973). However, if this principal were correct, the Arms segment ω should not have decreased. It is argued that maintaining a high angular velocity in a segment with considerable mass such as the Torso uses a large amount of kinetic energy that may otherwise be transferred to the club head.

7.2.3 Angular Acceleration

The angular accelerations (α) of the player segments were analyzed during the downswing. The Arms segment α was the first to reach a maximum, followed by the Hips, Torso and Club segments, respectively. While the timings of the body segments α were found to be significantly different from each other, the differences between peak timings were relatively small when compared to the Club peak. The three body segments all showed an α peak at approximately MT 50%, while the Club segment did not peak in α until MT 90%. In terms of α, the pattern of the golf swing can be described as a double

pendulum consisting of a rotating body segment and a club. It is not surprising that the early 2D double pendulum models of the golf swing were able to realistically predict the kinematics of a real swing (Cochrane and Stobbs, 1968; Jorgensen, 1970; Pyne, 1977).

Body segment α can be produced either actively by a muscle moment acting on a joint, or passively, by a reaction force acting on a joint (Nesbit and Serrano, 2005). It appears that the work being supplied to the body segments, whether actively or passively, began to decline half-way through the downswing. Ideally, each segment α should approach zero prior to impact. This implies that all energy being made available to increase speed has been imparted to the ball before it is too late to matter (Nesbit and Serrano, 2005). The reversal of Club α just prior to impact supports the finding by Nesbit and Serrano (2005) that total body power switches from positive to negative around the time of impact. Those authors went on to say that a golfer's ability to time the zeroing of total body power with impact was a strong indicator of that golfer's skill. The large negative accelerations of the Club and Arms segments before impact could indicate that on average, our sample population was premature in reversing their segment power. It should be noted that presence of joint power has been speculated based on segment α. Joint power has not been determined in this study.

The largest gain in α peak magnitude between adjacent segments happened at the connection point between the Torso and Hips segments. This result supports the finding of Nesbit and Serrano (2005) who calculated that the lumbar region of the spine does the majority of the mechanical work in the golf swing.

7.3 Angular Kinematics Summary

The angular kinematics of the golf segments did not follow a simple P-D motion pattern. Movement of the Hips and Arms segments initiated the downswing motion. The maximum relative angular displacement between adjacent segments may be an indicator of how much relative velocity can be generated between those segments. This was supported by the pattern of peak ω, which closely resembled the shape of the θ magnitude peaks. It was noted that the segments' peak θ in the backswing might be the best indicator of how much ω may be achieved in the downswing. The small increase in peak ω between the Torso and Arms segments might be influenced by the inability to achieve a large difference in peak θ at the shoulder connection point. The geometrical constraints of the left shoulder joint during the backswing may be a limiting factor in swing speed generation.

At approximately MT 80%, the θ of the Arms segment was closer to its position at impact than the Torso segment, its proximal neighbour. The Arms, therefore, travelled with a decreased ω for the remainder of the downswing in order to avoid overshooting the impact position. In this way, the non-sequential angular displacement of body segments coincided with a speed progression that moved proximally toward the core. This was evidenced by the mean ω traces of the segments during the downswing. From MT 75% to ball impact, the ω of the Arms segment underwent a drastic decrease, while the ω of the Torso segment was maintained at a peak plateau. Maintaining a high ω in a segment of such large mass is likely a waste of kinetic energy that could otherwise be made available to the club.

From an α standpoint, the golf swing may be effectively described as a double pendulum. This evidence helps to explain why early 2D double pendulum models of the golf swing were able to recreate realistic kinematics (Cochrane and Stobbs, 1968; Jorgensen, 1970; Pyne, 1977).

Club segment α reverses and becomes negative just prior to impact. This finding supports the phenomenon reported by Nesbit and Serrano (2005) of players being able to "zero" their total power output around ball contact.

The largest gain in α between neighbouring segments occurred at the connection point between the Torso and Hips. This supported the finding by Nesbit and Serrano (2005) that the lumbar region in the spine created the greatest amount of mechanical work of any joint in the golf swing.

7.4 Kinetic Energy

Previous studies of dinosaur tails (Myhrvold and Currie, 1997) and overhand throwing (Joris *et al*, 1985) have shown that P-D whip like motion can create fast and efficient musculo-skeletal movements. One purpose of this investigation was to compare the patterns of KE development in the golf swing with a P-D pattern, as seen in a whip.

7.4.1 Total Kinetic Energy

The earlier work of Nesbit and Serrano (2005) used a joint energetics approach to calculate mechanical work performed in the golf swing. At the time of writing, Nesbit and Serrano's joint energetics method is the gold standard for estimating mechanical work in the golf swing. Those authors reported a maximum figure of 355 J for the total

work performed by a scratch golfer during the downswing. In this investigation, a segmental energetics approach was used: the system's total kinetic energy (KE_T) was found by summing KE_T for the golfer segments. The system mean KE_T peak was found to be 310 J. The difference in energy magnitude found between this study and theirs is likely explained by study population sizes; the estimation of total work in this paper represents the swings of 447 near scratch golfers while the Nesbit and Serrano figure is based on an *n* of 1.

Potential energy was not taken into account into the total system energy in this study. It is speculated that the downswing should produce an overall loss in potential energy, which would increase the difference between the two estimations. Despite the differences between the two methodologies, the difference between the work values represents only 12.5% of the gold standard total. This gives support to the method employed in this study as the total energy calculated was similar to the current literature standard. This is the first known comparison of segmental and joint energy calculations in the golf swing.

The KE_T of the player segments did not peak in timing in a P-D fashion. The body segments (Hips, Torso and Arms) all peaked simultaneously around MT 80%. The Club segment peaked just prior to impact. The only connection point that showed a delay in KE peaks between adjacent segments was the wrist. It is speculated then that the only connection point that may allow for an efficient transfer of energy between neighbouring segments could be the wrist. In terms of KE, the golf system may faithfully be represented as two segments: the body and the club. This result mirrors the finding of body-club delay found in α.

The magnitudes of segmental KE_T increased in a P-D fashion. This is unlike the situation found in whip energetics where we would expect segmental peaks to be conserved. The addition of KE_T in each segment peak suggests that the golfer is doing additional work on the segments at the joints. This was supported by the model of Nesbit and Serrano (2005), which showed that the lumbar spine, shoulders and wrists do positive work.

It should be noted that the planes of segment motion tend to become more vertical moving from the Hips out to the Club. It is possible that gravity is responsible for some of the additional energy gained by segments whose motion contains components in the vertical plane. However, the gain in energy between segments is too great to be explained by converted potential energy alone.

The majority of the gain in energy between segments was found at the wrist, followed by the shoulder connection point. This finding is counter-intuitive from the viewpoint of the article by Nesbit and Serrano (2005), who found that joint work generally decreased in a P-D manner. It is unknown why this study found the biggest difference in energy magnitudes at distal joints while Nesbit and Serrano calculated that those joints performed the least mechanical work. It is speculated that joints displaying a high level of efficiency of energy transfer may not have created large magnitudes of net mechanical work in the Nesbit and Serrano model.

KE_T was calculated as the sum of translational KE (KE_{TR}), local rotational KE (KE_{LR}) and remote rotational KE (KE_{RR}). KE_T in the Torso segment was mostly comprised of KE_{LR}. KE_T in the Arms segment was nearly evenly divided between KE_{RR} and KE_{TR}. In the Club segment, KE_T was almost entirely comprised of KE_{TR}. The golf

swing may then be thought to convert rotational kinetic energy in the core to translational kinetic energy at the club head. This result is intuitive as the Torso segment COM and Arms segment COM are nearer to the system center of rotation while the Club segment COM is close to the distal end of the club, which has a high translational velocity.

Interestingly, the Hips segment contains a nearly equal balance between $KE_{\mathbf{LR}}$, $KE_{\mathbf{RR}}$ and $KE_{\mathbf{TR}}$. The division in rotational energy between $KE_{\mathbf{LR}}$ and $KE_{\mathbf{RR}}$ is largely determined by how a segment is divided into its rigid body elements; thus the relative differences found between these two types of rotational energy is largely arbitrary. The addition of $KE_{\mathbf{TR}}$ at the Hips is evidence that this segment not only rotates during the downswing but also translates during a lateral weight shift as reported by McTeigue (1994).

7.4.2 Translational Kinetic Energy

The majority of the energy contained in both the Club segment and the system as a whole was $KE_{\mathbf{TR}}$. The pattern displayed by the timing and magnitude of $KE_{\mathbf{TR}}$ peaks was generally P-D. Interestingly, this was the only KE measurement that showed this trend. This is most likely because the proximal segments generally contained more rotational energy than $KE_{\mathbf{TR}}$.

$KE_{\mathbf{TR}}$ comprised nearly one third of the Hip $KE_{\mathbf{T}}$. It is speculated that the lateral hip shift, as reported by McTeigue (1994), is responsible for this translational energy. The Hips segment $KE_{\mathbf{TR}}$ is roughly 5 J, approximately 2.4% of the Club segment $KE_{\mathbf{T}}$. McTeigue noted that the lateral hip shift was a swing characteristic indicative of skilled players. It is generally accepted that this hip shift is important in a successful swing,

however the purpose is generally not well understood. From the relative magnitude of the Hips and Club KE_{TR} peaks, it would seem that the translational energy gained from shifting the hips does not have a large effect on the overall energy contained in the Club segment. Instead, it is likely that the lateral hip segment is related to the relative positioning of the spine and shoulder joints, allowing for efficient energy transfers to the Club segment.

7.4.3 Local Rotational Kinetic Energy

KE_{LR} describes the rotational energy of a segment's rigid bodies rotating about their own COM's. The patterns for timing and magnitude of the KE_{LR} peaks were not P-D. The magnitudes of KE_{LR} were relatively small compared to other kinds of energy measurements. The Club segment contained almost none of this type of energy.

The Torso segment contained the greatest amount of KE_{LR}; the KE_{LR} accounted for nearly two thirds of the segment KE_{T}. The high amount of KE_{LR} seen in the Torso segment is because this segment contained large rigid bodies with high moments of inertia. The largest increases in rotational energy between adjacent segments occurred at the connection point between the Hips and Torso. This data supports the finding of Nesbit and Serrano (2005) that the lumbar spine region was responsible for the greatest amount of mechanical work in the swing.

7.4.4 Remote Rotational Kinetic Energy

KE_{RR} describes the rotational energy of a segment rotating around its own COM. The patterns of timing and magnitude peaks were not P-D for this type of energy. The Arms

contained the most KE_{RR} of any segment. The Arms segment shows a clear decrease in KE_{RR} after its peak. This data would suggest that the hands are being actively slowed before ball contact. This finding supports the work by Pyne (1977), who was the first author to show that slowing of the hands before ball contact may increase the effectiveness of "wrist snap".

The onset in Club segment KE_{RR} at MT 50% does not coincide with the peaking of the Arms segment KE_{RR} at MT 80%. The peaking of Arms segment KE_{RR} does however coincide with the rapid increase in Club segment KE_{TR}. The Club segment gains KE_{RR} early in the downswing through positive rotation of the proximal segments. It is not until rotation of the Arms segment begins to slow down that the Club segment shows a rapid increase in KE_{TR}. These data suggest that the changes in Club KE in the downswing can be described in 2 phases: increasing Arms KE_{RR} and decreasing Arms KE_{RR}. These phases have been called pre and post wrist-cocking (Pyne, 1977). In the first phase, the segments rotate simultaneously. This is not unlike the optimum motion pattern described by the "*superpositioning*" principle (Koniar, 1973). The body segments reach a peak in KE_{T} collectively at approximately MT 75%. Next, the Arms segment begins a clear decrease in KE. At this time, the Club segment undergoes a rapid gain in KE_{TR} and the Hips and Torso segments show a delayed and subtler decline in KE. The delay in KE peaks between the Arms and Club segments is caused by what previous authors have called a "cocking" of the wrists (Pyne, 1977; Pickering and Vickers, 1999). From this point onward, there is a whip-like transfer of KE P-D from the Arms segment to the Club. This effect is also visible in the angular kinematics of the golfer segments. It should be

noted that while the Arms KE goes through a clear decrease post wrist-cock, the Hips and Torso segments remain at an energy plateau.

7.4.5 Suggested Interventions

Achieving the optimum magnitude or efficiency of speed generation in the golf swing may be approached in 2 manners. Firstly, it may be possible to increase club head speed by promoting a P-D energy transfer to precede the wrist-cock, at either the shoulder or Torso-Hips connection point. For this to be viable, the sequence of segment kinematics must be altered to enable a sequential delay in motion. It has been mentioned that the geometry of the shoulder may limit such a delay when the left arm is swung in front of the chest. In order to have the Arms segment motion follow the Torso, a change in the conventional stance and grip would be required. This is discussed in greater depth in section 7.5.2 below.

The second means to increase Club KE would be to address the energy transfer from the Arms segment. There is a clear decrease in Arms segment KE during the rapid increase of Club KE_{TR}. However, the KE of the Torso and Hips segments seem to plateau post wrist-cock. It is possible that the decreasing energy in the Arms segment may be due to a proximal flow of energy to the Torso and Hips. In order to protect against this type of energy loss, it may be possible to increase the rotational stiffness of these segments post wrist-cock. The mechanisms for this solution will be described in greater detail in the section 7.5.3. A decrease in KE in the Hips and Torso segments post wrist-cock may allow for greater energy transfer to the Club.

7.4.6 Kinetic Energy Summary

The timing of KE_T did not progress in a P-D sequence. The magnitudes of KE_T however, did increase P-D. This data suggests that the whip model is not a good comparison for the entire downswing in golf.

The golf swing is a complex three-dimensional movement that converts rotational kinetic energy in the core to translational kinetic energy at the club head. The KE and angular kinematic data suggest that the only connection point showing a delay in peaks between neighbouring segments is the wrist. This is the only point where a whip-like transfer of P-D kinetic energy may be possible in the swing. From a KE perspective, it is possible to realistically describe the golf swing as a double pendulum, where the body represents the entire proximal link. This finding supports the use of 2D golf models where realistic golf kinematics were recreated using a two-link system (Cochrane and Stobbs, 1968; Jorgensen, 1970; Budney and Bellows, 1979).

It was speculated that the lateral hip shift, as described by McTeigue (1994), is responsible for a peak in Hips segment KE_{TR}. This energy amounted to 2.4% of the Club segment KE_T. It is unlikely that the sole benefit of this hip movement is a direct addition of KE_{TR} to the club head. Instead, it is likely that the lateral hip segment is related to the relative positioning of the spine and shoulders, allowing for efficient energy transfers to the Club segment.

The rapid increase in Club KE_{TR} coincided with a peaking of Arms KE_{RR} at MT 80%. The increase in Club KE_{RR} occurs earlier, half way through the downswing. In the pre wrist-cock phase of the downswing, the segments rotate simultaneously. Post wrist-

cock, the Arms rotation slows and the Club shows a large increase in KE_{TR}. It is only after wrist-cock that a whip-like, P-D pattern of KE flow is visible.

There were two interventions presented to improve KE generation in the golf swing. First, KE of the Arms may be increased by altering the sequence of segment rotations to allow a P-D progression. Second, the whip-like transfer of KE from the Arms to the Club may be made more efficient by limiting the flow of KE back to the Torso and Hips. Both interventions will be described in greater detail in sections 7.5.2 and 7.5.3 below.

7.5 Angular Momentum

Bahamonde (2000) observed Angular Momentum (***H***) in the tennis serve and showed how momentum is transferred from the feet to the racquet head. He used a method that calculated local and remote ***H*** about the system COM. That author concluded that the tennis serve is a three-lever system that transfers ***H*** sequentially from the Torso, to the Right Arm, to the Racquet. That author also noted that tennis segments undergo an ***H*** decrease P-D after peaking. It is suggested that the sequential decrease in ***H*** is what allows for an effective transfer of momentum in the distal direction. In this way, the pattern of ***H*** peaks in the tennis serve resembles that of a whip.

The goal of the golf drive is similar to the tennis serve in many ways. Rotations at the core are used to accelerate the upper body. Speed created in the hands is transferred through the wrist out to an external implement for collision with a relatively stationary ball. In both sports, speed is created in the distal end point to maximize the energy of the collision. If the golf swing were optimized in a manner similar to the tennis serve, we

would expect to see body segments of the player behave like a whip. That is, we would expect a sequential timing of ***H*** peaks. However, unlike the tennis racquet, the golf club itself has a large radius of gyration. The question remains, is a whip-like progression of ***H*** visible in the golf swing? And if not, how may the golf swing be altered to allow for an efficient transfer of ***H***? In the following section, patterns of peak golf swing ***H*** will be discussed in each plane of the global coordinate system, as in the method used by Bahamonde (2000).

7.5.1 Angular Momentum X

In the global coordinate system, the X-axis was oriented in the direction of the golf target and was normal to the golfer's sagittal plane at takeaway (see figure Figure 7.5.1). Positive ***H*** in the sagittal plane represented counter-clockwise rotation towards the ball, about the golfer's center of mass.

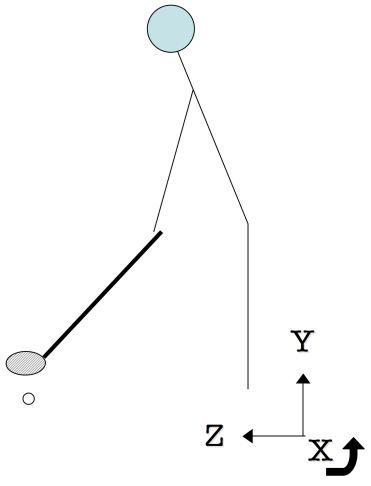

Figure 7.5.1: The global plane normal to the X-axis. This plane approximated the sagittal plane of the golfer at takeaway.

The total angular momentum in the X direction ($\boldsymbol{H}_{\mathbf{T\text{-}X}}$) did not show a P-D pattern in the magnitude or timing of golfer segment peaks. In general, magnitudes of $\boldsymbol{H}_{\mathbf{T\text{-}X}}$ peaks were smaller than in other components of $\boldsymbol{H}_{\mathbf{T}}$. This is likely because the segment swing planes were generally aligned with the frontal and transverse planes. $\boldsymbol{H}_{\mathbf{T\text{-}X}}$ data showed that the Torso segment rotated in the opposite direction from other segments in this plane. The Torso segment rotated towards the ball during the backswing and away from the ball during the downswing. The Hips and the Arms segment peaked in positive $\boldsymbol{H}_{\mathbf{T\text{-}X}}$ at nearly the same time that the Torso segment peaked in negative $\boldsymbol{H}_{\mathbf{T\text{-}X}}$. The Torso segment links the Arms with the Hips. It is speculated that the Torso segment must rotate in the opposite direction to permit the simultaneous rotation of the Hips and Arms. It is further speculated that this movement pattern would not allow for an effective transfer of momentum from the Hips segment to the Arms. The speed of any point along a kinetic chain depends on the $\boldsymbol{\omega}$ of preceding segments. Therefore, any segment containing $\boldsymbol{H}$ in the opposite direction of other segments should not benefit the speed of the distal end point.

Remote solar angular momentum ($\boldsymbol{H}_{\mathbf{RS}}$) describes the momentum due to a segment's COM rotating about the system COM. The majority of $\boldsymbol{H}_{\mathbf{T}}$ found in the sagittal plane was $\boldsymbol{H}_{\mathbf{RS}}$. For this reason, mean $\boldsymbol{H}_{\mathbf{RS\text{-}X}}$ closely resembled mean $\boldsymbol{H}_{\mathbf{T\text{-}X}}$. It should be noted that in $\boldsymbol{H}_{\mathbf{RS\text{-}X}}$, the Torso segment showed momentum in the direction opposite of the other segments. The suggested reason for this negative $\boldsymbol{H}$ is to accommodate the positive, simultaneous rotation of its neighbouring segments, as previously stated.

7.5.2 Angular Momentum Y

The global Y-axis pointed vertically, with positive pointing upwards. This axis was approximately normal to the transverse plane of the golfer at takeaway (see Figure 7.5.2). Positive ***H*** in the transverse plane represented counter-clockwise rotation towards the ball.

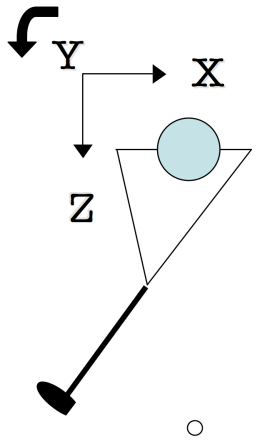

Figure 7.5.2: The global plane normal to the Y-axis. This plane approximated the transverse plane of the golfer at takeaway.

The Y and Z-axes may be more interesting for the golf swing as the planes of segment movement had larger components in these directions. The magnitudes of the largest peaks in $\boldsymbol{H}_{\mathbf{T\text{-}Y}}$ were about 10 kgm^2/s; nearly double those found in $\boldsymbol{H}_{\mathbf{T\text{-}X}}$.

In the transverse plane, the timings and magnitudes of $\boldsymbol{H}_{\mathbf{T\text{-}Y}}$ peaks did not follow a P-D progression. The Torso segment was the first to show a positive peak in $\boldsymbol{H}_{\mathbf{T\text{-}Y}}$ in the transverse plane, although this segment had a small amount of ***H*** in this direction. This small amount of Torso segment rotation in the transverse plane is surprising given that the axis is nearly aligned with the golfers spine. This suggests that the constraints of a conventional golf configuration limit the magnitude of rotation of the Torso in the

transverse plane. The decrease in Torso $\boldsymbol{H}_{\mathbf{T\text{-}Y}}$ was followed by an increase in $\boldsymbol{H}_{\mathbf{T\text{-}Y}}$ in the Torso's neighbouring segments, the Arms and Hips. The increase in Club segment $\boldsymbol{H}_{\mathbf{T\text{-}Y}}$ followed the decrease in Arms $\boldsymbol{H}_{\mathbf{T\text{-}Y}}$ before impact. It seemed that the angular position of the Torso was nearly square to impact in the transverse plane near the mid point of the downswing. To compare the golf swing to a whip, the Torso would need to continue to rotate in sequence between the Hips and Arms segments for optimum flow of $\boldsymbol{H}$ in this plane. Instead, $\boldsymbol{H}_{\mathbf{T\text{-}Y}}$ begins to increase in the Hips segment when the Torso slows rotation. This could mean that momentum is flowing proximally to the core instead of being transferred to the club head. This pattern is likely less than optimal for producing maximum club speed.

Local angular momentum ($\boldsymbol{H}_{\mathbf{L}}$) describes momentum due to the rotation of rigid body about its own COM. As in the sagittal plane, $\boldsymbol{H}_{\mathbf{L\text{-}Y}}$ was found almost entirely in the Torso segment. This is likely because this segment contains the rigid bodies with the highest rotational inertia.

At approximately MT 78%, $\boldsymbol{H}_{\mathbf{RP\text{-}Y}}$ showed a positive peak in the Hips and Arms segments and negative peak in the Torso. It is suggested that the negative $\boldsymbol{H}_{\mathbf{RP\text{-}Y}}$ of the Torso is necessary to offset the simultaneous positive peaking of $\boldsymbol{H}_{\mathbf{RP\text{-}Y}}$ in both of its neighbours. In this way, the pattern found in $\boldsymbol{H}_{\mathbf{RP\text{-}Y}}$ was similar to that found in $\boldsymbol{H}_{\mathbf{T\text{-}X}}$. It is likely that this motion pattern does not allow for an efficient transfer of $\boldsymbol{H}$ from the Hips to the Arms. The reasoning has been explained in greater detail in section 7.5.1 above.

The majority of $\boldsymbol{H}_{\mathbf{T}}$ found in the transverse plane was $\boldsymbol{H}_{\mathbf{RS}}$. For this reason, mean $\boldsymbol{H}_{\mathbf{RS\text{-}Y}}$ closely resembled those of $\boldsymbol{H}_{\mathbf{T\text{-}Y}}$. Torso segment $\boldsymbol{H}_{\mathbf{RS\text{-}Y}}$ was the first to peak. Its decrease in $\boldsymbol{H}_{\mathbf{RS\text{-}Y}}$ was followed by an increase in Arms and Hips segment $\boldsymbol{H}_{\mathbf{RS\text{-}Y}}$. The

Arms segment showed a clear decrease in $\boldsymbol{H}_{\mathbf{RS\text{-}Y}}$ preceding a sharp increase in Club segment $\boldsymbol{H}_{\mathbf{RS\text{-}Y}}$. In a distal direction, there was a sequential peaking of $\boldsymbol{H}_{\mathbf{RS\text{-}Y}}$ from the Torso to the Arms to the Club. Proximally, the gain in Hips $\boldsymbol{H}_{\mathbf{RS\text{-}Y}}$ plateaued until impact. The early decrease in Torso $\boldsymbol{H}_{\mathbf{RS\text{-}Y}}$ may lead to a transfer of $\boldsymbol{H}$ proximally to the core. This type of momentum transfer may limit the amount of rotational momentum available to the Club segment and potentially increase the amount of momentum transferred proximally at the connection point between the Torso and Hips.

To improve the transfer of $\boldsymbol{H}$ in the transverse plane, the Torso would have to be positioned so that its rotation could follow the rotation of the Hips segment and precede the rotation of the Arms segment. The geometry of the golfer's left shoulder does not permit this positioning when the left arm is swung in front of the chest and the feet are facing the ball. This transfer would be possible if the Arms segment could be swung behind the body. This type of movement can be seen when chopping wood with an axe or during the tennis serve. However, one achieves arm positions behind the Torso while chopping wood or serving in tennis by swinging the axe or racquet above one's head. Since the ball is teed on the ground, another solution must be found for the golf swing.

If one were to swing at the ball with only the right arm, the Arms segment would be free to trail in angular position behind the Torso (see Figure 7.5.3.b). The Torso could, in turn, trail in angular position behind the Hips segment if the feet were positioned in the direction of the target. Offsetting the angular positioning in this way would allow for rotation to occur in a sequential order. This would produce a "polo" style swing. This type of swing may produce greater angular momentum transfer in the transverse plane as compared to a conventional golf configuration (see Figure 7.5.3.a).

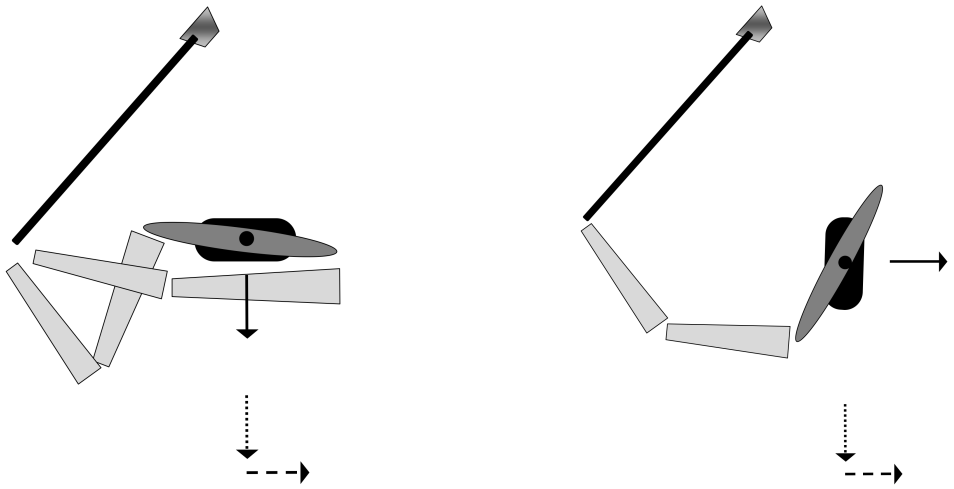

a) b)

Figure 7.5.3: Diagram of Torso position relative to Arms and Hips segments in the transverse plane for a right-handed player at the top of the backswing. A two-handed conventional golf swing is shown in part a). Part b) shows a one-handed "polo" style of swing. The Hips segment is shown as a black, rounded rectangle. The Torso segment is a thin, dark grey ellipse. The Arms segment consists of upper and lower arm rigid bodies and are colored light grey. The Club segment has a black shaft and silver club head. The solid black arrow shows the anterior direction of the golfer's body as dictated by the direction of the feet. The dotted arrow shows the relative direction of the ball position. The dashed arrow shows the direction of the target.

It should be noted that swinging a golf club in a "polo" type swing style might be of benefit in speed creation at the cost of losing accuracy in ball contact. It may be possible to gain a momentum transfer benefit by trailing the right arm and an accuracy benefit by using a two-handed grip and separating the placement of the hands on the club; this type of grip can be found in a hockey or lacrosse shot. In a future study, it would be interesting to determine if a two-handed, "hockey-grip" golf swing can produce a greater momentum transfer and retain a level of contact accuracy, *a la* Happy Gilmore (Dugan, 1996).

7.5.3 Angular Momentum Z

The Z-axis was oriented towards the ball at takeaway. This axis was approximately normal to the golfer's frontal plane at takeaway (see Figure 7.5.4). Positive $\boldsymbol{H_Z}$ represented counter-clockwise rotation towards the ball.

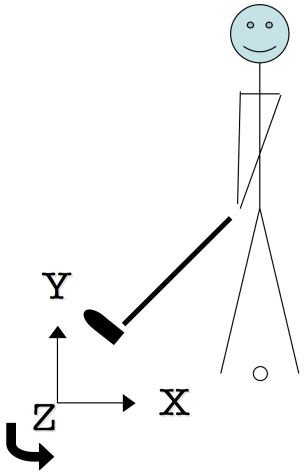

Figure 7.5.4: The global plane normal to the Z-axis. This plane was approximately normal to the golfer's frontal plane at takeaway.

In the frontal plane, $\boldsymbol{H_{T\text{-}Z}}$ segmental peaks followed a distinctly non P-D order. The Arms segment was the first segment to peak in $\boldsymbol{H_{T\text{-}Z}}$ during the downswing. The Arms segment peak was followed shortly by the Hips segment and later, by the Torso and Club segments, which both peaked just prior to impact. The peak timing of the Torso, Arms and Club segments showed very little variability. This would suggest that the pattern of an initial Arm $\boldsymbol{H_{T\text{-}Z}}$ peak before the Torso and Club is common among most golfers.

The decrease of the Arms segment $\boldsymbol{H_{T\text{-}Z}}$ nearly coincided with a decrease in Hips segment $\boldsymbol{H_{T\text{-}Z}}$. It is possible that the decrease in $\boldsymbol{H}$ in both of the Torso's neighbouring

segments contributed to its large momentum increase late in the downswing. This would mean that the Torso gains $\boldsymbol{H_Z}$ in a distal direction from the Hips segment, and also that $\boldsymbol{H}$ may flow proximally from the Arms segment at the shoulder.

The gain in $\boldsymbol{H_{T\text{-}Z}}$ in the Torso was relatively large; so large, in fact, that the peak in Torso $\boldsymbol{H_{T\text{-}Z}}$ surpassed the magnitude of the Club segment $\boldsymbol{H_{T\text{-}Z}}$ at impact. The $\boldsymbol{H_{T\text{-}Z}}$ found in the Torso was four times larger than the amount contained in the Hips segment. If the Hips were the only segment to supply the Torso with flow of $\boldsymbol{H_Z}$, the muscles responsible for rotating the Torso segment would need to have supplied the remainder of the momentum gained. However, the muscles supporting the spine generally work to stabilize rotations in the frontal plane, not to promote large rotations about the Z-axis. If this momentum were not gained by muscular work, it would have to have come from another source, such as being transferred from another segment.

The Arms segment experienced a large decrease in momentum at the same time as the Torso $\boldsymbol{H_{T\text{-}Z}}$ increased in this plane. It is likely that some of the $\boldsymbol{H_{T\text{-}Z}}$ contained in the Arms segment flowed proximally to create an increase in Torso $\boldsymbol{H_{T\text{-}Z}}$. The whip model created by McMillen and Goriely (2003) showed that the direction of $\boldsymbol{H}$ flow was dependant on the rotational inertia of neighbouring elements. From this perspective, it is speculated that the relative rotational inertia of the Club segment was comparatively high enough to allow a portion of the $\boldsymbol{H}$ from the Arms segment to flow proximally back into the Torso.

$\boldsymbol{H_{T\text{-}Z}}$ entering the Torso from the Arms segment would potentially decrease the amount of $\boldsymbol{H}$ made available to the Club segment. In addition, a large gain in Torso $\boldsymbol{H}$ in

the frontal plane would cause spinal rotations that may have to be stabilized by supporting muscles or joint structures.

The purported flow of Arm $\boldsymbol{H}_{\mathbf{T\text{-}Z}}$ to the Torso segment could likely be decreased by altering the rotational inertia of the Torso in the frontal plane. This may be achieved by adding mass to the Torso segment that is radially displaced in the frontal plane. In this way, the rotational inertia of the Torso segment will be increased in the frontal plane. In addition, stiffening of the connection point between the Torso and Hips segment may be achieved through strength training or athletic taping. It is hypothesized that either of these solutions would increase club head speed or decrease the amount of frontal plane rotation in the lower spine by creating greater resistance to proximal Arm segment $\boldsymbol{H}_{\mathbf{T\text{-}Z}}$ flow.

McTeigue (1994) also reported a positive rotation of the Torso in the frontal plane. This author found that a late Torso rotation in the frontal plane was characteristic of players with a high registered handicap. McTeigue also found that professional golfers tended to display a lateral hip shift instead of rotating the spine in this fashion. It is possible that the purpose of the lateral hip shift may be to reposition the shoulders and spine relative to the golf grip at impact. This may have the effect of stabilizing Torso rotations in the frontal plane, thus allowing for greater $\boldsymbol{H}$ transfer to the Club segment.

It may also be possible that the large increase in Torso $\boldsymbol{H}_{\mathbf{T\text{-}Z}}$ is related to the simultaneous decrease of $\boldsymbol{H}_{\mathbf{T\text{-}Z}}$ in the Arms and Hips segments. It is suggested that if the Torso segment were able to rotate in sequential order following the Hips segment and preceding the Arms segment, the proximal flow of Arms $\boldsymbol{H}_{\mathbf{T\text{-}Z}}$ may be decreased. This could be achieved by using the “polo” style or “hockey-grip” swing configurations described in section 7.5.2 above.

A P-D, whip-like sequence was found in the pattern of $\boldsymbol{H}_{\mathbf{RP\text{-}Z}}$ peaks. It seems that the timing of rotational momentum peaks about segment COM resembles a whip in the golfer's frontal plane. However, the magnitudes of these peaks do not proceed in a P-D manner. $\boldsymbol{H}_{\mathbf{RP\text{-}Z}}$ peaks gain in magnitude through each of the body segments, and then decrease at the wrist, as momentum type is most likely converted as it reaches the club. The timing of the $\boldsymbol{H}_{\mathbf{RP\text{-}Z}}$ peaks shows a pattern that suggests an efficient transfer of momentum. The magnitude of $\boldsymbol{H}_{\mathbf{RP\text{-}Z}}$ seen in the Arms segment represents 41% of the $\boldsymbol{H}_{\mathbf{T}}$ created in the Club segment as a whole. It is likely that a whip-like P-D progression of $\boldsymbol{H}_{\mathbf{RP\text{-}Z}}$ peaks in the frontal plane is responsible for a significant portion of $\boldsymbol{H}$ gained by the Club.

$\boldsymbol{H}_{\mathbf{RS\text{-}Z}}$ was the highest contributing component to the Torso, Arms and Club $\boldsymbol{H}_{\mathbf{T\text{-}Z}}$. The pattern of timing in $\boldsymbol{H}_{\mathbf{RS\text{-}Z}}$ peaks showed a distinctly non-P-D progression. The Arms segment peaked quite early in the downswing, at MT 45.8%. The Arms then went through a marked decrease before showing a negative peak. Following this, the Torso and Club segments went through a large increase in $\boldsymbol{H}_{\mathbf{RS\text{-}Z}}$ just prior to impact. It is likely that $\boldsymbol{H}$ transfer to the Club segment is compromised when the Arms $\boldsymbol{H}_{\mathbf{RS\text{-}Z}}$ peak precedes the Torso. The efficiency implications of this pattern order have been explored above in the section on $\boldsymbol{H}_{\mathbf{T\text{-}Z}}$.

Unexpectedly, at approximately MT 70%, the Arms segment $\boldsymbol{H}_{\mathbf{RS\text{-}Z}}$ became negative. This represents rotation in a clockwise direction, away from the ball. While it has been observed that golfers slow their hands before impact (Pyne, 1977), it is highly unlikely that golfers would rotate their Arms segment backwards during the downswing. $\boldsymbol{H}_{\mathbf{RS}}$ is a measurement of segment COM rotation about the system COM. The negative

Arm $\boldsymbol{H}_{\mathbf{RS\text{-}Z}}$ implies that the path of the Arms COM relative to the system COM became inconsistent in this plane. As the Arms segment passes in front of the chest, the COM passes superior to the navel (or approximate system COM). When this happens, the $\boldsymbol{H}_{\mathbf{RS\text{-}Z}}$ cross-product (of the Arms radius of gyration and the Arms COM velocity vector) switches directions. This must be taken with consideration then, when the Arms segment $\boldsymbol{H}_{\mathbf{RS}}$ showed a negative rotation in this plane. Results of momentum patterns in any of the 3 global coordinate planes should be compared with patterns of absolute momentum. The phenomenon of proximal Arms $\boldsymbol{H}$ transfer to the Torso segment will be discussed in absolute terms in section 7.5.4 below.

7.5.4 Club Plane and Absolute Angular Momentum

The Angular Momentum described in the club plane ($\boldsymbol{H}_{\mathbf{CP}}$) is the total Angular Momentum of the segments projected onto the 2D surface of the path of the club head during the downswing. This particular projection is of interest because it represents the $\boldsymbol{H}_{\mathbf{T}}$ components that are directly relative to the club-ball collision.

The Arms segment was the first to peak in $\boldsymbol{H}_{\mathbf{CP}}$ during the downswing. The decrease in Arms $\boldsymbol{H}_{\mathbf{CP}}$ in the downswing is followed by an increase in Club and Torso momentum. First, the amount of $\boldsymbol{H}_{\mathbf{CP}}$ that was transferred to the Arms from proximal segments was likely minimal. Second, this suggests that a portion of the Arms segment $\boldsymbol{H}_{\mathbf{CP}}$ was transferred proximally to the Torso, supporting the result found in the frontal plane.

$\boldsymbol{H}_{\mathbf{CP}}$ was not conserved; peak magnitudes increased P-D from the Hips segment to the Club. This mirrored the peak magnitude pattern found in KE_T. Also, similar to the KE

peaks, the largest increase in $\boldsymbol{H}_{\mathbf{CP}}$ was found at the wrist linking the Arms segment and the Club. Post wrist-cock, the Club segment undergoes a momentum increase amounting to roughly 60% of peak Club $\boldsymbol{H}_{\mathbf{CP}}$. The whip-like progression of movement at this connection point likely enhances the efficiency of $\boldsymbol{H}$ transfer to the Club.

$\boldsymbol{H}$ was also presented in absolute terms. Absolute total angular momentum (H_{AT}) is a scalar that describes a directionless quantity of $\boldsymbol{H}$ as a Euclidean norm of the 3D vector $\boldsymbol{H}_{\mathbf{T}}$. H_{AT} includes components of $\boldsymbol{H}$ that may not have been projected onto the club plane. The timing of the segment peaks in H_{AT} was similar to that found in $\boldsymbol{H}_{\mathbf{CP}}$. The Hips and Arms moved in unison, as did the Torso and Club segments. The Torso segment increased in H_{AT} near the end of the downswing. As in $\boldsymbol{H}_{\mathbf{CP}}$, the late Torso H_{AT} peak likely represents inefficient transfer of Arms H_{AT} to the Club segment. Also, as in $\boldsymbol{H}_{\mathbf{CP}}$, it seems unlikely that the Arms segment gained much $\boldsymbol{H}$ from other segments at the beginning of the downswing.

The progression of peak magnitudes was unlike that found in the club plane. The Torso, Arms and Club segments all showed a peak H_{AT} magnitude that was not statistically different (near 12.3 $kg\ m^2/s$). It would appear that in an absolute sense, $\boldsymbol{H}$ seems to be conserved, unlike the peak magnitude pattern found in KE. This result may be a function of the point about which $\boldsymbol{H}$ is calculated. For this investigation, the method of Bahamonde (2000) was employed which calculates $\boldsymbol{H}$ about the system COM. Since Nesbit and Serrano (2005) have found that the joints connecting these segments perform positive work, it is to be expected that $\boldsymbol{H}$ would not be conserved. The phenomenon of a common H_{AT} peak magnitude may not be repeated with a change in $\boldsymbol{H}$ focal point.

7.5.5 Angular Momentum Summary

$\boldsymbol{H}$ has been explored in this study using a method adapted from Bahamonde's investigation of the tennis serve (2000). The patterns of peak timing and magnitudes in golfer segment $\boldsymbol{H}$ have been compared to a P-D pattern as observed in a whip (McMillen and Goriely, 2003). This type of motion pattern has been shown to create optimal speed generation in overhand throwing (Joris *et al*, 1985) and the tennis serve (Bahamonde, 2000). It is speculated that this type pattern motion allows an efficient transfer of $\boldsymbol{H}$ to the distal end point of a human kinetic chain.

$\boldsymbol{H}_{\mathbf{T}}$ describes total angular momentum and was initially explored in the 3 axes of the global coordinate system as in the method used by Bahamonde (2000). The patterns of $\boldsymbol{H}_{\mathbf{T}}$ peak timings and magnitudes did not follow a P-D progression in any of the 3 global axes directions: X, towards the golf target; Y, vertical upward; and Z, towards the ball at address.

The Torso segment $\boldsymbol{H}_{\mathbf{T\text{-}X}}$ peaked clockwise, in the direction opposite to the other segments during the downswing. The simultaneous downward rotation of the Hips and Arms segments may have necessitated an upward rotation of the Torso segment that links them. This order of rotation probably does not allow for an efficient transfer of $\boldsymbol{H}$ from the Hips segments to the Arms.

The magnitudes of $\boldsymbol{H}_{\mathbf{T}}$ were much higher in the directions of the global Y and Z-axes. This result is intuitive as the segment swing planes were generally aligned in planes with components normal to these axes.

The conventional configuration of the golf swing allows for little Torso rotation in the transverse plane. The Torso segment peaked first in $\boldsymbol{H}_{\mathbf{T\text{-}Y}}$ as it began to stop rotating

in this plane halfway through the downswing. The decrease in Torso segment $\boldsymbol{H}_{\mathbf{T\text{-}Y}}$ was followed by an increase in Hips segment $\boldsymbol{H}_{\mathbf{T\text{-}Y}}$. This may suggest that $\boldsymbol{H}$ flows proximally from the Torso segment to the Hips and may represent inefficient momentum transfer to the Club segment. Altering the swing configuration to allow for a P-D sequencing of rotations might improve generation of Arms $\boldsymbol{H}$ or increase $\boldsymbol{H}$ transfer efficiency in the golf swing. Such a change in configuration might come at the cost of accuracy in the club-ball contact. Further research should be undertaken to determine if a P-D progression of the Hips, Torso and Arms segments would create higher speed generation in the golf swing.

In the frontal plane, the Arms segment $\boldsymbol{H}_{\mathbf{T\text{-}Z}}$ peaked first and then a marked decrease was observed. This decrease was followed by a large increase in $\boldsymbol{H}_{\mathbf{T\text{-}Z}}$ in the Torso and Club segments prior to impact. The low level of Hips $\boldsymbol{H}_{\mathbf{T\text{-}Z}}$ and the high rotational inertia of the Club segment might have allowed a portion of $\boldsymbol{H}_{\mathbf{T\text{-}Z}}$ to flow proximally from the Arms segment to the Torso. This would support the finding of McTeigue (1994), who observed frontal plane Torso rotations late in the downswing in low skilled players. McTeigue noted that professional players limited this Torso rotation by using a lateral hip slide. This hip slide likely stiffens the connection point between the Torso and Hips segments in the frontal plane. Furthermore, such an intervention would allow for greater transfer of Arms $\boldsymbol{H}_{\mathbf{T\text{-}Z}}$ to the Club segment.

The large increase in Torso segment $\boldsymbol{H}_{\mathbf{T\text{-}Z}}$ may have been due to the simultaneous decrease in $\boldsymbol{H}_{\mathbf{T\text{-}Z}}$ in both of its neighbouring segments. In addition, the early peaking of the Arms segment $\boldsymbol{H}_{\mathbf{T\text{-}Z}}$ in the frontal plane suggests that the Arms did not benefit from

an earlier $\boldsymbol{H}_{\mathbf{T\text{-}Z}}$ transfer from other segments. These results support the idea that a P-D ordering of segment motions may increase momentum made available in the swing.

$\boldsymbol{H}_{\mathbf{RS}}$ is used to denote remote solar angular momentum, and describes the momentum due to a segment's COM rotating about the system COM. $\boldsymbol{H}_{\mathbf{RS\text{-}Z}}$ showed a negative peak in the Arms segment prior to impact. It is highly unlikely that the arms rotate clockwise at any point during the downswing. This result is most likely due to the proximity of motion between the Arms segment COM and the system COM prior to contact in the frontal plane. This phenomenon suggests that patterns of $\boldsymbol{H}$ expressed in global coordinates must be compared to absolute values or planes relative to the motion of golfer segments.

$\boldsymbol{H}_{\mathbf{CP}}$ expresses segment $\boldsymbol{H}$ in the plane relative to the club-ball collision. The timing of $\boldsymbol{H}_{\mathbf{CP}}$ peaks did not follow a P-D progression. The Torso segment showed a large gain in $\boldsymbol{H}_{\mathbf{CP}}$ just prior to ball contact, suggesting an inefficient transfer of $\boldsymbol{H}$ to the Club. The peak magnitudes increased in a P-D progression, mirroring the pattern of peak magnitudes found in KE.

The timing and magnitudes of absolute total angular momentum, H_{AT}, did not follow a P-D progression. The Torso segment showed a large increase in H_{AT} just prior to impact. This result mirrored the findings in $\boldsymbol{H}_{\mathbf{CP}}$ and $\boldsymbol{H}_{\mathbf{RS\text{-}Z}}$. These data suggest that the flow of $\boldsymbol{H}$ from the Arms segment transfers proximally to the Torso segment just prior to impact. This is evidence that $\boldsymbol{H}$ is not effectively transferred to the Club in the golf swing. $\boldsymbol{H}$ transfer may be improved by altering the sequence of segment rotations or by stiffening the connection point between the Torso and Hips segments against rotations in the frontal plane.

The peak magnitudes of H_{AT} in the Torso, Arms and Club segment were nearly equal. It would appear that absolute momentum is conserved in these segments, similar to momentum transfer in a whip. Work by Nesbit and Serrano (2005) showed that upper body joints perform positive work during the downswing. In this case, we would expect that momentum should not be conserved in the golf swing. It is more likely that this is a chance phenomenon dependent upon the placement of the ***H*** focal point.

7.6 Study Limitations

A central limitation of this study has been examining flow of KE or ***H*** using a segment based perspective. By looking at only the destinations of energy or momentum, we can only speculate about the origins or direction of flow. For a full understanding of the flow of KE or ***H*** in the golf swing, a full-body inverse-dynamics approach must be undertaken to calculate power and work at each of the joints. At the time of writing, only Nesbit and Serrano (2005) have been able to provide data on joint power, using a hybrid motion analysis / simulation approach. It is suggested that human inverse-dynamics studies in golf may be possible if the resultant forces and moments could be resolved at the wrist joints. There has yet to be a study to show an improvement in the quality of club acceleration data or to determine the relative club loading contribution of each hand. Each of which are crucial for realizing wrist power calculations.

Another limitation of this study is the unknown error in estimated rigid body motion using the MATT system. It is possible that inter-subject resolution may be a concern with the MATT optical motion analysis system. The system is designed to alter the scaling and motion of a generic swing to fit the motion of reflective markers on real

golfers. As such, it is conceivable that some characteristic kinematics of the base swing may be visible in all golfer data. At the time of writing, it is unknown how the MATT system kinematic data differs from conventional optical measurement systems. Anecdotally, observers are able to correctly identify individual's swings by watching animations of the MATT data. However, the MATT system has yet to be verified against a conventional optical measurement tool.

For future work with the MATT system, a comparison of rigid body motion with a conventional system needs to be performed. One of the problems encountered in performing such a comparison is in executing a simultaneous data collection using both systems. The MATT system must see it's own limited marker set in order to make the necessary assumptions needed to process a swing. A conventional optical system would require a minimum of 3 markers per rigid body. In order to implement a simultaneous data collection, it is suggested that retro-reflective markers only be used in the MATT configuration. For the conventional comparison, active LED markers with a sample timing offset may be used.

Lastly, data collection repeatability may be a limitation in this study. In order to gain the large number of subjects for this investigation, motion analysis data needed to be collected from 5 different lab locations. It is unknown what noise is encountered by using data collected by different lab technicians. It is speculated that the least-squares optimization of the MATT model minimizes errors gained due to small differences in marker placement. For future work using data from different collection locations, it would be interesting to compare the repeatability of kinematic data of a single subject at each lab.

Chapter Eight: Conclusion

The purpose of this thesis was to develop a basic understanding of speed generation in the golf swing. The primary question addressed in this investigation was: Do the magnitudes and timings of peaks in segment angular kinematics, kinetic energy and angular momentum follow a P-D order in the golf swing?

The timing of peaks did not follow a P-D order in angular kinematics, kinetic energy or angular momentum. The only connection point to show a consistent delay in peaks between neighbouring segments was the wrist, or the interface between the Arms and Club segments. Wrist delay was shown in the timing of peak $\boldsymbol{\omega}$, $\boldsymbol{\alpha}$, KE_T and $\boldsymbol{H}$. This suggests that the only segment connection allowing a whip-like, P-D transfer of energy was the wrist. This was supported by the KE, $\boldsymbol{\omega}$ and $\boldsymbol{\alpha}$ results, where the wrist showed the largest gain in magnitude between adjacent segment peaks.

The timing of the Arms peak $\boldsymbol{H}$ preceded the peak $\boldsymbol{H}$ of all other segments. It is unlikely that the Arms segment receives an $\boldsymbol{H}$ transfer from either the Torso or Hips segments in the downswing. A change in the configuration of a conventional swing to a "polo" style or "hockey-grip" swing may improve Arms segment $\boldsymbol{H}$ and result in more efficient club speed production.

The peak magnitudes of $\boldsymbol{H}$ did not follow a P-D order. There was a large increase in Torso $\boldsymbol{H}$ momentum immediately prior to impact. It is likely that $\boldsymbol{H}$ flows proximally from the Arms segment to the Torso. The efficiency of $\boldsymbol{H}$ transfer in the golf swing may be improved by limiting rotation of the Torso in the frontal plane. This finding supports

the work of McTeigue (1994) who found that frontal plane Torso bending was characteristic of low-skilled players.

8.1 Notable Findings

The pattern of peak θ magnitudes at the top of the backswing closely resembled the pattern of peak ω magnitudes during the downswing. It appeared that swing plane peak θ was a strong predictor of attainable segment speed in the swing plane.

The timing of peak KE_T and α showed that the body segments peaked as a unit and preceded the Club segment peak, immediately prior to impact. From the standpoint of KE_T and α data, the golf player may be realistically represented by a two-link system in which the body segments comprise the proximal link. This supports the double pendulum modelling work that founded the field of golf biomechanics (Jorgensen, 1970; Pyne, 1977; Milburn, 1982; Vaughn, 1981).

Golf segment energetics were compared against a value of golf joint energetics from the literature (Nesbit and Serrano, 2005). The system peak KE was found to be within 12% of the total joint work for a scratch golfer by the Nesbit simulation. It is likely this difference represents inter-subject variability as the joint energetics value is based on a subject group of n=1. This is the first known comparison of this kind for the golf swing.

In conclusion, a basic understanding of speed generation in the golf swing has been afforded by exploring the patterns of peak angular kinematics, kinetic energy and angular momentum. The results found in this study will be of benefit to players, teachers and equipment manufacturers in the game.

APPENDIX A: REFERENCES

Baker, R., (2006). Gait analysis methods in rehabilitation: a review. *Journal of NeuroEngineering and Rehabilitation.* Mar 2, 3:4

Berme, N., Cappozzo, A., and Meglan, J., (1990). *Kinematics in Biomechanics of Human Movement: Applications in Rehabilitation, Sports and Ergonomics*, Cappozzo, A., Berme, N., ed. Bertec Corporation. Worthington, OH. 89-102

Budney, D.R., and Bellow, D.G., (1979). Kinetic Analysis of a Golf Swing. *Research Quarterly*. 50 (2), 171-179

Bunn, J.W., (1972). *Scientific Principals of Coaching*, 2nd ed. Prentice Hall Inc. New Jersey.

Burden, A.M., Grimshaw, P.N., and Wallace, E.S., (1998). Hip and shoulder rotations during the golf swing of sub-10 handicap players. *Journal of Sport Sciences.* 16, 165-176

Cappozzo, A., Catani, F., Leardini, A., Benedetti, M.G., and Della Croce U., (1996). Position and orientation in space of bones during movement: experimental artefacts. *Clinical Biomechanics.* 11 (2), 90-100

Chapman, A.E., and Sanderson, D.J., (1990). Muscular Coordination in Sporting Skills. *Multiple Muscle Systems: Biomechanics and Movement Organization.* Winters, J.M., and Woo, S.L., ed. Springer-Verlag. 608-620

Cochran, A., and Stobbs, J., (1968). *The Search for the Perfect Swing*. J.B. Lippincott Company, Philadelphia.

Coleman, S.G., and Rankin, A.J., (2005). A three-dimensional examination of the planar nature of the golf swing. *Journal of Sport Sciences.* 23 (3), 227-234

Cooper, J.M., Bates, B.T., Bedi, J., and Scheuchenzuber, J., (1974). Kinematic and kinetic analysis of the golf swing. *Biomechanics IV*. Nelson, R.C., and Morehouse, C.A., ed. Baltimore, MD. University Park Press. 298-305

Craig, J.J., (1986). *Introduction to Robotics: Mechanics and Control.* Addison-Wesley Publishing Co. Reading, MA.

Dapena, J., (1978). A Method to Determine the Angular Momentum of a Human Body About Three Orthogonal Axes Passing Through Its Center of Gravity. *Journal of Biomechanics.* 11, 251-256

Dugan, D., dir. (1996). Happy Gilmore. Writ. Hurlihy, T. Sandler, A; Prod. Simmonds, R; Perf. Sandler, A. Barker, B; Universal.

Dillman, C.J., and Lange, G.W., (1994) How has biomechanics contributed to the understanding of the golf swing? In: Cochrane, A.J., Farrally, M.R., ed. *Science and Golf II: Proceedings of the 1994 World Scientific Congress of Golf*. E & FN Spon. London. 3-13

Egret, C.I., Vincent, O., Weber, J., Dujardin, F.H., Chollet, D., (2003). Analysis of 3D Kinematics Concerning Three Different Clubs in Golf Swing. *International Journal of Sports Medicine.* 24, 465-470

Farrally, M.R., Cochran, A.J., Crews, D.J., Hurdzan, M.J., Price, R.J., Snow, J.T., and Thomas, P.R., (2003). Golf science research at the beginning of the twenty-first century. *Journal of Sports Sciences*. (21), 753-765

Feltner, M.E., and Dapena, J., (1989). Three-Dimensional Interactions in a Two-Segment Kinetic Chain; Part I: General Model. *International Journal of Sport Biomechanics.* 5, 403-419

Gillmeister, H., (2002). Golf on the Rhine: On the Origins of Golf, with Sidelights on Polo. *International Journal of History of Sport*. 19 (1), 1-30

Goriely, A., and McMillen, T., (2002). Shape of a Cracking Whip. *Physical Review Letters.* 88 (24), 1-4

Herring, R.M., and Chapman, A.E., (1992). Effects of Changes in Segmental Values and Timing of Both Torque and Torque Reversal in Simulated Throws. *Journal of Biomechanics.* 25 (10), 1173-1184

Hoffman, J.D., (2001). *Numerical Methods for Engineers and Scientists,* 2nd ed. Marcel Dekker Inc. New York.

Hume, P.A, Keogh, J., and Reid, D., (2005). The Role of Biomechanics in Maximizing Distance and Accuracy of Golf Shots. *Sports Medicine*. 35 (5), 429-449

Jorgensen, T., (1970). On the Dynamics of the Swing of a Golf Club. *American Journal of Physics.* 38 (5), 644-651

Jorgensen, T., (1999). *The Physics of Golf,* 2nd ed. Springer-Verlag. New York.

Joris, H.J., Edwards van Muyen, A.J., van Ingen Shenau, G.J., and Kemper, H.C.(1985). Force, Velocity and Energy Flow During the Overarm Throw in Female Handball Players. *Journal of Biomechanics.* 18 (6), 409-414

Kim, D.H., Millett, P.J., Warner, J.J., and Jobe, F.W., (2004). Shoulder Injuries in Golf. *American Journal of Sports Medicine.* 32 (5), 1324-1330

Koniar, M., (1973). The Biomechanical Studies on the Superposition of Angular Speeds in Joints of Lower Extremities of Sportsmen. *Biomechanics III.* Karger, ed. Basel.. 426-428

Krehl, P., Engemann, S., and Schwenkel, D., (1998). The puzzle of whip cracking – uncovered by a correlation of whip-tip kinematics with shock wave emission. *Shock Waves.* Springer Verlag. 8, 1-9

Kreighbaum, E., and Barthels, K.M., (1990). *Biomechanics; a Qualitative Approach for Studying Human Movement,* 3rd ed. MacMillan Publishing Company. New York.

Kwon, Y.H., (1998). Mechanical Basis of Motion Analysis. *http://www.kwon3d.com/theories.html*

Lampsa, M.A., (1975). Maximizing Distance of the Golf Drive: An Optimal Control Study. *Journal of Dynamic Systems, Measurement, and Control.* December, 362-367

Lowe, B., (1994). Centrifugal force and the planar golf swing. *Science and Golf II: Proceedings of the World Scientific Congress of Golf.* Cochran, A.J., and Farrally, M.R., ed. E & FN Spon, London.

Marshall, R.N., (2000). Long-axis rotation: The missing link in proximal-to-distal segmental sequencing. *Journal of Sports Sciences.* 18, 247-254

Marshall, R.N., (2002). Proximal-to-distal Sequencing Research: Application to Throwing. *International Research in Sports Biomechanics.* Hong, Y. ed. Routledge. New York. 9-14

Martino, R., (2005). Sweet Release. Golf Tips, PGA.com, Retrieved January 29, 2007, from http://www.pga.com/improve/tips/rickmartino/improve_martino110805.cfm

McLaughlin, P.A., and Best, R.J., (1994). Three-dimensional kinematic analysis of the golf swing. *Science and Golf II: Proceedings of the World Scientific Congress of Golf.* Cochran, A.J., and Farrally, M.R., ed. E & FN Spon, London.

McMillen, T., and Goriely, A., (2003). Whip waves. *Physica D*. Elsevier Science Publishing. 184, 192-225

McTeigue, M., (1994). Spine and hip motion analysis during the golf swing. *Science and Golf II: Proceedings of the World Scientific Congress of Golf.* Cochran, A.J., and Farrally, M.R., ed. E & FN Spon, London.

Milburn, P.D., (1982). Summation of segmental velocities in the golf swing. *Medicine and Science in Sports and Exercise*. 14 (1), 60-64

Miura, K., (2001). Parametric acceleration – the effect of inward pull of the golf club at impact stage. *Sports Engineering.* 4, 75-86

Myhrvold, NP., and Currie, PJ., (1997). Supersonic sauropods? Tail dynamics in the diplodocids. *Paleobiology.* 23(4), 393-409

Neal, R.J., and Wilson, B.D., (1985). 3D Kinematics and Kinetics of the Golf Swing. *International Journal of Sport Biomechanics*. 1, 221-232

Nesbit, S.M., (2005). A Three Dimensional Kinematic and Kinetic Study of the Golf Swing. *Journal of Sports Science and Medicine.* 4, 499-415

Nesbit, S.M., and Serrano, M., (2005). Work and Power Analysis of the Golf Swing. *Journal of Sports Science and Medicine.* 4, 520-533

Nigg, B.M., Cole, G.K., and Wright, I.C. (1999). Optical Methods. *Biomechanics of the Musculo-skeletal System 2nd ed.* Nigg, B.M. and Herzog, W. ed. John Wiley & Sons. West Sussex, UK. 302-331

Pickering, W.M., and Vickers, G.T., (1999). On the double pendulum model of the golf swing. *Sports Engineering*. 2, 161-172

Putnam, C.A., (1993). Sequential Motions of Body Segments in Striking and Throwing Skills: Descriptions and Explanations. *Journal of Biomechanics*. 26 (Suppl 1), 125-135

Pyne, I.B., (1977). A Clubhead Speed Coefficient for the Golf Swing. *Quarterly Journal of Mechanics and Applied Mathematics.* XXX (3), 269-280

Sanders, R.H., and Owens, P.C., (1992). Hub Movement During the Swing of Elite and Novice Golfers. *International Journal of Sport Biomechanics.* 8, 320-330

Soderkvist, I., and Wedin, P.A., (1993). Determining the Movements of the Skeleton Using Well-Configured Markers. *Journal of Biomechanics.* 26 (12), 1473-1477

Sprigings, E.J., and Neal, R.J., (2000). An Insight into the Importance of Wrist Torque in Driving the Golfball: A Simulation Study. *Journal of Applied Biomechanics.* 16, 356-366

Sprigings, E.J., and Neal, R.J., (2002). Examining the delayed release in the golf swing using computer simulation.. *Sports Engineering.* 5, 23-32

Stefanyshyn, D.J., (1996). *Mechanical Joint Energy in Athletics*. Doctor of Philosophy Thesis. University of Calgary

Vaughan, C.L., (1981). A three-dimensional analysis of the forces and torques applied by a golfer during the downswing. *Biomechanics VII-B.* Morecki, A., Fidelus, K., Kedzior, K., and Witt, A., ed. University Park Press, Baltimore MD. 325-331

Vinogradov, O., (2000). *Fundamentals of Kinematics and Dynamics of Machines and Mechanisms.* CRC Press. London.

von Tscharner, V. 2002. Time-frequency and principal-component methods for the analysis of EMGs recorded during a mildly fatiguing exercise on a cycle ergometer. *Journal of Electromyography in Kinesiology*. 12 (6) 479–492

Williams, D., (1967). The Dynamics of the Golf Swing (with Conclusions of Practical Interest). *Quarterly Journal of Mechanics and Applied Mathematics*, 20 (2) 247-264

Williams, R., (2002). Live on Broadway. DVD. Sony.

Winter, D.A., (1987). Mechanical Power in Human Movement: Generation, Absorption and Transfer. *Current Research in Sports Biomechanics.* Karger, Basel. 25, 34-45

Wood, G.A., (1982). Data Smoothing and Differentiation Procedures in Biomechanics. *Exercise and Sport Science Reviews.* 10, 380-362